Structure and Swelling Behaviour of Polyelectrolyte Multilayers

vorgelegt von
Samuel Dodoo, M.Sc
Accra, Ghana

von der Fakultät II -Mathematik und Naturwissenschaften
an der Technischen Universität Berlin
zur
Erlangung des akademischen Grades

Doktor der Naturwissenschaften
(Dr. rer. nat.)

genehmigte Dissertation

Vorsitzender: Prof. Dr. Reinhard Schomäcker
1. Berichter: Prof. Dr. Regine von Klitzing
2. Berichter: Prof. Dr. Eva Blomberg
Tag der wissenschaftlichen Aussprache: 23.09.2011

Berlin 2011
D 83

I dedicate this work to my love Josephine, my children Ken, Keona, Kinsly and my mother Linda Okine. Your love, support and encouragement toward the dream of attaining the highest level of education have seen me through. With the finishing of this work, your dreams come true

Acknowledgements

Contents

Chapter 1

Introduction

Outline of the thesis

In this thesis, the relation between structure, growth and swelling in water of polyelectrolyte multilayers are investigated. Polyelectrolyte multilayers are fabricated by alternating adsorption of polyanions and polycations on a silicon substrate. The multilayer is sensitive to external stimuli, which often counteracts the stability of the multilayer. Also the many applications of polyelectrolyte multilayers have made the *interphase* between the substrate and the film bulk to be of interest. The thesis addresses the effect of preparation parameters such as type of ion and ionic strength on the thickness, roughness, mobility and amount of water in the polyelectrolyte multilayers. The effect of the substrate on the multilayer is also studied.

1.1 Introduction

Polyelectrolytes are polymers with charged groups attached to the repeat unit and can dissociate in aqueous solution. Polyelectrolyte multilayers (PEM) are fabricated through the self assembly layer-by-layer adsorption technique introduced by Decher.[1–3] PEM can be assembled on variety of hydrophilic substrates such as silica, glass, mica or gold wafers by alternating exposure to solutions of polyanions and polycations.[4,5] This self assembly technique[6–9] is very simple and offers a lot of opportunities in which it can be applied. Applications are optical devices,[10] sensors,[11,12] functional materials, surface modification, encapsulation,[8,11,13,14] catalysis,[15] separations,[16,17] nanofiltration,[18,19] surface coatings, light-emitting diodes,[20] electrochromic,[21] membranes and bioactive thin films of controlled thickness,[22,23] selective area patterning[24] and nanotubes.[25,26] As building blocks, for example, inorganic nanoparticles such as gold colloids,[27] temperature-sensitive compounds,[28] orientable chromophores,[29,30] charged biopolymers[31,32] and mesogenic units including local order[33] have been employed.

The layer-by-layer adsorption method has gone through many advancement from dipping in the early stages to spraying in recent times.[34] Polyelectrolyte multilayers are known to be driven not only by electrostatic interactions[3,35] but also entropic gain due to release of counterions, hydrophobic interactions and hydrogen bonding.

Type of salt[36–40] used in the multilayer preparation influences the thickness of the multilayer according to the Hofmeister effect. The amount of salt also affects the multilayer

thickness which can be explained by different conformations of the chains: Without salt the polyelectrolyte chains are oriented flat and parallel to the substrate, with higher salt concentrations of the aqueous solutions the chains form coils[41,42] which are then adsorbed at the interface. Because of screening of charges along the polyelectrolyte chains the polymer is more entangled with larger thickness. TIRF (Total Internal Reflection Fluorescence) kinetic experiments, where the fluorescence of a fluorescein labeled polyelectrolyte is measured, indicate an increasing amount of adsorbate with increasing salt concentration. Measurements of the rhodamine transport through the polyelectrolyte multilayer reveal a higher diffusion coefficient of rhodamine for multilayers prepared without salt. These findings lead to the conclusion that the polyelectrolyte density of multilayers prepared without salt is lower than the polyelectrolyte density of multilayers prepared with salt additive.[43]

Reflectivity techniques, especially neutron and x-ray reflectometry, are well suited for the characterization of multilayer films, as they allow the determination of concentration gradient along the layer normal. X-ray reflectometry have only exhibited Kiessig fringes that arise from the interference of x-ray beams reflected at the substrate-film and film-air interfaces.[44–46] Neutron reflectivity measurements of polymer films of super lattice structure showed that the polyelectrolytes are deposited as layers with an interdigitation larger or equal to a single layer thickness and indicate that there is no distinct layer-by-layer separation between polyelectrolytes of opposite charges.[20,47,48] Measurements of the surface potential resulted in a change of (surface) potential (but not with opposite sign) after each adsorption step, i.e. after each additional single deposited polyelectrolyte layer.[11,14,49,50]

The properties of PEM are not fully understood up to now and more work needs to go into investigating their structural behaviour. PEM can be fabricated with Å precision by tuning preparation parameters like type of ion, ionic strength, pH, temperature, type of polyelectrolyte and degree of charge. Depending on which application of the PEM is of interest it is necessary to have a broad knowledge of the PEM as well as in-depth knowledge of specific properties of the multilayer.

The content of this thesis covers characterization of PEM using different experimental techniques such as: Ellipsometry, Neutron and X-ray reflectometry, Quartz Crystal Microbalance with Dissipation, Contact Angle measurements, Atomic Force Microscopy, and Fluorescence Recovery After Photobleaching. These techniques are used to study the structural behaviour of PEM, both external and internal structures. The external structure includes, thickness, type of growth, morphology, surface roughness, hydrophobicity and swelling whereas the internal structure include, amount of void and swelling

water, internal roughness towards substrate, and mobility. These structural properties are studied as a function of type of salt (or type of ion) and the amount of salt (or ionic strength) during preparation.

The results are presented in the form of papers (articles) which are either published, accepted or in preparation. The chapters of this thesis are named depending on the specific properties of PEM under discussion. The layout of the thesis is as follows.

Chapter 2 - Scientific background and theory will cover some basic definitions like, polyelectrolytes, polyelectrolyte complexes, polyelectrolyte multilayers, type of growth as well as the principles of intermolecular interaction theory necessary to explain this thesis.

Chapter 3 - Experimental Section: Materials and Techniques will present the various materials used and the detailed description of the experimental procedures and techniques including instruments and parameters.

Chapter 4 - Effect of ionic strength and type of ions on the structure of water swollen polyelectrolyte multilayers will discuss thickness, roughness, void water and swelling water as a function of various amounts of Sodium Fluoride (NaF), Sodium Chloride (NaCl) and Sodium Bromide (NaBr).

Chapter 5 - Effect of ionic strength and layer number on swelling of polyelectrolyte multilayers in water vapour will discuss the the swelling behaviour of PEM in water vapour as well as the interphase and continuum behaviour of PEM.

Chapter 6 - Long Chains versus Short Chains will discuss structural differences and analogies of long chains and short chains PEM

Chapter 7 - Types of multilayer growth will discuss the linear growth, exponential growth and unstable growth as influenced by preparation parameters.

Chapter 8 - Summary and Outlook will summarize the key findings of this thesis and highlight possible project for the future.

Chapter 2

Scientific background and theory

2.1 Polyelectrolytes

Polyelectrolytes are polymer chains having charged groups attached to the repeat unit.[51] Examples of natural polyelectrolytes are proteins, DNA and polysaccharides. Because of synthetic polyelectrolytes are water soluble, they allows a wide range of non-toxic, environment friendly and inexpensive formulation. Super-absorbing diapers, low fat food, washing detergent and their additives, waste water purifiers are amongst the most common examples. After dissociation in aqueous media polyelectrolytes break into charged polymer chains and counterions. Based on the degree of dissociation, a polyelectrolyte can be considered as "strong" or "weak" and the type of charge that the polymer carries determines whether it is a polyanion or polycation. In cases where a polyelectrolyte dissociates completely it is termed as strong polyelectrolyte. But in cases where a polyelectrolyte only partially dissociates, this is termed as weak polyelectrolyte.

Polyelectrolyte solutions are characterized by a wide range of interactions varying from molecular distances (counterion-chain interaction) to almost micrometer lengths (long-range electrostatic forces). The properties of electrolytes as polyions can be seen in the electrostatic interactions between charges on the polymer chain and also between charged chains and the counterion cloud around it which influences the chain conformation considerably. Considering polymer molecules with like-charges, the chains are more stretched than the chains of uncharged polymers as a result of electrostatic repulsion. Considering electrostatic interactions of polyelectrolytes, the Debye-Hückel theory[52] can be applied as first approximation to explain their interactions. An important parameter in the description is the Bjerrum length l_B, which is defined as the distance where the electrostatic interaction between two unscreened elementary charges e in a dielectric medium equals the thermal energy $(k_B T)$,

$$\frac{e^2}{4\pi\epsilon l_B} = k_B T \tag{2.1}$$

where ϵ is the dielectric constant of the medium. At room temperature the l_B for water is 7 Å. The electrostatic repulsion leads to an increased persistence length of the chain, l_τ.

The excluded volume statistics can be used to describe semi-rigid charged chains, but with an increased persistence length l_τ, and thus an increased end-to-end distance R_0 of $R_0^2 = 2Nal_\tau$. In salt solutions, the electrostatic interaction is screened and decays with

the Debye length $\lambda_D = \kappa^{-1}$, where $\kappa^2 = 8\pi c_{salt}l_B$, and c_{salt} is the salt concentration. Given l_0 as the persistence length of the uncharged chain, the self-repulsion of the polyion chain leads to an increase of the persistence length, which is dependent on the extent of salt screening, resulting in

$$l_\tau = l_0 + (\tau^2 l_B)/(4\kappa^2), \tag{2.2}$$

with $\tau = f/a$ given as the charge density per unit length, calculated from f as the fraction of charged monomers along the chain, and a as the monomer length. Here, Manning condensation, which occurs at higher charge densities on the chain, is neglected.[53]

2.2 Complexes

Polyelectrolyte complexes (PECs) are formed by mixing a solution of polyanion and a polycation solution.[54,55] Electrostatic and entropy gain due to counterion release drive this self-assembly process.[56] The same process is also necessary for the association between oppositely charged polyelectrolytes and surfactants, colloidal particles, and biomolecules. Dautzenberg[57] found that mixing of strong polyelectrolyte with low concentration of salt, leads to formation of low amount of aggregates. However, at high concentrations, a secondary aggregations is formed which causes the large aggregates to precipitate out of solution. In a complex of a weak polyelectrolyte and a strong polyelectrolyte, the addition of salt causes a complete dissolution of the complex.[58] For a weak polyelectrolyte, the charge density changes depending on the pH. Combination of a polyelectrolyte with a high charge density and a polyelectrolyte with a low charge density leads to the formation of non-stoichiometric PECs[55,59–61] which are normally formed when polyelectrolytes are mixed with an excess of one type of polyion charge. Non-stoichiometric PECs are usually in two categories: (i) highly aggregated PECs made up of several polyelectrolyte chains that are stabilized by the polyion in excess, which charges the PEC surface and prevents macroscopic precipitation; (ii) water-soluble molecular PECs that form at special conditions.[62] Stoichiometric polyelectrolyte complexes contain equal amounts of positive and negative charges. They are usually insoluble and precipitate out of solution upon formation. However, the precipitation of stoichiometric PECs can be avoided if a hydrophilic nonionic block is attached to at least one of the polyelectrolytes.[63] In such a case uncharged water soluble PECs are formed, comprising of a water-insoluble core (the insoluble PEC) surrounded and stabilized by a hydrophilic corona.

2.3 Polyelectrolyte Multilayers

2.3.1 The layer-by-layer self-assembly procedure

Coulombic interactions do not only take place between polyelectrolytes. A charged surface immersed in a polyelectrolyte solution will adsorb the polyelectrolyte onto the surface. When the adsorbing polyelectrolytes completely cover the surface, in most cases the charge of the system will now carry the charge of the polyelectrolyte. This is termed to as charge reversal. If this occurs the surface can be washed in water and then immersed in a solution of another polyelectrolyte having a charge opposite to that of the initial polyelectrolyte. The subsequent polyelectrolyte will be adsorbed on top of the initial polyelectrolyte. The difference between complexes and a surface is that this process can be repeated as many times as desired. This procedure is termed as layer-by-layer (LbL) assembly and leads to a multilayer formation, with the early idea being developed by Decher et al.[2,3] The internal structure of the films are investigated by neutron reflectivity. These investigations revealed that the structure is continuous with interdigitation of the chains.[40,47] If the film consist of a species that induces some water structuring, like a hydrophobic species, a less interdigitated film could be realized.[64] Films consisting of as many as 200 layers have been reported.[65]
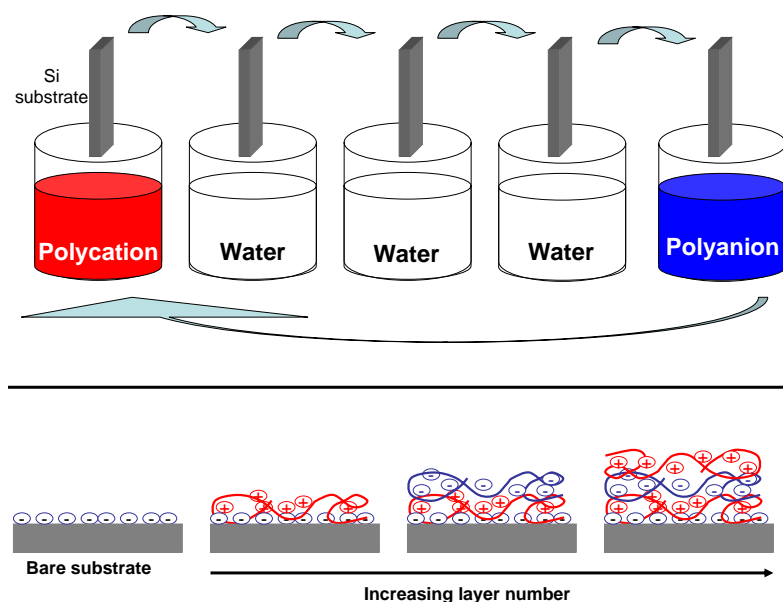
Figure 2.1: *Setup of layer-by-layer alternating adsorption of polycations and polyanions from aqueous polyelectrolyte solutions unto a charge planar substrate.*

After the earlier work by Decher in 1992, the work done on LbL has largely increased due to its ease and versatility. A number of substrates have been used so far which include

glass, quartz, silicon wafers, mica, and gold surfaces. Apart from the many available substrates, many layer constituents have been realized also, including polyelectrolytes, biopolymers, inorganic particles, and many others.[7,66] Usually multilayers are fabricated using electrostatic interaction between oppositely-charged polyelectrolytes. Aside the electrostatic interaction, there are other interactions involved during multilayer formation. For example, hydrophobic interaction arising from the carbon backbone of the polymer also plays a major role.[67] Furthermore, interactions like hydrogen bonding[68,69] and specific interactions[70] are also involved in multilayer formation. Preparation parameters such as type of ion and ionic strength,[9,53,71–74] pH and temperature affect the structure of polyelectrolyte multilayers. Atmospheric humidity can also influence the thickness of the film.[75]

2.3.2 Kinetics of multilayer build-up

The adsorption of each layer takes place simultaneously with complexation of polyelectrolytes, due to charge interactions between previously deposited layers. The level of interdigitation is determined during the adsorption process of each layer, assuming the internal chains in the multilayer to be immobile. One way to view the adsorption-complexation process is as a time dependent process at a polymer concentration larger than the saturation concentration. The timescale differs a lot in kinetic studies of multilayer build-up.[7,76] The kinetics is considered to be a two-step process where the first adsorption occurs in seconds to minutes, and a much slower process, which can occur as slowly as over hours.[7] Movement of chains to the surface and a quick mass adsorption is the first steps of kinetics.[76,77] In this case the rate of adsorption is controlled by the diffusion of polyelectrolyte coils. Rearrangement of chain takes place at the surface and mass adsorption continues at a slower rate until reaching saturation.[76] The second kinetic step involves chain rearrangement making the diffusion of chains into the areas of previously deposited layer possible. The irreversible complexation of charges is finally achieved by combining positive and negative polyelectrolytes.[33,77] The proof of layer interdigitation experimentally is concluded not only from the properties of preformed multilayers, but is evident already during the formation process of the assembly. Kinetics and equilibrium properties influence the multilayer build-up. Rearrangement of slower chains allows for equilibration and adsorption of more chains. The flexibility of the final layers ensures the interdigitation and thus the complexation. Finally, further adsorption is hindered by repulsive interaction, while the deposited amount in each layer is determined by the efficiency of interdigitation and complexation.

2.3.3 Multilayer growth

The adsorption of the first layer on the charged substrate is the start of the multilayer growth. With each deposition step the layer thickness changes characterizing multilayer build-up. A linear growth of the multilayer thickness with number of deposition step is usually observed for most polyelectrolyte multilayer systems.[2,14,31,33,78] However, the few initial layers don't follow this growth order where a relatively lower amount is adsorbed leading to thinner layer thickness and only after many deposition steps is a constant thickness increase observed.[79] Multiplication of surface functionality is shown to cause a nonlinear growth of the few initial layers.[3] The substrate surface charge is considered an important parameter determining the first layer properties. This zone in the multilayer growth where the properties of the multilayer is influence by the underlying substrate is termed the precursor zone.[80]

A constant regime is reached after many layers where the multilayer properties no longer depend on substrate surface charge. In this regime the layer by layer thickness become constant with roughness and thickness increasing with increasing number of deposition layers. This second zone is considered the core zone.[80] The outer zone is made up of the outer layers carrying the excess charges making contact with the electrolyte solution where the polyelectrolyte chains are weakly bound, with their chain ends protruding into the solution. The local properties of the multilayer in the outer zone differ from those of the core zone.

There are instances where no linear regime of multilayer growth is observed but rather the amount of adsorbed polyelectrolyte and thickness increase more rapidly than linearly with the number of deposited pairs. This type of growth is called "exponential growth" in literature and is mainly due to the mobility of polyions used. Examples of such multilayer systems include poly(L-glutamic acid) (PDA)/poy(L-lysine) (PLL)[78] or hyaluronic acid (HA)/PLL.[81] The adsorption of more chains with increasing number of layers indicates a layer structure that changes with layer increase. Observations such as these are correlated with an increase in surface roughness which provides an increase of total surface and thus with each deposition step a lager number of charges are available for complexation.[82] A complete rearrangement of the multilayer with each new layer addition is said to lead to an exponential growth, and evidence of a very large chain mobility shown by polymer diffusion experiments.[83] Apart from the polyelectrolyte pairs that determine the type of multilayer growth, certain parameters are also known to influence the type of growth. These parameters include ionic strength, type of ion, polymer charge density, pH

of weak polyelectrolyte solutions, type of solvent, temperature, adsorption time, polymer concentration and molecular weight of the polyelectrolytes.

2.4 Theory of polyelectrolytes

In this section specific interactions explaining the behaviour of polyelectrolyte multilayers are discussed in detail.[84–86]

2.4.1 Chain extension at infinite dilution

The effect of the repulsive interaction between like charges on the chain can be understood by a Flory-type calculation. Let us consider a chain with N monomers and assume that a fraction f of those are ionizable. Thus, in solution the chain contains fN charged monomers and $(1-f)N$ neutral monomers. all randomly distributed. In a mean-field approach, the Flory-type energy for a chain of size R is

$$E_F = k_B T \frac{R^2}{Na^2} + k_B T \frac{(Nf)^2 l_B}{R}. \tag{2.3}$$

The first term is the elastic energy where we assume that the chain has a Gaussian configuration when all electrostatic interactions are switched off. The second term is the electrostatic energy due to the Nf monomers of charge e. Minimization with respect to R leads to

$$R \approx N f^{2/3} (l_B a^2)^{1/3} \tag{2.4}$$

where a monomer length. This simple calculation leads to the important result that the size of a polyelectrolyte is proportional to the number of monomers and to the two third power of the charge fraction.

2.4.2 Van der Waals forces

Considering two freely rotating permanent dipoles, there exist orientation forces or Keesom forces between them. Let u_1 and u_2 be the dipole moments of the two dipoles and r be the distance between them. The Keesom interaction energy between them is given by equation 2.5.[85]

$$w_K(r) = -\frac{u_1^2 u_2^2}{3(4\pi\epsilon\epsilon_0)^2 kTr^6} = -\frac{C_K}{r^6} \tag{2.5}$$

where ϵ is the dielectric constant of the medium, ϵ_0 is the dielectric constant of vacuum, k is Boltzmann constant and T is the temperature.

For a permanent dipole and an induced dipole, the interaction force between them is induction forces or Debye forces. Two different molecules possessing permanent dipole u_1 and u_2 and polarizabilities α_{01} and α_{02}, their net dipole-induced dipole interaction energy can be described by equation 2.6,[85] Debye interaction energy.

$$w_D(r) = -\frac{u_1^2\alpha_{02} + u_2^2\alpha_{01}}{(4\pi\epsilon\epsilon_0)^2 r^6} = -\frac{C_D}{r^6} \tag{2.6}$$

The third interaction is between two non-polar species and this is called London forces or dispersion forces. If h be the Planck constant, $h\nu_1$ and $h\nu_2$ be the ionization potentials of the two molecules respectively, the London dispersion interaction energy is given by equation 2.7.[85]

$$w_L(r) = -\frac{3\alpha_1\alpha_2(h\nu_1)(h\nu_2)}{2(4\pi\epsilon_0)^2 r^6 h\nu_1 + h\nu_2} = -\frac{C_L}{r^6} \tag{2.7}$$

Since these three equations are attractive and possess an r^6 dependence, summing them up will result to the total Van der Waals interaction energy, which is written as

$$w_{VdW}(r) = \frac{C_K + C_D + C_L}{r^6} \tag{2.8}$$

Now, to calculate the interaction energy between two planes at a distance, d, an integration over all Van der Waals forces of points within these planes is necessary. The integration will result in a d^{-2} dependence having interaction constants merging into a Hamaker constant A, according to equation 2.9.

$$w_{VdW}(d) = \frac{A}{12\pi d^2} \tag{2.9}$$

2.4.3 Double layer forces

Double layer forces are repulsive in nature and arise when a surface with ionizable groups is placed in water. The dissociating charges will be compensated by opposite charges in solution or adsorbed at the surface. The Poisson-Boltzmann equation describes the electrolyte distribution near the interface. The equation requires that a non-linear second-order differential be solved. The ionic strength in the solution affects the charge distribution, σ. The Debye length, κ^{-1}, is the characteristic decay length of the diffuse (double) layer.

This refers to the "thickness" of the double layer. Equation 2.10 gives the interaction energy of the electric double layer.

$$w_{el}(d) = \frac{2\sigma^2}{\kappa\epsilon\epsilon_0}e^{-\kappa d} \tag{2.10}$$

The DLVO theory after Derjaguin, Landau, Verwey and Overbeek combines the Van der Waals forces and the electric double layer force. It describes the total interaction energy between two surfaces as a function of distance. With reference to equations 2.9 and 2.10, one can see that the Van der Waals contribution to the total potential is dominant at long ranges and at extremely short distances, while at intermediate distances the electric double layer forces become dominant. The interaction between two surfaces is described by the DLVO theory but at very, very close range, the DLVO no longer completely describes all the effects seen between two interacting bodies. These forces are referred to as non-DLVO forces.

2.4.4 Non-DLVO forces

At distances that are within a few nanometers from a surface, the DLVO theory does not describe completely all the interactions that occur, except for atomically flat surface like mica. These non-DLVO forces, which are not described by the DLVO theory, are attractive, repulsive or oscillatory in nature. These forces are steric forces, hydration forces, solvation forces, and hydrophobic forces. Steric forces normally refer to the case at small distances that the Stern layer overlaps. Primarily the geometry of molecules and their arrangement around a constraining boundary determine the solvation (or structuring) of solvent molecules at a surface. Solvation forces do not arise simply because liquid molecules tend to arrange in semi-ordered layers at surfaces, but they result from the disruption or change of this ordering during the approach of a second surface. In the absence of change, there would be no solvation force. Chemical and physical properties of the surfaces as well as the properties of the intervening medium influence the solvation forces. Short distance interactions are usually referred to as solvation forces, structural forces or when the medium is water, hydration forces. Hydrophobic forces arise from species that are inert to water or cannot bind to water. The case where a hydrophobic species is in an aqueous environment is an entropically unfavorable one. Therefore the hydrophobic species are drawn together to reduce the surface to water.

2.4.5 Hydrogen bonding

Hydrogen bonding is a special case of attractive directional dipole-dipole interactions force that cannot be explained by the DLVO theory or by the non-DLVO forces. In particular, if hydrogen is bonded to an electronegative atom, the electron will spend more time around the electronegative atom, leaving a partial positive charge on the hydrogen and a partial negative charge on the electronegative atom. Species that take the role of the electronegative atom are known as hydrogen bonding donors; examples of good hydrogen bonding donors are oxygen, nitrogen, and fluorine. Hydrogen bonding is useful in nature because of its directional dependence as well as its semi-strong nature. It has strength from 10-40 kJ/mole which is between Van der Waals forces (about 1 kJ/mol) and covalent bonds (500 kJ/mol), which means it is a strong interaction but not so strong to be unbreakable. Water is a special case of an associated liquid, or liquids that display hydrogen bonds. The oxygen of a water molecule has two lone pairs of electrons, each of which can form a bond with hydrogens on two other water molecules. This can repeat so that every water molecule is H-bonded with four other water molecules.

Chapter 3

Experimental Section: Materials and Techniques

Abstract

This section deals with the objectives behind the work and the experimental approach towards fulfilling these objectives. As stated in the outline, understanding the structural behaviour of polyelectrolyte multilayers (PEM) is the main objective. The structural properties of PEM are different under different length scales and for that reason different experimental setups have to be designed to probe these properties. Different techniques provide different structural information about the multilayers. Some techniques are suitable for studying the external properties while others are suitable for studying the internal ones. To gain an insight to specific knowledge of the polyelectrolyte system various techniques are needed to complement each other. The techniques used to analyze the systems discussed in the work are a mixture of microscopy, spectroscopy, and reflectivity methods. Combining the knowledge gained from all the measurements with one another gives a better understanding of the system as a whole. The principles and setups of the techniques used in this work are described in this chapter.

3.1 Materials

3.1.1 Polyelectrolytes and Salts

The polyelectrolytes used in this work include poly(ethylenimin) (PEI), 750 kDa, 50 wt.% solution in water, poly(allylamine hydrochloride), (PAH) 65 kDa, poly(sodium 4-styrenesulfonate), (PSS) 70 kDa and are purchased from Sigma-Aldrich (Steinheim, Germany). The linear copolymers poly[(diallyl dimethyl ammonium chloride) -stat- (N-methylactamide)], (PDADMAC-stat-NMVA) 300 kDa are synthesized by free radical polymerization of positively charged diallyldimethylammonium chloride monomers and neutral N-Methyl-N-vinyl-acetamide with different percantages which corresponds to different degree of charge in the resulting polycation. The synthesis was done by Dr. W. Jaeger (Fraunhofer Institut für Angewandte Polymer Forschung). Throughout this thesis, fully charged PDADMAC or PDADMAC100% is denoted as "PDADMAC" otherwise the respect degree of charge is denoted accordingly, e.g. PDADMAC75%. Sodium carboxymethylcellulose (CMC) with the degree of charged substitution of 0.89 and the average molecular weight of 250 kDa was purchased from AQualon Inc. France. Hyaluronic

acid (HA) in the sodium hyaluronate form, 150 kDa was obtained from Amersham Bio-science GmbH, Germany. The type of salts used in preparing the electrolyte solutions are sodium floride NaF, sodium chloride NaCl and sodium bromide NaBr (purity $> 99\%$) purchased from Merck (Darmstadt, Germany). Deionized and ultrapure Milli-Q water (specific resistance 18 M$\Omega\cdot$cm^{-1}) was used as solvent. The chemical structures of all the polyelectrolytes are shown in 3.1.
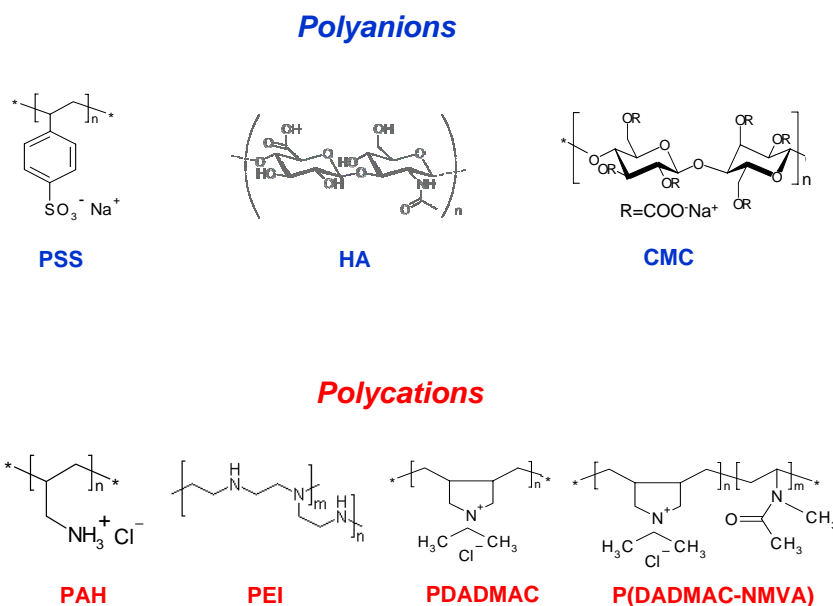
Figure 3.1: *Chemical structures of all the polyelectrolytes used in the sample preparation.*

3.1.2 Preparation of fluorescently labeled PAH (FITC-PAH, RITC-PAH)

Fluorescein labelled PAH, was prepared according to the labeling procedure suggested by Nargessi et al.[87] 25 mg PAH was gently dissolved in 2 ml buffer solution of Na$_2$CO$_3$ and NaHCO$_3$ (pH = 9.5). Either 1 mg fluorescein isothiocyanate FITC or 1.38 mg rhodamine B isothiocyanate was dissolved in 1 ml buffer after which 200 ml of FITC or RITC solution (in a similar buffer solution) was added drop by drop. After two hours of stirring, the mixture was filtered through a separating column (Deasalting and buffer exchange HiPrep 26/10 columns, Amersham Bioscience GmbH, Germany) in order to separate the single dye molecules not attached to the polyelectrolyte from those attached according to their different elution time in the column. After the labeling process, the FITC or RITC molecules are bound covalently to the PAH chain. The polymer was then freeze dried in

order to have a precise concentration of 10^{-2} monomolar polyelectrolyte in the solution. The ionic condition associated with the solution was fixed at 0.5 M NaCl.

3.2 Sample Preparation

3.2.1 Cleaning and Preparation of Negatively Charged Planar Substrate

Since surfaces and interfaces of polymers are very sensitive to dirt and contamination, it is very necessary to thoroughly clean everything that will have contact with the polyelectrolytes during the sample preparation. Before the actual sample preparation all glassware, tweezers, magnetic stirrer bars to be used are soaked in a solution of Q9 (5 %) from Ferak Berlin GmbH and Miili-Q water (95 %) for at least 24 hours, after which they are rinsed with Milli-Q water very well before drying in an oven at 70°C.

Layer-by-layer PEM adsorption requires a solid charged substrate onto which the multilayers will be adsorbed. In this thesis planar substrate is employed because it offers advantages over colloidal particles as substrate, sometimes used in PEM buildup. Silicon wafers (Wacker Siltronic AG, Germany) or silicon blocks of dimension $(80 \times 50 \times 15)$ mm^3 (Silizium Bearbeitung A. Holm, Tann, Germany) used as solid substrates are etched with a 1:1 mixture of piranha solution (H$_2$O$_2$:H$_2$SO$_4$; 1:1) for 30 min followed by extensive rinsing with Milli-Q water until the pH of the solution around the Si wafers/blocks was about 6 or 7. The Si wafer/block is held with a pair of tweezers from underneath to prevent washing contaminants from the tweezers onto the wafer/block. A gentle flow of nitrogen gas is blown over the wafer/block to dry it.

3.2.2 Cleaning of Quartz Crystals with Gold Electrodes

The surface properties of the sensor crystal are crucial for the interaction of sample material with the surface. Therefore, the use of proper procedures for cleaning and surface preparation are required to obtain reproducible measurements. The quartz crystals used in the Quartz Crystal Microbalance with Dissipation QCM-D (Q-Sense Sweden) measurements are cleaned according to the RCA 1 cleaning procedure followed by a plasma cleaning (recommended by Q-Sense). A safer protection of the sensor crystals is by using the Q-Sense crystal cleaning Teflon holder while working with them. A mixture of (H$_2$O:H$_2$O$_2$:NH$_4$; 5:1:1) is heated to 80°C and then the quartz crystal is put into the boiling mixture for 5 min after which it is rinsed with Milli-Q water thoroughly. The crystal

is held with a pair of tweezers from underneath to prevent washing contaminants from the tweezers onto the crystal. Liquid is chased off the crystal with a flow of nitrogen gas. The cleaned crystals are then plasma cleaned at 30 W for 10 min to get rid of organic contaminants.

3.2.3 Polyelectrolyte Multilayer Adsorption onto Si Substrate

The polyelectrolyte multilayers are deposited on silicon wafers or blocks (for X-ray and neutron reflectivity measurements) by immersion for 20 min into aqueous solutions containing 10^{-2} monoM (concentration of monomer units) of the respective polyelectrolytes in H_2O and by rinsing three times with Milli-Q water for 1 min after each deposition step. First, the wafer is immersed in aqueous solution of PEI for 30 min and then rinsed gently in Milli-Q water. This extra step is found to be efficient in the reduction of substrate influence on the adsorption of the next polyelectrolyte layers.[88] After that, PSS and PDADMAC are deposited consecutively via the self-assembly technique. The multilayers are dried in a gentle stream of nitrogen for 3 minutes after completion of the multilayer assembly.

3.3 Measurement Procedure and Techniques

3.3.1 Reflectometry

Reflectometry is an analytical technique for investigating thin layers using the effect of total external reflection of x-rays or neutrons. In reflectivity experiments, the x-ray reflection of a sample is measured around the critical angle. Below the critical angle of total external reflection, x-rays penetrate only a few nanometers into the sample. Above this angle the penetration depth increases rapidly.[89] At every interface where the electron density changes, a part of the x-ray beam is reflected. The interference of these partially reflected x-ray beams creates the oscillation pattern observed in reflectivity experiments. From these reflectivity curves, layer parameters such as thickness and density, interface and surface roughness can be determined.

X-rays are electromagnetic radiation occupying the spectrum from about 10^{-2} to 10^{2} Å in wavelength, but those used for the study of structure of materials have wavelengths more narrowly confined to the approximate range of 0.5-2.5 Å. Studies on polymers are performed mostly with the $K\alpha$ characteristic radiation from copper target tube having a

wavelength of 1.5418 Å. X-ray wavelength of around 1 Å is of the same order of magnitude as most interatomic distances, that is why it plays such important role in probing the structure of matter.[90] X-rays are characterized by their energy E and momentum p, which are related to the wavelength λ and frequency ν by

$$E = h\nu \tag{3.1}$$

and

$$p = \frac{h}{\lambda} \tag{3.2}$$

where h is Planck's constant (6.626×10^{-34} Js) and equation 3.2 is known as the de Broglie relation. A photon does not possess a mass or an electric charge.

On the other hand, a neutron is an uncharged elementary particle, possessing a mass m equal to 1.675×10^{-24} g and spin $1/2$. Its kinetic energy E and momentum p are

$$E = \frac{1}{2}mv^2 \tag{3.3}$$

and

$$p = mv \tag{3.4}$$

where v is its velocity. Neutrons also exhibit wave-like behaviour, with the wavelength λ given by the de Broglie relation

$$\lambda = \frac{h}{p} = \frac{h}{mv}. \tag{3.5}$$

When a radiation is incident on an interface between two materials, part of the energy is reflected at the interface and the rest is transmitted through it.[89] Irrespective of whether the radiation involved is a beam of light, x-rays or neutrons, the geometry and the relative intensities of the reflected and refracted rays can be described by the principles of optics,[91] once the refractive indices of the two media are known (Figure 3.2).

With reference to Figure 3.2a, consider an incident radiation with intensity I_0 which is partly reflected and partly transmitted with intensities I_r and I_t respectively. By definition, reflectivity R is given by

$$R = \frac{I_r(\theta)}{I_0} \tag{3.6}$$

where θ is the incident angle. From Figure 3.2a, k is the wave vector of the radiation with

(a) Surface reflection

(b) Surface reflection: simple coatings

(c) Reflection at interfaces: simple coatings

(d) Reflection at interfaces: multilayers
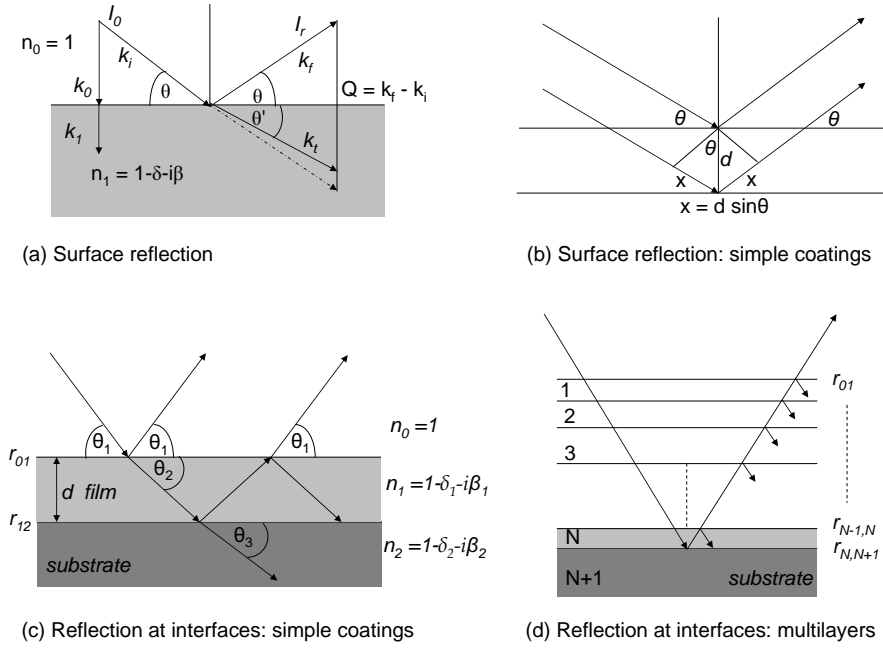
Figure 3.2: *Schematic of x-ray / neutron reflection at surface and interface.*

k_0 given by

$$k_0 = \frac{2\pi}{\lambda} sin\theta. \tag{3.7}$$

k_0 is the z-component of the k_i and it is perpendicular to the substrate. k_1 is given by

$$k_1 = k_0 n_1 \tag{3.8}$$

where n_0 and n_1 are the refractive indices of air and film respectively. The reflection coefficient r at the air/film interface is given by equation 3.9.

$$r = \frac{k_0 - k_1}{k_0 + k_1} \tag{3.9}$$

Now let's consider Snells Law which is given by

$$n_0 cos\theta = n_1 cos\theta' \tag{3.10}$$

for $\theta' < \theta$. When the incident angle is lowered, the transmitted angle gets smaller till the transmitted beam is parallel to the surface. This is the limiting condition for total external reflection, $\theta \leq \theta_c$ where θ_c is called the critical angle. Equation 3.10 therefore becomes

$$n_0 cos\theta_c = n_1 \tag{3.11}$$

which implies

$$cos\theta_c = 1 - \delta \tag{3.12}$$

where δ is the real part of the refractive index of the film. Using the series expansion of $cos(x)$ which is given by

$$cos(x) = 1 - \frac{x^2}{2} + \frac{x^4}{24} - ... \tag{3.13}$$

equation 3.12 becomes

$$1 - \frac{\theta_c^2}{2} = 1 - \delta \Rightarrow \theta_c = \sqrt{2\delta}. \tag{3.14}$$

For x-rays, δ is given by

$$\delta = \frac{\lambda^2}{2\pi}\rho_e r_0 \tag{3.15}$$

where ρ_e is the electron density and r_0 is radius of the free electron (2.82×10^{-5} Å) or the Thompson radius. For neutrons, δ is given by

$$\delta = \frac{\lambda^2}{2\pi}Nb \tag{3.16}$$

where N is the Number density [$1/\text{Å}^3$] and b is the coherent neutron scattering length [Å]. From Figure 3.2b, the path length difference between the waves scattered by the atoms in consecutive lattice planes is $2x$, which is

$$2x = 2dsin\theta \tag{3.17}$$

From Bragg's law (condition for constructive interference)

$$n\lambda = 2dsin\theta; sin\theta \approx \theta \tag{3.18}$$

and

$$(2 - 1)\lambda = 2d(\theta_2 - \theta_1) \tag{3.19}$$

then

$$\lambda = 2d\Delta\theta \tag{3.20}$$

with

$$k = (\frac{2\pi}{\lambda})\theta \tag{3.21}$$

and

$$\Delta k = (\frac{2\pi}{\lambda})\Delta\theta \tag{3.22}$$

therefore

$$d = \frac{\pi}{\Delta k}. \tag{3.23}$$

Mostly the reflectivity R is plotted as $R(Q)$ with $Q = 2k$; explicitly

$$Q_z = 2k_z = 2k sin\theta = 2(\frac{2\pi}{\lambda}) sin\theta. \tag{3.24}$$

Hence

$$d = \frac{2\pi}{\Delta Q} \tag{3.25}$$

Neutron Reflectometry

The homemade sample cell for neutron reflectivity studies of solid/liquid interfaces represents a modified version of the design by Satija and co-workers.[92] It consists of a Teflon trough of inner dimensions $(72 \times 42 \times 3)$ mm^3 stainless steel inlet and outlet tubes for the fluid mounted in opposite corners of the trough. It is sealed with a Viton O-ring against the silicon block. A more detailed description of the sample cell is given elsewhere.[93] All measurements are conducted at room temperature. Neutron reflectivity measurements are performed at the V6 instrument at the HZB Berlin. A detailed description of the instrument can be found in the literature.[94] A neutron wavelength of 4.66 Å is selected by a graphite monochromator in the incident white beam. The resolution is set by a slit system on the incident side to $\Delta Q = 0.001$ Å^{-1} for $Q \leq 0.0518$ Å^{-1}, and $\Delta Q = 0.002$ Å^{-1} otherwise. A beam of rectangular cross section 0.5×40 mm^2 for $Q \leq 0.0518$ Å^{-1} and 1×40 mm^2 for Q > 0.0518 Å^{-1} impinged on the samples at the solid/vacuum interface through vacuum and at the solid/liquid interface through the silicon block. The scattered neutrons are recorded with a ^{3}He–detector in single $\theta/2\theta$ steps with a complete run from 0.0047 to 0.1646 Å^{-1} taking typically 6-9 hours. Every run is repeated in the low Q-range to check for changes in structure during this time. The off-specular signal is collected simultaneously in a ^{3}He counter offset from the specular position by $0.44°$ toward larger angle 2θ. The extinction coefficient of the silicon blocks is found to be $\kappa = 0.0038$ mm^{-1} for the monochromatic neutrons used in this work. In the neutron reflectivity experiment at the V6 instrument, the background to the measured intensity is determined to $(1.5 \pm 0.5) \times 10^{-5}$ for measurements against both liquid phases and $(8 \pm 1) \times 10^{-6}$ for measurements against vacuum. The intensity is normalized on the measured incident intensity I_0 to obtain the reflectivity R(Q), of the interface. The centerpiece of the experimental setup is shown in figure 3.3.[95] A complete measurement cycle consisted of four steps: Recording neutron reflectivity from the multilayer 1) against vacuum (Pressure:
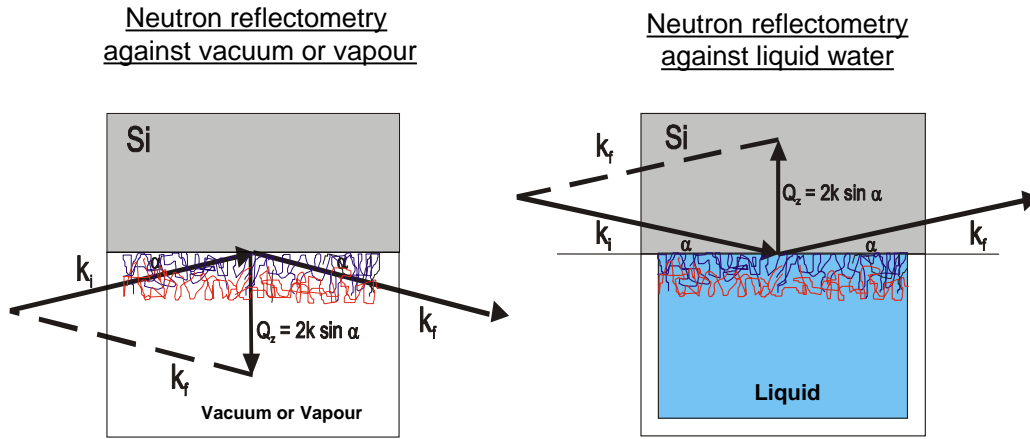
Figure 3.3: *Schematic setup of neutron scattering at planar surface. Image is taken from elsewhere.*[95]

from $(0.2\text{-}2.7)\times10^{-2}$ mbar) after preparation i.e. after exposure to H_2O (H_2O vac), 2) against H_2O (H_2O liq), 3) against D_2O (D_2O liq) and 4) against vacuum after exposure to D_2O (D_2O vac).

X-ray Reflectomery

X-ray reflectivity experiments are made using a triple axis diffractometer built at the Helmholtz Zentrum Berlin. The primary beam of this instrument is defined by the line focus of a sealed x-ray tube (0.04×8 mm^2, Cu anode) and a diaphragm (0.24×8 mm^2) at a distance of 500 mm. The reflected beam is monochromatized by a pyrolytic graphite crystal and the pulse height discriminator of the scintillation detector. The graphite crystal is set to reflect the Cu Kα doublet (1.541 Å). For measurements at high intensities, e.g., primary beam and region of total external reflection, a remote-controlled Ni absorber is inserted in the reflected beam. The Si wafers are placed in a homemade closed-cell made of stainless steal containing a reservoir which is filled with water during vapour measurements or P_2O_5 drying powder for measurements in the dry state.

Scan	FROM /deg	TO(OM) /deg	ZT /deg	OM /deg	TIM millisec	NS1	DOM2 /deg	NS2	DZT2 /deg
1	0.1	0.3	0.4	0.2	5000	1	0.01	21	0.02
2	0.3	0.7	1.0	0.5	10000	1	0.01	41	0.02
3	0.7	1.5	2.2	1.1	40000	1	0.02	41	0.04
4	1.5	3.1	4.6	2.3	80000	1	0.04	41	0.08

Table 3.1: *X-ray scan parameters: ZT is detector angle (2-Theta-Position), OM is sample angle (Omega-Position), TIM is measuring time per step, NS1 is repetition factor, DOM2 is step width of Omega (increment of sample angle), NS2 is number steps, and DZT2 is step width of 2-Theta (increment of the detector angle)*

Table 3.1 shows the scan parameters of the X-ray reflectivity measurements. For the adjustment of the 2-Theta Zero point and the Omega angle the slit width is set to 0.2 mm after which it is set to 2 mm just before the scan is started. The primary intensity I_0 is scan by removing the sample from the holder and setting ZT = 0°, OM = 0°, TIM = 10000 milliseconds, NS2 = 3, DOM2 = 0°, and DZT2 = 0°.

Fitting procedure

The reflectivity data are fitted with Parratt's dynamic approach[96] using the Parratt32 fitting software (provided by HZB). Since all the fabricated multilayers are assumed to have a homogeneous density a so-called one-box model is used to fit the experimental data. Thereby, the multilayer is described by a certain thickness, scattering length density (SLD) and roughness towards the outer medium (vacuum or water). A SiO_2 layer with thickness between 5 and 25 Å and with SLD of 1.891×10^{-5} Å^{-2} (x-rays) or 3.475×10^{-6} Å^{-2} (neutrons) representing the native oxide layer is established between Si substrate and PEM. The roughness of the SiO_2-interlayer towards silicon and towards the polymer multilayer is kept at zero. The SLD for Si is fixed at 2.073×10^{-6} Å^{-2} throughout the fitting. First, the H_2O vac data are fitted. Then, the best fit for the SiO_2 thickness is kept fixed for a particular substrate for all other conditions, i.e. H_2O liq, D_2O liq and D_2O vac. This fitting procedure is applied to all the polyelectrolyte multilayers except for $(PSS/PDADMAC)_6$ prepared from 0.25 M NaCl (neutron reflectivity data only). In this case, the SiO_2 layer went to thickness values smaller than 5 Å, which is physically senseless. For the very reason the SiO_2 layer is omitted from the model and replaced by a roughness term instead. All previously fitted samples are cross-checked with this second fitting approach and no significant differences are observed in the derived parameters.

3.3.2 Ellipsometry

Ellipsometry has become one of the most important and powerful tools for the characterization of optical properties, in particular, of thin-film- and multi-layered materials.[89] It is the most accessible of direct interfacial probe of surfaces. This method measures the change in polarization state of light reflected upon a planer interface and, based on the refractive indices of the surface, second medium and interfacial layer. The null ellipsometer provides information about the layer thickness of the adsorbed layer.[97] In the context of ellipsometry a thin film ranges from essentially zero thickness to several thousand Angstroms. The sensitivity of an ellipsometer is such that a change of film thickness of a few Angstroms is usually easy to detect. Ellipsometry is sensitive to several material characteristics, such as layer thickness, optical constants (refractive index and extinction coefficient), composition, and optical anisotropy. A beam of light is incident on a sample at an angle of incidence θ_i; the angle of incidence is defined as the angle between the input beam direction and the direction normal to the sample surface. At the boundary of the medium, part of the light will be reflected at angle θ_r while the other part will be transmitted through the sample at angle θ_t. Snell's law requires that all three beams be in the plane of incidence. The plane of incidence is defined as that plane which contains the input beam, the output beam, and the direction normal to the sample surface.

The measured values are Psi (Ψ) and delta (Δ), which are related to the ratio of Fresnel reflection coefficients, R_p and R_s for p and s-polarized light, respectively.

$$tan(\Psi)e^{i\Delta} = \frac{R_p}{R_s} \tag{3.26}$$

From equation 3.26 the ratio is seen to be a complex number, thus the "phase" information is contained in Δ, which makes the measurement very sensitive. A linearly polarized input beam is converted to an elliptically polarized reflected beam. For any angle of incidence greater than 0° and less than 90°, p-polarized light and s-polarized will be reflected differently. The optical constants define how light interacts with a material. The complex refractive index is represented by

$$\tilde{n} = n + ik \tag{3.27}$$

The real part or the refractive index, n, defines the phase velocity of light in a material:

$$v = \frac{c}{n} \tag{3.28}$$

where v is the speed of light in the material and c is the speed of light in vacuum. The imaginary part or extinction coefficient, k, determines how fast the amplitude of the wave decreases. The extinction coefficient is directly related to the absorption of a material and is related to the absorption coefficient by:

$$\alpha = \frac{4\pi k}{\lambda} \qquad (3.29)$$

where α is the absorption coefficient and λ is the wavelength of light.

Ellipsometry in air and under controlled humidity condition.

Ellipsometric measurements are performed with a polarizer - compensator - sample - analyzer (PCSA) ellipsometer, Multiscope from Optrel GbR (Wettstetten, Germany) in Null-Ellipsometry mode. The measurements are performed using a He-Ne laser light (wavelength 632.8 nm) at an incident angle of 70° against the air/film interface and 60° against the water/film interface. The instrument is controlled by the software Multi, which measures Δ and Ψ the phase shift and magnitude respectively, of change in polarization of light after reflection at the sample surface. The data analysis for the determination of thickness d and refractive index n of the multilayers is performed by using the software Elli (Optrel).

The data are analyzed by a least-squares fit with four-layer box model: (i) air ($n = 1$) or water ($n = 1.3325$), (ii) multilayer, (iii) SiO_x ($d = 1.5nm$, $n = 1.4598$) and (iv) Si ($n = 3.8858$, $k = -0.020$). For most of the multilayer both thickness and refractive index are fitted simultaneously without any assumption for the refractive index (otherwise the assumed n is stated) due to in-built algorithm which can fit both d and n even below thickness of 10 nm. The Garnet equation[98] is used to cross check the obtained thickness (below 10 nm) and refractive index. The thickness and refractive index obtained from the Garnet equation showed no significant difference from those obtained from the software.

For the measurements under controlled humidity, a locally made humidity cell is used (Figure 3.4). The cylindrical cell made of stainless steal is 57 mm long with 55 mm inner diameter. It is mounted on a ($90 \times 53 \times 4$) mm³ metal plate for stability. Humidity and temperature sensors are connected to the cell from the top. The channels of the sensors are connected to the computer and the readings are recorded. The height of the round sample table (35 mm) inside the cell can be adjusted by rotating it clockwise or anticlockwise. The front window of the cell is closed with a transparent Plexiglas 5 mm thick. Attached to the Plexiglas is a rubber O-ring to ensure air-tight closure of the cell.

1. Adjustable sample table **5. Temperature sensor** **9. Ellipsometer detector arm**

2. Nitrogen gas in-let **6. Rubber gasket** **10. Ellipsometer laser arm**

3. Nitrogen gas out-let **7. Light guide** **11. Humid nitrogen gas tube**

4. Transparent plastic lid **8. Humidity sensor** **12. Dry nitrogen gas tube**
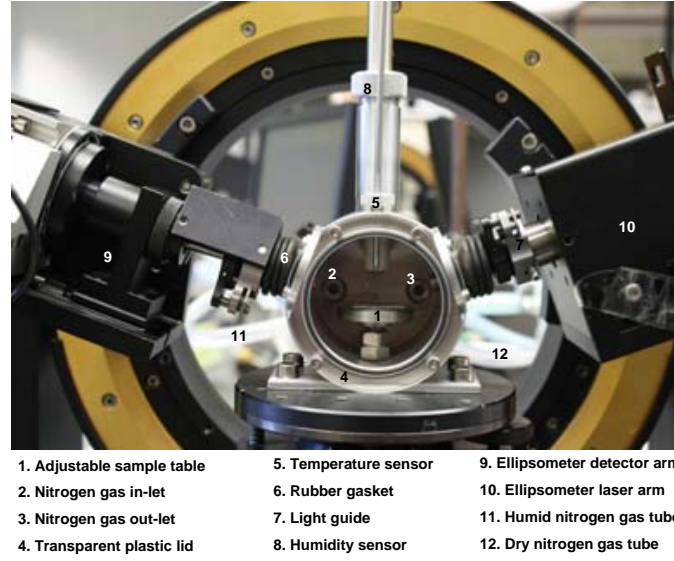
Figure 3.4: *Cross-section of the humidity cell showing the various components of the cell.*

Light guides are connected to the cell through a rubber gasket attached to two openings on the upper sides of the cell. The openings allow up to 10° movement of the laser and detector arms of the ellipsometer. For the water vapour, nitrogen gas is blown through water and the saturated water vapour flows through a tube into the cell. Both the water vapour and the dry nitrogen gas are connected to the in-let tube of the cell and circulates out of the cell through the out-let tube to avoid pressure in the cell. The relative humidity could be controlled between 1% and 98% by adjusting the right amount of nitrogen and water vapour flowing into the cell (Figure 3.4). The height of the round sample table (35 mm) inside the cell can be adjusted by rotating it clockwise or anticlockwise. The front window of the cell is closed with a transparent plexiglass 5 mm thick. Attached to the plexiglass is a rubber O-ring to ensure air-tight closure of the cell.

The condition of 100% relative humidity means the sample is immersed in water and the measurement performed with a homemade cell which is described elsewhere.[99]
The amount of swelling water is determined by using equation 3.30[75]

$$\frac{d_{swollen} - d_{dry}}{d_{swollen}} \cdot 100 \tag{3.30}$$

where $d_{swollen}$ is the thickness of the swollen PEM at r.h. > 1 % or against liquid water (100 % r.h.) and d_{dry} is the thickness of the dry multilayer at 1% r.h..

3.3.3 Atomic Force Microscopy under ambient conditions

AFM is a technique which helps to study the structure of polyelectrolyte multilayers in terms of information on morphology and surface roughness. AFM can be operated in Contact Mode, Tapping Mode and Non-Contact Mode. Tapping Mode is chosen for probing the samples since it is developed as a method to achieve high resolution without inducing destructive frictional forces both in air and fluid. With the Tapping Mode technique, very soft and fragile samples can be imaged successfully.

Two different AFM apparatus are employed for the surface probe of the samples in order to check for consistency in the images produced and for better resolution using the second instrument. The first AFM instrument used for most part of the thesis is Nanoscope III (Veeco), Digital instrument, Santa Barbara, USA, model MMAFM-2. It has a liquid cell for fluid measurements where the temperature of the cell environment could be adjusted from a NanoScope Temperature Controller. The Nanoprobe SPM Tips are made from non-conductive Silicon Nitride. The cantilevers are 125 μm long. The type of tips (0.4 μm - 0.7 μm) for measurements in liquid and ambient conditions are NP-S10 and TESP respectively. The resonance frequency ranges from 302 - 396 KHz. The second instrument is Asylum Research Cypher Scanning Probe Microscope. It has a better resolution than the Nanoscope III and because of that it is possible to make zoom-in scan of size 500×500 nm^2 which is not possible with the Nanoscope III. The tips are made of silicon, having spring constant of 42 N/m and resonance frequency in the range of 294 - 346 kHz. A scan speed of 1 Hz and scan sizes of $(5 \times 5$ and $2.5 \times 2.5)$ μm^2 are made. The roughness is determined by using a 1×1 μm^2 box so as to be comparable to neutron reflectivity measurements with 1 μm neutron correlation length. The final value is an average of those calculated at different positions on each image.

3.3.4 Quartz Crystal Microbalance with Dissipation

An applied electric field across a piezoelectric material will subject the material to a mechanical strain, and vice versa: when a piezoelectric material comes under a mechanical strain, an electric field is being generated within the material. The magnitude and direction of the piezoelectric strain is directly dependent on the direction of the applied electric field relative to the crystal axis. Mostly, so-called AT-cut quartz crystal is used for QCM measurements. The crystal which is normally circular disc, has diameter of (0.5 - 1.5) cm and is (0.1 - 0.3) mm thin, with metal electrodes (mostly gold, or silicon) evaporated on the crystal, see Figure 3.5.
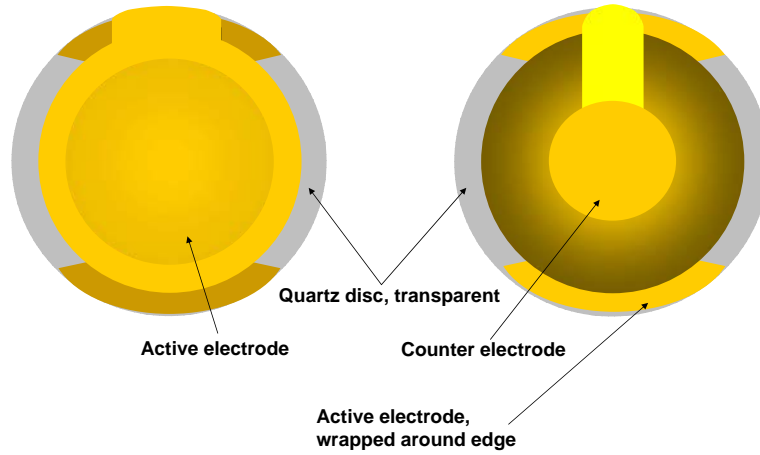
Figure 3.5: *Schematic illustration of the Quartz Crystal with gold electrodes used in the QCM measurements. Sketch is not to scale.*

The measurements are performed with QCM-D from Q-Sense, Sweden. An AT-cut crystal (Q-sense) having fundamental resonance frequency of 5 MHz is used. The crystal with gold electrodes is mounted in a fluid cell with the active electrode side (see Figure 3.5) in contact with the solution. The mass sensitivity constant, C of the crystal is 17.7 ng/cm^2 Hz. The minimum measurable frequency shift is 1 Hz in liquid medium.

The crystal oscillates when excited in the thickness shear mode at its fundamental resonance frequency, f_0 when voltage near the resonance frequency is applied across the electrodes. An adsorbed polyelectrolyte onto the electrodes induces a change in the resonance frequency Δf, which is proportional to the adsorbed mass Δm. In air or vacuum, provided the adsorbed layer is rigid, evenly distributed, and much thinner than the crystal, Δf is related to Δm and the overtone number (n = 1, 3, 5, 7...) by the Sauerbrey equation.[100]

$$\Delta m = -\frac{\rho_q l_q}{f_0} \frac{\Delta f}{n} \tag{3.31}$$

where f_0 is the fundamental frequency, ρ_q and l_q are the specific density and thickness of the quartz crystal, respectively. The dissipation D is proportional to the energy dissipated in the oscillatory system.[101] The dissipation factor is the inverse of the more familiar Q factor and is defined by

$$\Delta D = \frac{1}{Q} = \frac{E_{dissipated}}{2\pi E_{stored}} \tag{3.32}$$

where $E_{dissipated}$ is the energy dissipated during one period of oscillation and E_{stored} is the energy stored in the oscillating system.[102] The ΔD measurement is done knowing that when the driving power of a piezoelectric oscillator is switched off the voltage across the crystal decays exponentially as a damped sinusoidal.[103] Periodic switching of the driving voltage on and off, leads to a series of changes of the resonance frequency and the dissipation factor which can be obtained simultaneously. For data acquisition the software Q-Soft from Q-Sense is used and for data analysis the software Q-Tools (Q-Sense) is used.

3.3.5 Fluorescence Recovery After Photo-bleaching (FRAP)

FRAP is a technique which can be used to measure the lateral mobility of fluorescein labelled polyelectrolytes. Through this method one can determine the diffusion coefficient of the polyelectrolyte chains by measuring the rate of recovery of fluorescence which results from transport of fluorophore into a bleached spot from unirradiated parts of a sample. The procedure involves bleaching a small region of the surface of the sample containing the mobile fluorescein molecules with an intense light coming from the reflected illumination optics of a fluorescent microscope. The intense illumination causes an irreversible photochemical bleaching of the fluorophores at that spot.

The instrument used is a fluorescent microscope (Axioskope plus, CARL ZEISS) having a CCD camera (Hamamatsu) to capture the images and a camera controller (Hamamatsu) which are digitized by an image grabber of WASSABI (Hamamatsu, photonics Deutschland GmbH). The Image-J software is used to process the images.

The experiment starts by illuminating a small spot on the sample with an intensive light with the wavelength of 488 nm (FITC-PAH terminated samples) or 530 nm (RITC-PAH terminated samples) through for at least 5 minutes. At this moment the controlling aperture of the microscope is half-closed and the intensity of illumination is adjusted to 100%. In order to get sharp borders between bleached and unbleached area the objective must be well focused. Using Nicon (Nicon Fluor, 20×0.5) immersion objective, it is possible to bleach the surface of the sample under water as the objective could be immersed into the liquid. After 5 min, when the bleached spot darkens, the aperture is gently opened while the intensity is adjusted to 50% after which a snap shot of the image is taken. The sample is treated also in water to investigate the mobility of the chains in liquid. After

some time (hours or days), new snap shots of the bleached area is taken and compared with the initial image taken just after the bleaching. The images are processed with Image-J by applying the microscopic scaling to the image and to draw the image profile. The latter shows the change in the brightness measured in the so-called Grey scale (arbitrary units) by moving from unbleached area to the bleached one on the image.

There are two diffusing processes taking place: (i) movement of single dye molecules and (ii) self-diffusion of the polyelectrolyte chains. Single molecules which are not bound to the polyelectrolyte chains during the labeling process diffuse into bleached area much faster than the labelled polyelectrolyte, leading to a rapid increase in the fluorescence intensity of the dark area. The actual diffusion process is considered to be the segmental movement of polymer chains which are interdigitated and entangled in the multilayer and are rather glassy at room temperature. This is a slow process which can be promoted by some stimuli. However, the whole process may happen in the micron scale around the borders of the bleached and unbleached areas, making the sharp borderlines fuzzy (Figure 3.6).
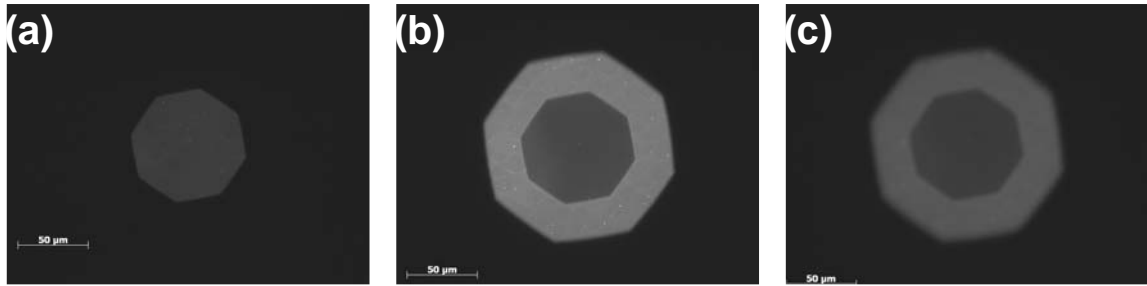
Figure 3.6: *Snap shots from the fluorescent microscope during FRAP measurement of FITC-PAH terminated polyelectrolyte multilayer. (a) Before bleaching, (b) after bleaching and (c) recovery after 3 days.*

To avoid noise and obtain good results, the raw data are fitted with a Sigmoidal (Boltzmann) function. The amount of material transport into the dark area during the measurement time is obtained from the change in slope of the resulting graphs with time. The diffusion process in an isotropic medium and can be simulated with a Gaussian-like function. To calculate the diffusion coefficient, the fitted Sigmoidal curve is differentiated into a Gaussian curve. The diffusion coefficient D_{dif} is given by

$$D_{dif} = \frac{\omega^2}{8t} \qquad (3.33)$$

where ω is the width of the Gaussian peak at half height, see Figure 3.7
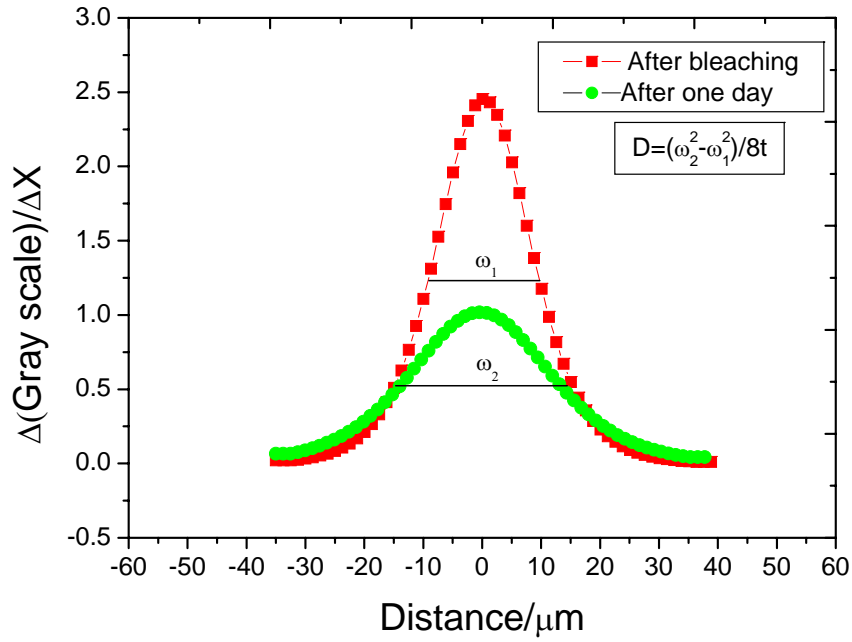
Figure 3.7: *Diffusion coefficient as determined from the deviation in peak width of Gaussian curves representing the diffusion process.*

3.3.6 Contact Angle measurements

When a drop of liquid is put on top of a solid surface, there are two competing effects. The interaction with the solid substrate makes it energetically favourable for the drop to spread such that it wets the surface. However, spreading increases the area of contact between the liquid and vapour, which also increases the surface energy between the drop and the vapour. When the interaction with the solid surface dominates, one gets complete wetting, and when the surface term dominates, one gets "partial wetting" as sketched in Figure 3.8. Contact angle measurements is the most accurate method of determining the interaction energy between a liquid (L) and a solid (S). The cosine of the macroscopic contact angle θ_e (measured through the drop), at the tangent to the drop, starting at the triple point solid-liquid-air; is a measure of the resultant of the energy of cohesion of the liquid with surface tension, γ_{LG} and the energy of adhesion between liquid and solid, expressed as ΔG_{SL}. In case of complete wetting, the interfacial tension γ_{SL} is given by the equation:

$$\gamma_{SG} = \gamma_{SL} + \gamma_{LG} \tag{3.34}$$

In case of incomplete wetting the interfacial tension is given by:

$$\gamma_{SG} - \gamma_{SL} = \gamma_{LG} cos\theta_e \tag{3.35}$$
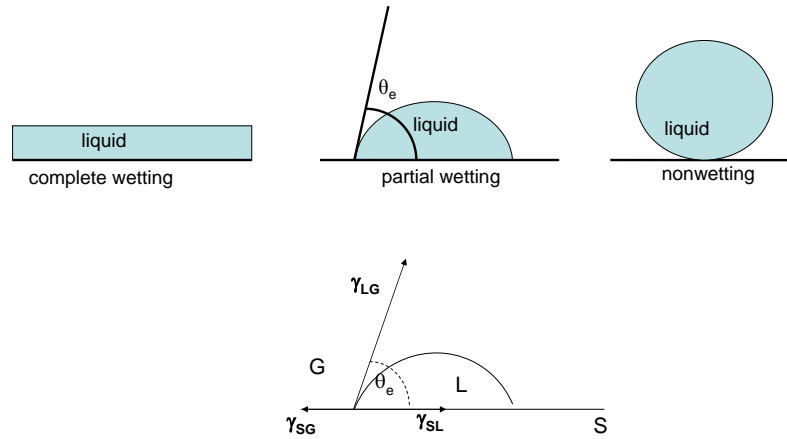
Figure 3.8: *Schmematic of wetting at hydrophilic and hydrophobic surfaces.*

The contact angle of water on polyelectrolyte multilayers is measured by the sessile drop method using an OCA 20 instrument (DataPhysics Instruments GmbH, Germany). The multilayers are freshly prepared on Si/SiO_2 substrates and placed in a cell made of transparent optical glass (Hellma, Germany) having a Teflon lid and sample support. The cell is filled with water up to two-thirds of the height of the cell just enough to saturate the cell when closed and the system is left equilibrating for 15 min; after that, a water droplet (Milli-Q water, specific resistance $\sim$19 MΩ·cm^{-1}) is placed on the multilayer through the hole of Teflon lid by using a syringe. The software SCA 20 (DataPhysics Instruments GmbH, Germany) is used in real time image mode to draw the baseline and the droplet contour by image analysis. The time-dependent measurement is run for a total time of 60 min by measuring the contact angle on the two sides of the droplet at intervals of 10 min.

Chapter 4

Effect of ionic strength and type of ions on the structure of water swollen polyelectrolyte multilayers [1]

Abstract

This Chapter addresses the effect of ionic strength and type of ion on the structure and water content of polyelectrolyte multilayers. Polyelectrolyte multilayers of poly(sodium-4 styrene sulfonate) (PSS) and poly(diallyl dimethyl ammonium chloride) (PDADMAC) prepared at different NaF, NaCl and NaBr concentrations, have been investigated by neutron reflectometry against vacuum, H_2O and D_2O. Both thickness and water content of the multilayers increase with increasing ionic strength and increasing ion size. Two types of water were identified, "void water" which fills the voids of the multilayers and does not contribute to swelling but to a change in scattering length density and "swelling water" which directly contributes to swelling of the multilayers. The amount of void water decreases with increasing salt concentration and anion radius while the amount of swelling water increases with salt concentration and anion radius. This is interpreted as a denser structure in the dry state and larger ability to swell in water (sponge-like) for multilayers prepared from high ionic strengths and/or salt solution of large anions. No exchange of hydration water or replacement of H by D is detected even after eight hours incubation time in water of opposing isotopic composition.

4.1 Introduction

Polyelectrolyte multilayers are very sensitive to the water content of the environment. This is of interest since polyelectrolyte multilayers are often used as cushions or junctions between different materials. Further, they present building blocks for novel stimuli responsive materials. Therefore, it is necessary to conduct structural investigations for clarifying the internal structure of the polyelectrolyte multilayers. Swelling behaviour of polyelectrolyte multilayers has been investigated in recent times by ellipsometry, X-ray and neutron reflectometry. Wong et al.[98] observed an "odd-even effect" which shows outer-layer dependence for poly(sodium-4 styrene sulfonate) (PSS)/poly(allylamine hydrochloride)

(PAH) multilayer in ellipsometric swelling experiments in 99% relative humidity. Ellipsometrically determined swelling percentages of PSS/PDADMAC multilayers prepared in 0.5 M NaCl show that water uptake can vary depending on whether the outermost layer is a polycation or a polyanion.[104] Steitz et al.[95] reported that PSS/PAH systems swell as much as 56% in outer layer and 42% in inner part by neutron reflectometry, where two boxes of different scattering length densities are needed to fit the reflectometry curves. PSS/PAH bilayers studied by X-ray and neutron reflectometry as a function of type of salt shows that the PSS/PAH bilayer thickness is independent of the type of salt (NaCl or KCl), yet its composition is different (more bound water for NaCl).[105] Especially in biologically relevant systems like in presence of proteins, specific ion effects[73] become important.

It is well known that the addition of salt induces changes in the water structure,[106] and it is likely to be different depending not only on the ionic strength and ion size but also on the type of ions in the salt solution. Ions have been ranked in the Hofmeister series[107] according to their ability to precipitate a given protein. Ions that have weaker interactions with water than water itself are known as structure breakers or chaotropes, whereas ions that have stronger interaction with water molecules are known as structure makers or kosmotropes. Ion specific effects are caused by short-range (direct) contact between, for example, polyelectrolyte and small ion.[73] Some experiments can be explained by the size, charge density, and related polarizability of small ions, but there are other experiments which show reverse effects of the same ion series in the presence of different macromolecules, micelles, or vesicles.

So far, a detailed study on specific anion effects on the water content and the inner structure of polyelectrolyte multilayers is missing. The problem in many studies is that the water content calculated by changes in scattering length density differs from the one calculated by the swelling ratio of multilayer thickness. Here the structural investigation of PSS/PDADMAC multilayers by neutron reflectivity is reported. In order to determine effect of type of salt and ionic strength on the water content and swelling behaviour of PSS/PDAMAC multilayers, neutron reflectometry experiments are conducted at the solid-liquid and solid-vacuum interface. The polyelectrolyte multilayers fabricated are Si/PEI/(PSS/PDADMAC100%)$_6$ at different NaF, NaCl and NaBr concentrations.

4.2 Results

4.2.1 Hydration water in dry polyelectrolyte multilayer

Figure 4.1 shows the raw neutron reflectivity data (symbols) of PSS/PDADMAC sample and the best fit (solid line). The spectra contain Kiessig oscillations but no Bragg peaks suggesting that there is no pronounced density variation within the repeat units of the multilayer.
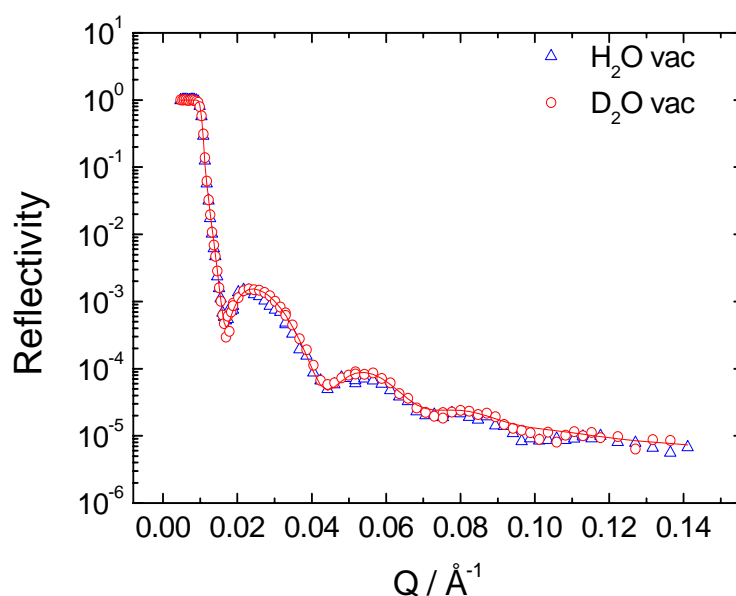
Figure 4.1: *Neutron reflectivity against vacuum of (PSS/PDADMAC)$_6$ prepared in 0.1 M NaBr aqueous solution and measured against vacuum after exposure to H_2O and D_2O, respectively. The data points are supplemented with continuous line representing the best fit model as described in the fitting procedure.*

The sample (PSS/PDADMAC)$_6$ prepared from aqueous solution of 0.1 M NaBr is measured against vacuum. The Kiessig oscillations of the multilayer against vacuum after exposure to H_2O (H_2O vac) and D_2O (D_2O vac) coincide i.e., the oscillation amplitudes and the minima positions are the same, which means equal thickness, SLD and roughness of the multilayer. The best fit of the experimental data results in a thickness of 229 ± 5 Å, SLD of $(1.04 \pm 0.02) \times 10^{-6}$ Å^{-2} and roughness of 23 ± 4 Å for both conditions. Throughout the experiment there is no difference between H_2O vac and D_2O vac which is consistent with all samples irrespective of their preparation parameters. This can be attributed to either no hydration water or strongly bound hydration water where

the displacement of H_2O by D_2O molecules is suppressed. An isotopic exchange of H by D atoms in the polyelectrolytes can be excluded since both PSS and PDADMAC do not possess any displaceable acidic protons. In case of an exchange of hydration water in the dry multilayer, it is to be expected that the SLD obtained from the measurement against vacuum after exposure to H_2O or D_2O is different. The interpretation that no hydration water is exchanged in the course of varied environmental conditions is in agreement with the report of Ivanova et al.,[108] who stated that most of the H_2O molecules found in polyelectrolyte multilayers at 0% relative humidity remain bound at 100% relative humidity D_2O.

4.2.2 Effect of ionic strength

Figure 4.2 shows three different spectra of $(PSS/PDADMAC)_6$ prepared in aqueous NaCl solutions of various ionic strength and against vacuum after exposure to H_2O. Upon adsorption of polyelectrolytes from solution of higher ionic strength the minima positions of the Kiessig fringes in the spectra shift towards low Q and the distance, ΔQ, between adjacent minima shrinks. The thicknesses derived from the fits for 0.1 M, 0.25 M and
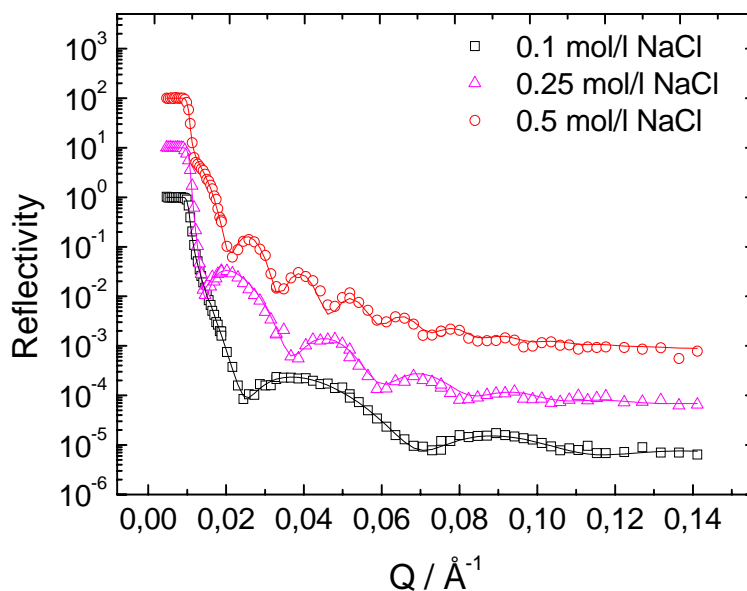
Figure 4.2: *Neutron reflectivity against vacuum after preparation (H_2O vac) showing the effect of ionic strength on multilayer thickness of $(PSS/PDADMAC)_6$ prepared from 0.1 M, 0.25 M and 0.5 M NaCl concentration. The spectra of 0.25 M and 0.5 M have been multiplied by 10 and 100, respectively, for clarity.*

0.5 M are 144 ± 1 Å, 267 ± 6 Å, and 481 ± 3 Å, respectively. The smearing out of the oscillations at high Q is due to the roughness of the samples. The roughness obtained for different ionic strengths is 10 ± 4 Å, 11 ± 4 Å, and 22 ± 5 Å in order of increasing ionic strength. Hence, both multilayer thickness and roughness increase with increasing ionic strength.[109,110] Addition of salt to the polyelectrolyte solution during multilayer preparation introduces counterions which also contribute to complex formation.[9,72,74] By adsorbing polyelectrolyte from salt solutions of varying ionic strength, the layer thickness can be controlled over a wide range. Screening of the polyelectrolyte charges in a strong electrolyte solution leads to a smaller radius of gyration. Thus, adsorption of coils will take place, which occupy a smaller surface area per chain, leading to a larger adsorbed amount of segments and consequently to a larger layer thickness.[41,53] The pronounced difference in roughness between 0.25 M and 0.5 M is attributed to strong interdigitation of more coiled chains caused by higher ionic strength. The scattering length density does not show any systematic change with increasing ionic strength.

4.2.3 Effect of type of ion

The type of salt used during the multilayer preparation can affect the growth of the multilayer strongly.[82,111] In order to investigate this effect $(PSS/PDADMAC)_6$ is prepared
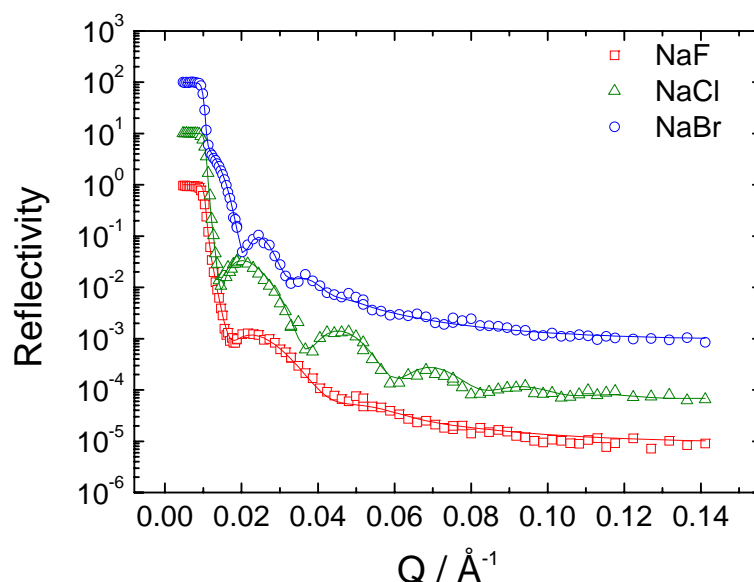
Figure 4.3: *Neutron reflectivity spectra of $(PSS/PDADMAC)_6$ containing 0.25 M concentration of NaF, NaCl and NaBr against H_2O vacuum.*

from NaF, NaCl and NaBr solutions at a fixed ionic strength of 0.25 M. Different anions are chosen since anions are known to have a significantly larger effect on the thickness of the multilayers than their cation counterparts.[73] Ion-specific effects become more important for cations above an ionic strength of 0.25 M at which stage the influence is not negligible anymore. The result of the neutron reflectivity measurements are shown in Figure 4.3. At first sight, the distance, ΔQ, between adjacent minima shrinks as the size of the anion of the respective salt increases. The position of the first minimum shifts towards low Q values. From the fits the thickness obtained is 218 ± 3 Å, 267 ± 6 Å and 498 ± 4 Å for NaF, NaCl and NaBr, respectively. This shows an increase in the thickness of the multilayer as the size of the anion gets larger. The roughness obtained is 25 ± 5 Å, 11 ± 4 Å and 50 ± 8 Å for NaF, NaCl and NaBr, respectively. The roughness is expected to show a pattern similar to that of thickness, however, NaF is seen to produce exceptionally rougher multilayers. That explains why there is only one Kiessig oscillation and strong damping of R at high Q values. The effect of the anion on thickness and of the polyelectrolyte multilayers is due to its respective position in the Hofmeister Series[107] and coincides with results of other studies on polyelectrolyte multilayers.[9,38,39,73]

4.2.4 Quantitative analysis of water content

A complete set of measurements as shown in Figure 4.4, i.e., H_2O vac, H_2O liq, D_2O liq and D_2O vac, is performed for all $(PSS/PDADMAC)_6$ multilayers which are prepared with different concentrations of NaF, NaCl and NaBr. In the following the quantitative analysis of the water content is described. The percentage of swelling in water is determined by:

$$\phi_{swell} = \frac{d_{swollen} - d_{dry}}{d_{swollen}} \times 100 \tag{4.1}$$

where ϕ_{swell} is the percentage of swelling, $d_{swollen}$ is the thickness in the water swollen state and d_{dry} is the thickness of the multilayer against vacuum. For example, the percentage of swelling in water of $(PSS/PDADMAC)_6$ prepared from aqueous solution of 0.1 M, 0.25 M and 0.5 M NaCl are 36%, 43% and 55%, respectively (see Figure 4.5a). In many former studies the percentage of swelling is equated with the amount of water within the polyelectrolyte multilayer. However, it differs from the amount of water calculated by the concurrent change in scattering length density of the multilayers. This leads to the conclusion that some hidden water exists which does not contribute to swelling in water but to the change in scattering length density only.

"Swelling" and "void water": Polyelectrolyte multilayers are deposited as layers that
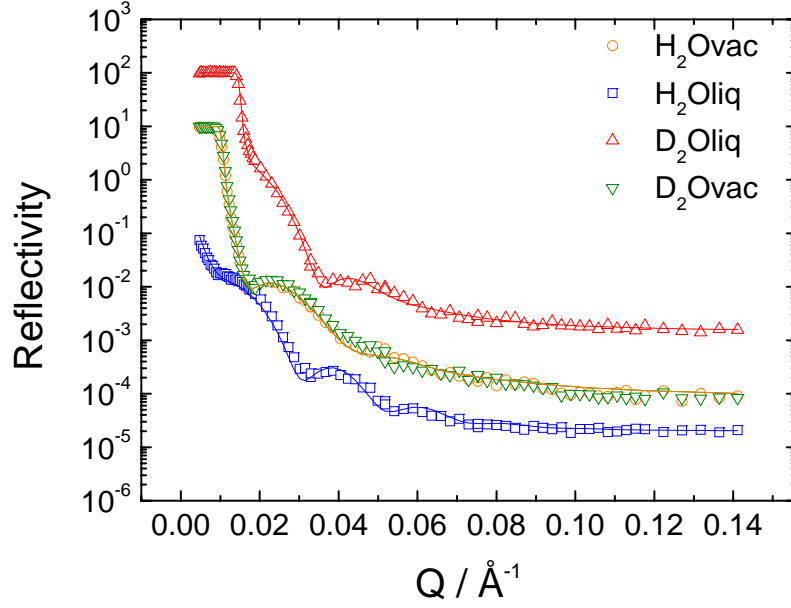
Figure 4.4: *Neutron reflectivity spectra on $(PSS/PDADMAC)_6$ multilayers prepared from 0.25 M NaF, showing the order of measurements. The reflectivities of the curves H_2O vac, D_2O vac and D_2O liq have been multiplied by 10, 10 and 100, respectively.*

form continuous molecular layers without distinct layer-by-layer separation between polyelectrolytes of opposite charges,[20,47,48] which in turn creates voids in the multilayer. In vacuum those voids within the multilayer are empty and the multilayer thickness is termed d_{dry}. Upon swelling the voids are filled with water called "void water". That water does not contribute to the swelling of the multilayers but exclusively to the change in scattering length density. Subsequent water absorbed by the multilayer, called "swelling water" on the opposite directly contributes to the swelling of the multilayer. The amount of "void water" ϕ_{void}, is retrieved from comparison of the amount of "swelling water", ϕ_{swell}, calculated from equation (1), with the total water content, ϕ_{total}, calculated from the respective changes in scattering length density and appropriate boundary conditions (see equation 4.6): At 0% relative humidity (r.h.), the SLD of the dry multilayer is given by

$$Nb_{dry} = x{\cdot}Nb_{polymer} + (1-x){\cdot}Nb_{voids}. \tag{4.2}$$

with $Nb_{voids}{=}0$, empty voids against vacuum, the SLD of the dry multilayer becomes proportional to the SLD of pure polymer, $Nb_{polymer}$. Equation 4.2 then becomes

$$Nb_{dry} = x{\cdot}Nb_{polymer}. \tag{4.3}$$

Concentration of salt	d(H_2O) d_{dry} (Å)	d(H_2O) $d_{swollen}$ (Å)	d(D_2O) $d_{swollen}$ (Å)	σ(H_2O) σ_{dry} (Å)	σ(H_2O) $\sigma_{swollen}$ (Å)	SLD(H_2O) ρ_{dry} (10^{-6} Å^{-2})	SLD(H_2O) $\rho_{swollen}$ (10^{-6} Å^{-2})	SLD(D_2O) $\rho_{swollen}$ (10^{-6} Å^{-2})
0.25 M NaF	218 ± 3	295 ± 5	295 ± 6	25 ± 5	40 ± 6	0.95 ± 0.02	0.53 ± 0.03	3.48 ± 0.3
0.5 M NaF	300 ± 5	486 ± 8	495 ± 10	34 ± 6	55 ± 5	1.20 ± 0.03	0.45 ± 0.02	4.04 ± 0.2
0.1 M NaCl	144 ± 1	226 ± 3	226 ± 2	10 ± 4	27 ± 4	1.33 ± 0.02	0.58 ± 0.01	3.47 ± 0.1
0.25 M NaCl	267 ± 6	465 ± 9	480 ± 15	11 ± 4	35 ± 13	1.34 ± 0.03	0.49 ± 0.02	4.00 ± 0.2
0.5 M NaCl	481 ± 3	1041 ± 18	1110 ± 30	22 ± 5	48 ± 19	0.74 ± 0.04	0.02 ± 0.07	4.11 ± 0.1
0.1 M NaBr	229 ± 5	395 ± 6	381 ± 9	23 ± 4	36 ± 9	1.04 ± 0.02	0.34 ± 0.05	3.45 ± 0.2
0.25 M NaBr	498 ± 4	1282 ± 20	1200 ± 40	50 ± 8	123 ± 9	1.05 ± 0.02	0.05 ± 0.01	4.36 ± 0.1

Table 4.1: *Structure parameters of (PSS/PDADMAC)$_6$ multilayer prepared from aqueous polyelectrolyte solution containing NaF, NaCl and NaBr, respectively. Data set H_2O vac and D_2O vac are the same. Error bars are set in accordance to a level of 10% increase in chi^2.*

At 100% r.h. (fully swollen), the SLD of the swollen multilayer is given by

$$Nb_{swollen} = (1 - \phi_{swell})[x \cdot Nb_{polymer} + (1 - x) \cdot Nb_{water}] + \phi_{swell} Nb_{water} \qquad (4.4)$$

where x, the volume fraction of polymer, is given by

$$x = \frac{Nb_{dry}}{Nb_{water}} - \frac{Nb_{swollen} - \phi_{swell} Nb_{water}}{(1 - \phi_{swell}) Nb_{water}} + 1 \qquad (4.5)$$

$$\phi_{total} = (1 - x)(1 - \phi_{swell}) + \phi_{swell} = \phi_{void} + \phi_{swell} \qquad (4.6)$$

Nb_{dry} is the SLD of dry multilayer, $Nb_{swollen}$ is the SLD of the swollen multilayer and Nb_{water} is the SLD of the water, D_2O or H_2O. Hence, the total water content ϕ_{total} of a swollen multilayer is the sum of the "void water" ϕ_{void} and "swelling water" ϕ_{swell}. The summary of the results for the amount of "void water" ϕ_{void}, "swelling water" ϕ_{swell} and

total water ϕ_{total} is represented in Figure 4.5. There is no significant difference in the water content for H_2O and D_2O in the multilayer. Therefore, the values presented in Figure 4.5 are the average water content in the multilayers. It is concluded that there is no isotopic effect in the thickness of the swollen multilayers as well as in the water content as can be seen from Table 1 and the supporting information, respectively.
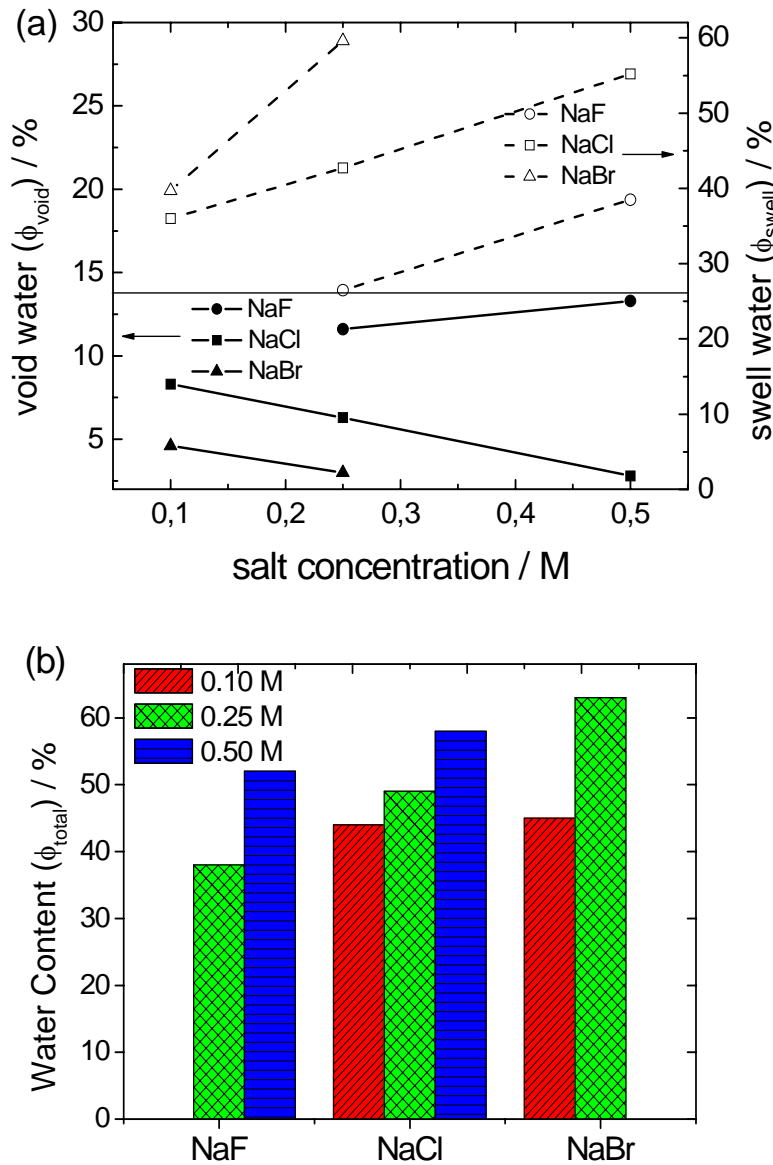
Figure 4.5: *(a) Amount of void water and swelling water in dependence of the salt concentration and type of ion of the preparation solutions. (b) Total amount of water in dependence of the salt concentration and type of ion of the preparation solutions.*

For each type of salt 3 different concentrations are used, i.e., 0.1 M, 0.25 M and 0.5 M. The results for 0.1 M NaF could not be provided because the multilayer is too thin to produce any oscillations and for 0.5 M NaBr the multilayer is unstable. With increasing ionic

strength and increasing ion size the amount of total water and swelling water increases. The amount of void water shows an opposite effect: It decreases with increasing ionic strength (exception for NaF). This means that the two water species (swelling and void water) partially compensate each other. In case of 0.1 M the ion type has no effect on the total amount of water but on the amount of void and swelling water. Obviously, the increasing ion size has qualitatively the same effect as increasing the ionic strength.

4.3 Discussion

The main findings can be summarized as follows: (i) There is no displacement of hydration water in the dry polyelectrolyte multilayers and there is no replacement of H by D. (ii) The thickness of the polyelectrolyte multilayers increases with increasing ionic strength of the polyelectrolyte solution. (iii) The thickness of the multilayers increases in accordance with the arrangement of the anions in the Hofmeister series. (iv) The total water content of the polyelectrolyte multilayers increases with increasing ionic strength and also type of ion. In order to qualitatively explain these findings, the hydrophobic effect will be discussed and the Hofmeister effect on polyelectrolyte multilayers.

4.3.1 Hydration water in polyelectrolyte multilayers

The generally accepted model of hydration[112] invokes a cage of water molecules around a nonpolar solute molecule or molecular part, i.e polymer backbone. Hydrogen bonds are preserved by partial ordering of water (a decrease in entropy), and contact with the solute can generate favorable, though small, enthalpies of dissolution. Hydrophobic interactions are generated when multiple nonpolar solutes, or fragments of molecules, associate to maximize contact of water with water, maintaining structure and hydrogen bonds. Polyelectrolyte multilayers prepared by alternating adsorption of polyanions and polycations from aqueous solution are assumed to contain hydration water in their dry state. Evidence is reported by Schwarz and Schönhoff[113] who applied ^{1}H NMR transverse relaxation to monitor the hydration water in polyelectrolyte multilayers. Schlenoff et al.[114] also reported hydration contributions to association in polyelectrolyte multilayers. The analysis based on neutron reflectivity indicates no structural change in the dry polyelectrolyte multilayers, prepared from light water H_2O, dried and subsequently exposed to heavy water D_2O for 8 hours and then dried. This result is proven at different salt concentrations of NaF, NaCl and NaBr. For all samples the reflectivity spectra of H_2O vac and D_2O vac are identical producing the same multilayer thickness, same scattering length density and

multilayer roughness. If hydration water exists in vacuum, then it is included in x, the volume fraction of polymer as fixed, not displaced (as integral part that cannot be resolved by the applied technique). The explanation for this phenomenon would be the presence of strongly bound hydration water surrounding the molecules of the polyelectrolytes making it impossible for the H in the hydrogen bonds to be displaced by D, which is not fully understood so far. Similar effects are reported by Ivanova et al,[108] who observed about 6 immobile protons at 0% r.h. in a PSS/PAH multilayer system. It could be imagined that by supplying the system with energy in the form of heat, more first-shell water conformations would be made accessible. Melting the cages of water molecules would then allow a closer approach of the polymer groups. The observed variations in SLD of the films in dry state are caused by two effects: (i) Variations in polymer volume fraction, x, and (ii) amount of bound water included in x. While with the present technique it is possible to resolve x, it is not possible to resolve the amount of bound hydration water associated to the polyelectrolyte with certainty.

However, the number of water molecules n_{H_2O}, dry for a pair of monomers PSS/PDAD-MAC can be calculated from the measured SLD. By definition, $SLD = \sum_i n_i b_i / \sum_i n_i V_i$, which is the ratio of the sum of the scattering lengths b_i and the volumes V_i of the atoms and molecular groups of the system. Hence the amount of H_2O molecules per PSS/P-DADMAC can be calculated as follows:

$$SLD = \frac{b_{PSS} + b_{PDADMAC} + n_{H_2O}b_{H_2O}}{V_{PSS} + V_{PDADMAC} + n_{H_2O}V_{H_2O}} \tag{4.7}$$

then

$$n_{H_2O} = \frac{b_{PSS} + b_{PDADMAC} - SLD(V_{PSS} + V_{PDADMAC})}{SLD{\cdot}V_{H_2O} - b_{H_2O}} \tag{4.8}$$

(The numerical values are[40,108,115] $b_{PSS} = 47.203 \times 10^{-5}$ Å, $b_{PDADMAC} = 3.587 \times 10^{-5}$ Å, $b_{H_2O} = -1.675 \times 10^{-5}$ Å, $V_{PSS} = 201$ Å³, $V_{PDADMACS} = 156$ Å³, $V_{H_2O} = 30$ Å³, SLD from Table 4.1.)

With these formulas the number of water molecules at 0% r.h. are calculated. For example, the number of hydration water molecules for PSS/PDADMAC pair of monomers having 0.1 M NaBr, with SLD $= 1.04 \times 10^{-6}$ Å^{-2}, is calculated to be $n_{H_2O} = 2.85$. Table 4.2 show the calculated amount of hydration water "void water", "swelling water" and total water content for H_2O. The upper limit for the SLD of the polymer complex itself without hydration water is 1.43×10^{-6} Å^{-2}. This number is based on published data on the molecular volumes of PSS and PDADMAC of 201 Å³[40] and 156 Å³[115] respectively, the latter based on the measured mass density of PDADMAC of 1.19 g/cm³. From measured

SLD values against vacuum, it is concluded that beside the polymer volume fraction also the amount of bound water varies as a function of preparation conditions.

Conc./ type of salt	No. of water mol. n_{H_2Odry}	void water $\phi_{void}(\%)$	swell water $\phi_{swell}(\%)$	total water $\phi_{total}(\%)$	fraction of polymer x(%)
0.25 M NaF	3.7	10.6	26.0	36.6	85.0
0.50 M NaF	1.5	13.2	38.3	51.5	78.4
0.10 M NaCl	0.6	9.1	36.2	45.3	82.7
0.25 M NaCl	0.5	7.2	42.6	49.8	88.6
0.50 M NaCl	6.3	2.7	53.8	56.5	94.1
0.10 M NaBr	2.9	4.2	42.1	46.3	92.7
0.25 M NaBr	2.8	2.8	61.2	64.0	92.8

Table 4.2: *Parameters of PSS/PDADMAC pair of monomers prepared from solutions of different type of ion and ionic strength. x is the volume fraction of polymer and n_{H_2Odry} is the number of water molecules bound to the pair of monomers.*

4.3.2 Effect of ionic strength and type of ion

The properties of the polyelectrolytes constituting the multilayer determine its structure and the charge compensation mechanism. The presence of salt in the solution can create electrostatic screening of the charge on the polyelectrolyte layer and also influence both the dynamics of polyanion/polycation complexes holding the layers together as well as the forces operating in the system.[116–118] Polyelectrolyte multilayers prepared from NaBr salt are thicker than those prepared from NaF due to the ion-specific effects of the anions and their position in the Hofmeister Series.[9,38,39,73,107] Br^- has larger size, higher polarizability, and small hydration shell than F^-, and this makes the Br^- interact stronger with the PDADMAC chains thereby forming coils which leads to thicker films. The Hofmeister Series usually presents an inversion point[73,107] at about Cl^- (for anions) and Na^+ (for cations). Hence, the position of these two ions is usually considered as a null point in the ion-specific effects. This explains why the NaCl multilayer has the smallest roughness in Figure Figure 4.3 and Table 4.1. In contrast to the thickness the roughness does not follow systematically the Hofmeister series. The increasing coiling of the chains leading to an increasing film thickness has two counteracting effects on the roughness. A slight increasing flexibility of the PDADMAC chains due to a stronger interaction with anions from F^- to Cl^- leads to a stronger ability for rearrangement and therefore to a smoother interface. A further increasing coiling (from Cl^- to Br^-) leads to rougher surfaces.[9,73,119]

The thickness of the multilayers prepared using different sodium salts (NaF, NaCl, NaBr) at an ionic strength of 0.25 M increased in the order of $F^-<Cl^-<Br^-$.[39,120] The roughness increases in the same order with increasing ionic strength due to an increase in coiling. The scattering length density of the dry multilayer varies from $(0.95 \pm 0.02) \times 10^{-6}$ Å^{-2} in the case of NaF to $(1.34 \pm 0.02) \times 10^{-6}$ Å^{-2} in the case of NaCl, with NaBr having $(1.05 \pm 0.02) \times 10^{-6}$ Å^{-2}. An opposite effect between roughness and SLD is observed among the multilayers of NaF, NaCl and NaBr. Whereas the multilayer of 0.25 M NaCl shows lowest roughness, it also has the highest SLD among the multilayers of the sodium salts.

At ionic strengths up to 0.1 M the counterions involved in extrinsic complex formation with the polyions are few. This increases electrostatic attraction between oppositely charged layers and causes the polyelectrolyte chains to conform flat to the substrate. In this case the layers are tightly bound to each other resulting in low multilayer thickness, roughness and voids. This accounts for the fact that multilayers prepared from 0.1M NaCl and 0.1M NaBr have the same total water content of 44% and 45%, respectively. Therefore at low ionic strength the electrostatic interactions are dominating and specific ion effects are minor as shown in the present study. Above an ionic strength of 0.1 M salt specific ion effects come into play. This observation supports findings of former studies.[73] It has been shown that at high ionic strength (above 0.1 M), where the electrostatic interactions are partially screened, the interion interactions are controlled by dispersion forces that depend on the polarizability of the ionic species.[121]

4.3.3 Swelling behavior and water content of polyelectrolyte multilayers

The results show that the amount of void water and swelling water show opposite dependencies on the ionic strength and the ion size leading to a partial compensation with respect to the total amount of water within the polyelectrolyte multilayers. Starting with the swelling water, the polyelectrolyte multilayer can be considered as a sponge. Due to stronger interaction of the PDADMAC with Br^- more loops are formed, which are less fixed by oppositely charged polyelectrolytes than in presence of F^- during preparation. These loops will be folded during drying and have a strong ability for unfolding, i.e. reswelling, in presence of water. The same effect occurs at high ionic strength.

In contrast, the amount of void water, which does not contribute to the swelling, rather probes the structure of the dry state. Less void water means a denser structure in the dry state. A higher flexibility of the chains leads to an easier reorganization of the chains and therefore a denser packing. A higher flexibility is reached by intrachain screening caused

by a high ionic strength and/or large counter ions. With increasing salt concentration and increasing size of ion, the total amount of water increases which indicates a decrease of polyelectrolyte density in the swollen state. This contradicts a former experiment on rhodamine transport through polyelectrolyte multilayers. An explanation might be that rhodamine also probes defects in the film.[43]

4.4 Conclusions

In this study, the influence of ionic strength and type of ion (during preparation) on the water content of polyelectrolyte multilayers has been investigated by neutron reflectivity. It is found that there is no exchange of hydration water or replacement of H by D when dry polyelectrolyte multilayers prepared from H_2O, are incubated in D_2O liquid for at least eight hours.

The polyelectrolyte multilayer acts like a sponge. The total amount of water of the polyelectrolyte multilayer is the sum of the "void water" which fills the empty space (excluded volume) between the polyelectrolyte chains and does not contribute to the swelling but to the change in scattering length density and the "swelling water" which contributes directly to swelling. "Swelling water" and total water content of the multilayer increase with increasing ionic strength and increasing size of the anions. With increasing ionic strength of the polyelectrolytes solutions the amount of counterions in the aqueous medium contributing to extrinsic polyelectrolyte complex also increases, resulting in screening of electrostatic attraction between oppositely charged polyelectrolyte segments. Increasing screening effect causes the polyelectrolyte chains to change from flat conformation to coil conformation thereby increasing the total thickness of the multilayer and the roughness.

In contrast, the amount of void water shows the opposite effect. It decreases with increasing ionic strength and anion size reflecting a denser structure in the dry state at high ionic strength and for large anions.

In the experiments shown increasing anion size acts like increasing the salt concentration. The specific ion effects become pronounced at an ionic strength larger than 0.1 M, where the electrostatics are mainly screened and dispersion forces between the ions and polyions become dominant.

Chapter 4 Effect of ionic strength and type of ions on the structure of water
swollen polyelectrolyte multilayers

49

Chapter 5

Effect of ionic strength and layer number on swelling of polyelectrolyte multilayers in water vapour [1]

Abstract

The swelling behavior of polyelectrolyte multilayers (PEMs) of poly(sodium - 4 styrene sulfonate) (PSS) and poly(diallyl dimethyl ammonium chloride) (PDADMAC) prepared from aqueous solution of 0.1 M and 0.5 M NaCl are investigated by ellipsometry and Atomic Force Microscopy (AFM). The study shows that from 1 double-layer up to 4 double-layers from 0.1 M NaCl, the amount of swelling water in the PEMs decreases with increasing number of adsorbed double layers. This is explained by an increase in polyelectrolyte density as a result of the attraction between the positively charged outermost PDADMAC layer and the Si substrate. From 6 double layers to 30 double layers, the attraction is reduced due to a much larger distance between substrate and outermost layer leading to a much lower polyelectrolyte density and a higher amount of swelling water. In PEMs prepared from aqueous solution of 0.5 M NaCl the amount of water constantly increases which is related to a monotonically decreasing polyelectrolyte density with increasing number of polyelectrolyte layers. Studies of the surface topology also indicate a transition from a more substrate affected *interphase* behavior to *continuum* properties of the polyelectrolyte multilayers. It is shown that the threshold for the transition from *interphase* to *continuum* behavior depends on the physical quantity that is investigated.

5.1 Introduction

Polyelectrolyte multilayers are known to be sensitive to external parameters such as salt concentration,[41,42] type of salt,[36–39] pH[117,122] and temperature.[123] The neutron reflectivity study described in 4 showed that increasing ionic strength and preparation with anions of increasing size lead to increasing thickness and swelling water of the multilayers.[75] There are some papers[40,77,95,124–128] on hydration and swelling behavior of polyelectrolyte multilayers. The typical amount of water uptake in high humidity environment or water varies between 39 vol % for PSS/PAH system[40,95] and 300 vol % in the case

---

[1]Similar content is included in: *Effect of ionic strength and layer number on swelling of polyelectrolyte multilayers in water vapour*, S. Dodoo, B. Balzer, T. Hugel, A. Laschewsky, and R. v. Klitzing, *Soft Material*, Accepted

of poly(acrylamide)/poly(diallyl dimethyl ammonium chloride) PAA/PDADMAC system.[117]

There are only a few studies addressing the effect of the substrate on the swelling water. Wong et al.[98] reported that swelling and deswelling of poly(sodium-4 styrene sulfonate) (PSS) and poly(allylamine hydrochloride) (PAH) multilayer are completely reversible and that at 99% relative humidity (r.h.), a pronounced "odd-even effect" in the swollen thickness (about 20% with respect to total thickness) is observed depending on the type of polyelectrolyte in the outermost layer. The swelling water decreases from about 50% to 25%, indicating an increase in polyelectrolyte density with increasing number of deposited layers. This study stops at 6 double layers and the ionic strength is fixed at 0.25 M. So far, it is unclear whether a PEM of 6 double layers presents already the *continuum* phase or still the *interphase* between substrate and *continuum* phase with respect to the amount of water. In addition the effect of the ionic strength has not been clarified.

In order to address these questions a multilayer system of PSS/PDADMAC (1, 2, 4, 6, 8, 14, 20 and 30 double layers) prepared from aqueous solution of 0.1 M and 0.5 M NaCl is studied under different relative humidities. For the reliability of the results two different methods for the determination of the swelling water are applied. Ellipsometric measurements are performed in a home-made humidity cell Figure 3.4 equipped with humidity and temperature sensors. Measurements at relative humidities between 1% and 98% are performed. For 100% r.h. the samples are immersed in liquid water.

5.2 Results

5.2.1 Surface roughness against ambient conditions

For studying the changes in morphology upon adsorption of polyelectrolyte layers onto Si/PEI, AFM images of PSS/PDADMAC PEMs are taken after different numbers of adsorption steps. Figure 5.1 (left) shows that a bare Si substrate is with a roughness of 0.09 nm. The adsorption of PEI onto Si substrate leads to a homogeneous layer with a low roughness of σ=0.12 nm (Figure 5.1 right).

Due to strong electrostatic attraction between the substrate and the PEI layer the chains have a flat conformation on the substrate. PEMs prepared from 0.1 M NaCl show a grain-like topography, and the roughness increases with increasing number of adsorbed layers (Figure 5.2, 0.1 M). PEMs prepared from aqueous solution of 0.5 M NaCl exhibit as well an increasing roughness with increasing number of adsorbed layers to a larger
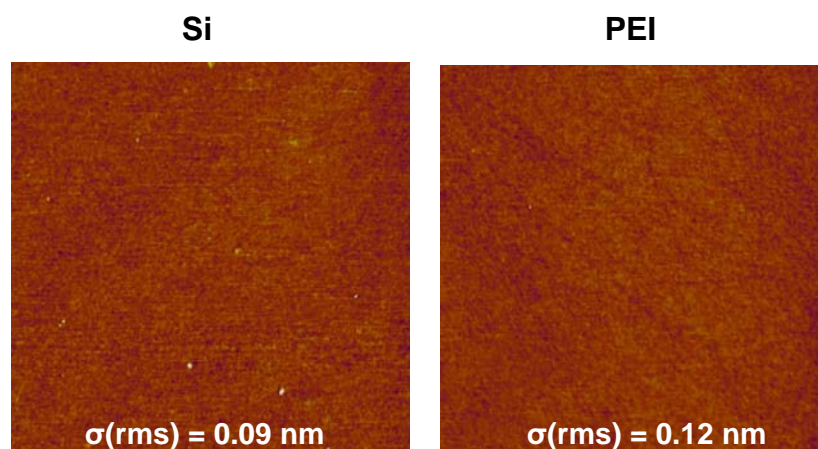
Figure 5.1: *AFM image of Si (left image) and Si coated with PEI prepared without addition of salt. Scan size: 2×2 μm^2.*

extent than PEMs prepared at an ionic strength of 0.1 M. The topography shows a development from grain-like via rod–like to blob or worm–like structures (Figure 5.2, 0.5 M). For multilayers prepared from 0.1 M NaCl, blobs are observed for a multilayer of 30 double layers. However, for an ionic strength of 0.5 M NaCl the blob formation is already observed from 14 double layers on. The roughness values determined over an area of 1 $\times$ 1 μm^2 are in good agreement with the ones of neutron reflectivity:[75] For instant the roughness of $(PSS/PDADMAC)_6$ are (10 ± 4)Å and (22 ± 5)Å for 0.1 M and 0.5 M NaCl, respectively.

It is important to point out that the ionic strength[82,111] of the multilayer affects the topography and the roughness in a pronounced way. For the same number of layers, PEMs prepared from 0.5 M NaCl solution show larger roughness than PEMs prepared from 0.1 M NaCl.

5.2.2 Swelling behavior

The correlation between the swelling behaviour at different relative humidities and the thickness of the multilayers is studied. Figure 5.3 shows ellipsometry results of thickness as a function of the relative humidity for PSS/PDADMAC multilayers prepared at an
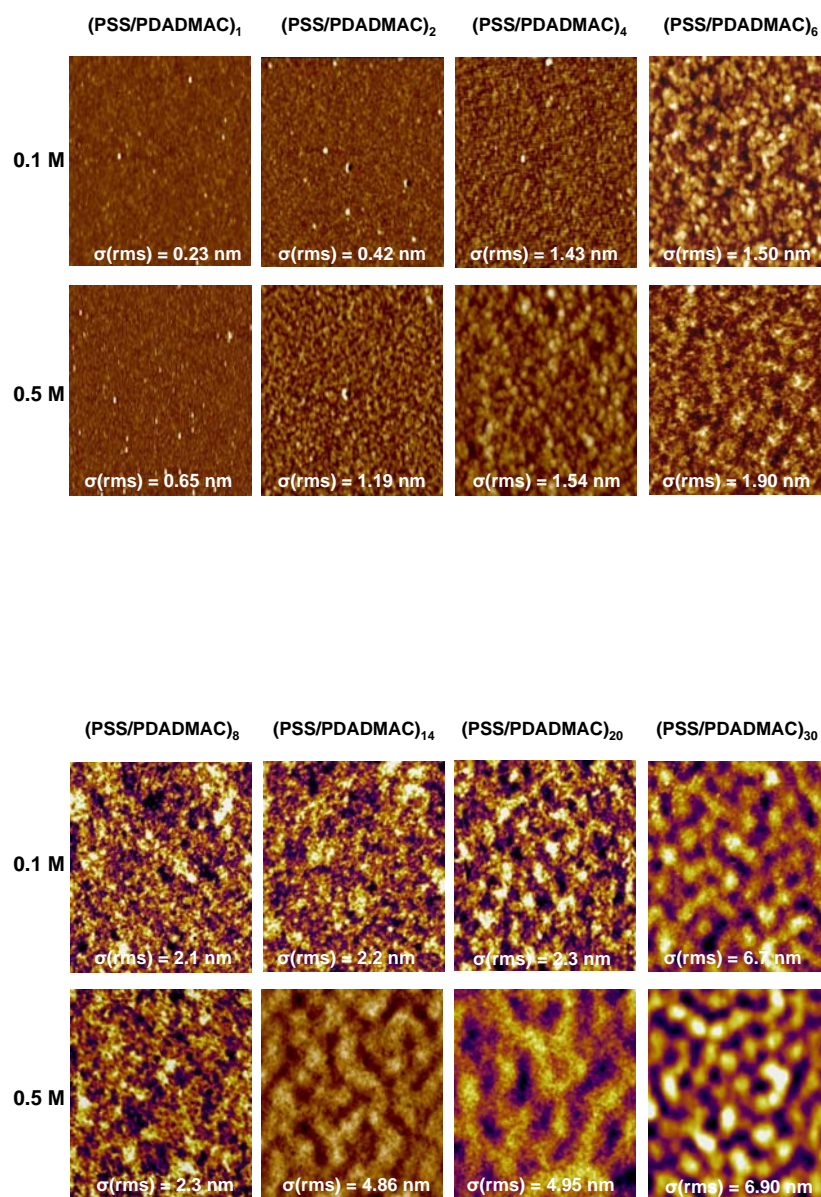
Figure 5.2: *AFM images in ambient conditions of PSS/PDADMAC multilayers prepared from aqueous solution of 0.1 M NaCl and 0.5 M NaCl. Top: multilayers having 1 to 6 double layers and Bottom: multilayers have 8 to 30 double layers. The images have scan size of $2.5 \times 2.5 \ \mu m^2$.*

ionic strength of 0.1 M and 0.5 M, respectively. The measured thicknesses are consistent within the experimental error with AFM measurements of similar films by Bizan Balzer.[129] The thickness increases with increasing r.h. and increasing ionic strength. Figure 5.4
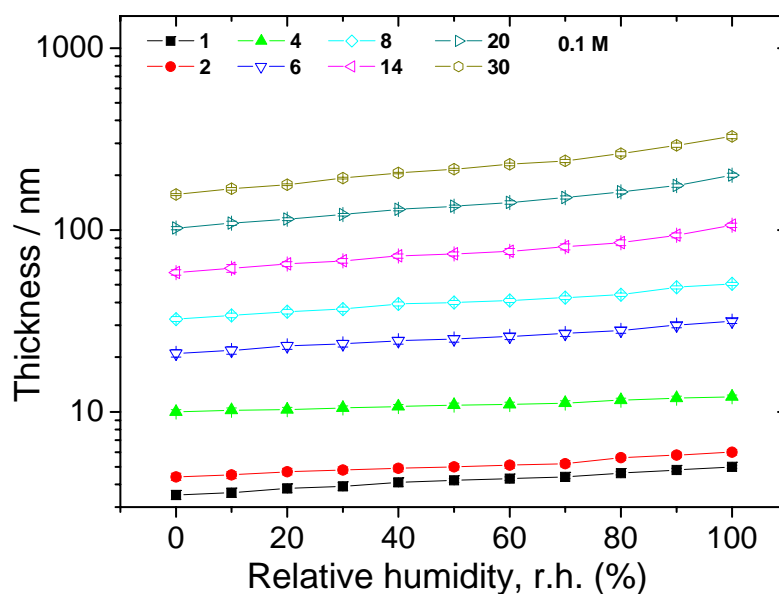
(a)
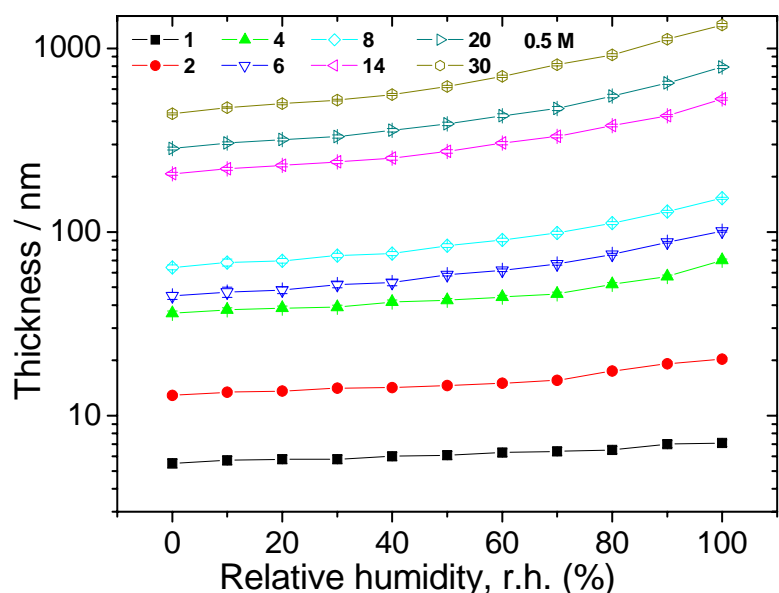
(b)

Figure 5.3: *Thickness against relative humidity of PSS/PDADMAC polyelectrolyte multilayers on Si/PEI prepared from aqueous solutions of 0.1 M NaCl (a) and 0.5 M NaCl (b). The data points at 100% r.h. are obtained from measurements against liquid water. The numbers in the legend correspond to number of PSS/PDADMAC double layers.*

demonstrates how the amount of swelling water varies with relative humidity. The swelling water is calculated using equation (1) for both ellipsometry and AFM data recorded under

(a)

(b)
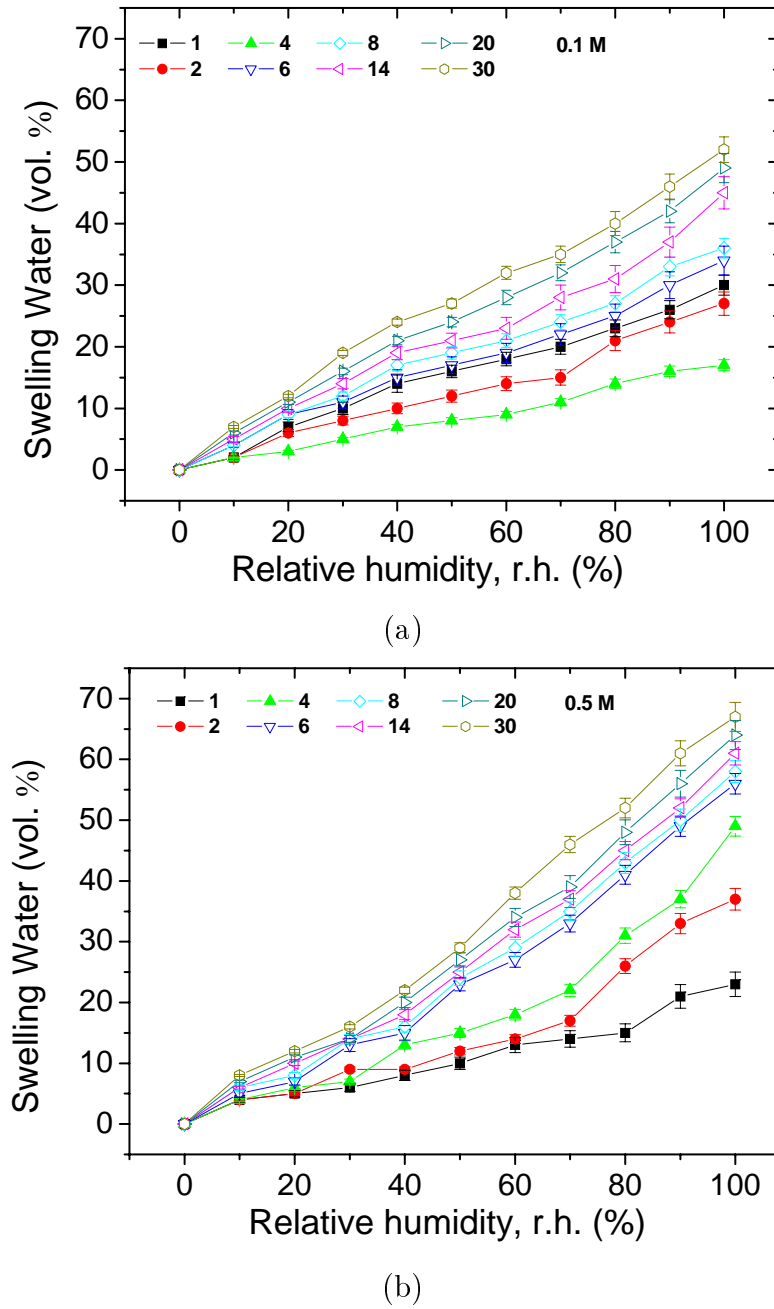
Figure 5.4: *Amount of swelling water as a function of relative humidity for PSS/PDAD-MAC multilayers on Si/PEI prepared from aqueous solutions of 0.1 M NaCl (a), and 0.5 M NaCl (b). The numbers in the legend correspond to the number of PSS/PDADMAC double layers.*

controlled relative humidity:

$$\phi_{swell}(r.h.) = \frac{d_{swollen}(r.h.) - d_{dry}}{d_{swollen}(r.h)} \times 100 \qquad (5.1)$$

where ϕ_{swell} corresponds to the swelling water, $d_{swollen}$ is the thickness of the swollen PEM at r.h.> 1% or against liquid water (100 % r.h.) and d_{dry} is the thickness of the dry multilayer at 1% r.h.. Firstly, all the plots in Figure 5.3 and Figure 5.4 indicate an increase in both thickness and swelling water as the relative humidity in the sample cell increases. Interestingly, in case of the thinner PEMs (1–4) the multilayers swell differently for 0.1 M and 0.5 M. For 0.1 M the swelling water increases in the order of (PSS/PDADMAC)$_4$ < (PSS/PDADMAC)$_2$ < (PSS/PDADMAC) (see Figure 5.4a. This means that the 1, 2, and 4 double layers prepared from 0.1 M NaCl exhibit swelling water decreasing with increasing number of layers. This observation is consistent with the work of Wong et al.[98] who reported a decreasing swelling water with increasing number of layers for PSS/PAH up to 6 double layers prepared from 0.25 M NaCl even though the polycation and the ionic strength is different from this work. From 6 to 30 double layers of 0.1 M NaCl, the swelling water increases again.

In contrast to this, for an ionic strength of 0.5 M , the swelling water shows a monotonous increase with increasing number of PSS/PDAMADC double layers (Figure 5.4b). For both 0.1 M and 0.5 M, the refractive index of the PEM decreases with increasing relative humidity but there is no systematic change between the PEMs of different number of layers.

5.3 Discussion and Conclusion

PSS/PDADMAC multilayers with different numbers of double layers (1, 2, 4, 6, 8, 14, 20 and 30) are prepared from two different ionic strengths (0.1 and 0.5) and are characterized by ellipsometry at different relative humidities. An influence of the substrate on the few adsorbed double layers is observed.

Ladam et al[80] reported a three zone model (precursor zone, core zone and outer zone) for PSS/PAH polyelectrolyte multilayer system. Both, with respect to the swelling behavior and the topography the transition from substrate dominated *interphase* structure to the *continuum* structure differs for 0.1 M NaCl and 0.5 M NaCl as shown in Figure 5.5, swelling water against number of double layers. The observations are discussed in the following:

Multilayers prepared from 0.1 M NaCl solution. The increasing roughness with increasing number of adsorbed layers is consistent with the literature[34,130] and is due to increasing coiling, interdigitation of oppositely charged chains and increasing chain mobility.[74] The chain conformation is rather flat and more stretched creating more contact
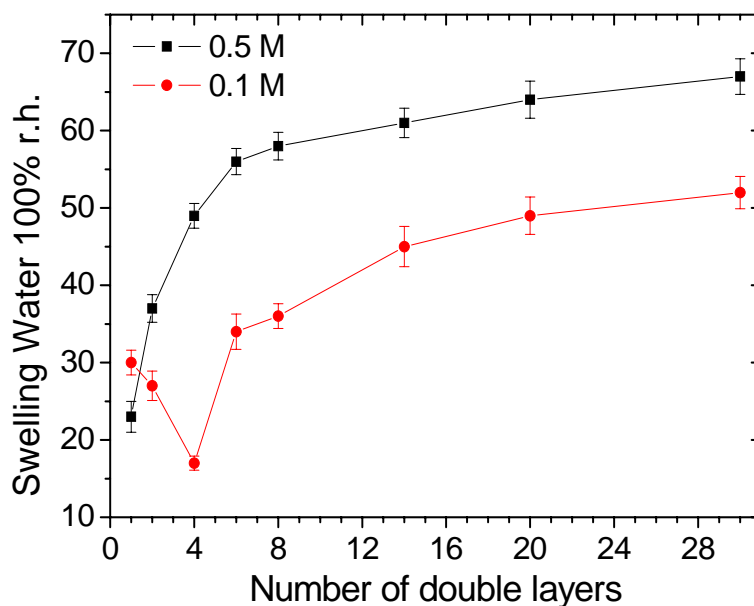
Figure 5.5: *PSS/PDADMAC multilayers on Si/PEI prepared from aqueous solutions of 0.1 M NaCl and 0.5 M NaCl. Amount of swelling water (100% r.h.) as a function of number of double layers.*

points to the surface which leads to rather grain–like structures. As more and more layers are adsorbed the interdigitation increases leading to the formation of worm (blob)–like structures.

The swelling structure of the PEM from low ionic strength is explained by the proposed model in Figure 5.6 (0.1 M NaCl). The first double layer has a quite loosely packed structure due to its close contact to the environmental aqueous phase. That is the common feature of all outer layer independent of the number of layers. That is confirmed by mobility and permeability measurements which show a higher diffusion coefficient of polyelectrolyte chains in the outer layer[74] and also a higher diffusion coefficient of probe molecules through this layer[43] . The adsorption of the next layer leads to a densification due to strong interdigitation with the former adsorbed double layer related to intrinsic charge compensation. Although the formation of complexes between oppositely charged polyelectrolytes is entropically driven (release of counterions) the overall increase in density is enhanced by the electrostatic attraction between the negatively charged Silicon substrate and the outermost PDADMAC layer. In addition the rather flat conformation at low ionic strength causes a higher density of adsorbed layers. This leads to decreasing chain mobility[74] and decreasing permeability[43] with increasing number of layers. This process explains the formation of multilayers at least up to a number of 4 double lay-

ers, i.e. the swelling water decreases in the order of 1 > 2 > 4 double layers. It is in good qualitative agreement with the findings of Wong et al.[98] where 6 double layers of PAH/PSS system exhibited an *interphase* structure. The present work shows 6 double-layers of PSS/PDADMAC system to have a *continuum* structure. The difference between the former work[98] and now is the adsorption of PEI as the first layer before the PSS/P-DADMAC multilayer. Also, the multilayers without PEI are relatively thin compared to those having PEI as a first layer. In the case of the PEMs consisting of more than 4 double layers, the attraction between the outer polycation layer and the substrate is screened. This leads to a less dense packing and they swell more when exposed to water vapour. In this context, PEMs consisting of 1, 2 or 4 double layers show *interphase* behavior, i.e. still affected by the substrate and only the 6, 8, 14, 20 and 30 double layers show rather *continuum* behavior with respect to the amount of swelling water.
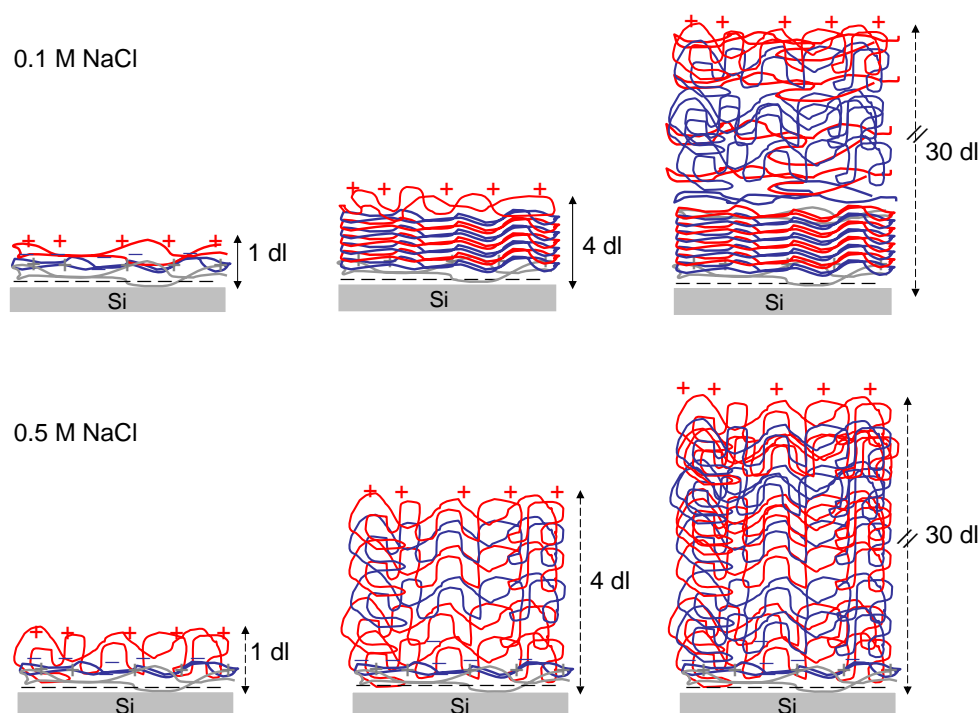
Figure 5.6: *Proposed model for the influence of substrate on the different number of adsorbed polyelectrolyte multilayers*

Multilayers prepared from 0.5 M NaCl solution. In contrast to this, the topology for an ionic strength of 0.5 M changes dramatically with the number of layers from grain–like via rod–like to worm(blob)–like structures. This indicates that in–plane interaction between interdigitating polyelectrolytes becomes almost as prominent as the interaction

between polyelectrolytes perpendicular to the surface. This leads to a 3D-bulk complex between oppositely charged polyelectrolytes. This might be a hint for a transition from the *interphase* to *continuum* behavior. Since the 30 double layers of both 0.1 M and 0.5 M NaCl have almost the same roughness (6.7 nm and 6.9 nm respectively) this indicate the beginning of constant roughness irrespective of ionic strength.

For the high ionic strength the PEM swelling structure is completely different from the low ionic strength PEM. First of all, due to the charge screening along the polycation chain, the chains adsorb in a more loosely packed structure, which enhances the amount of water. In addition the attraction between the outermost layer and the oppositely charged substrate is stronger screened which counteracts a denser packing of the layers close to the substrate. This is consistent with the swelling water increase in the order of $1 < 2 < 4 < 6 < 8 < 14 < 20 < 30$ double layers. The swelling of $(PSS/PDADMAC)_{30}$ prepared from 0.5 M NaCl solution shows that the polyelectrolyte multilayer can absorb up to 70 vol.% of water.

From this point of view it is concluded that the PEMs prepared at an ionic strength of 0.5 M show already a *continuum* behavior at quite a low number of polyelectrolyte layers, at least concerning the electrostatic attraction between substrate and outermost layer. Still unclear is from which number of layers on the amount of swelling water remains constant. Experiments concerning this point are underway.

In conclusion, this study shows that polyelectrolyte multilayers do not show one fixed threshold, i.e. number of layers, where all features switch from an *interphase* behavior, i.e. dominated by the substrate to a *continuum* properties. Rather the transition from one zone to the other depends on the physical quantity of the polyelectrolyte multilayers that is investigated.

Chapter 6

Long chains versus short chains polyelectrolyte multilayers: a comparison of structural and dynamic properties [1]

QCM-D and AFM measurements on short polymer chains have been performed by Samantha Micciulla in her master thesis under the supervision of Samuel Dodoo and Chloé Chevigny.

Abstract

Structural and viscoelastic properties of high and low molecular weight polyelectrolyte multilayers are investigated by the use of Ellipsometry, Atomic Force Microscopy (AFM), Contact Angle (CA) and Quartz Crystal Microbalance with Dissipation (QCM-D). The combination of the obtained results highlighted the effect of chain length for poly(sodium styrene sulfonate) PSS/ poly(diallyl dimethyl ammonium chloride) PDADMAC multilayers. First the structure, i.e. type of growth, thickness and external roughness is investigated for both systems. Short-chains systems are much thinner and grow slower, but the growth stays linear in every case in the observed range (up to 6 bilayers). The external roughness is found to be independent of chains length. Then the interactions with water (contact angle and swelling in humid atmosphere) are studied. While water uptake does not depend on chain length, the short-chain PEMs are much more hydrophilic than the standard long-chain system. Finally, a detailed analysis of the QCM-D results allowed to characterize the different adsorption behaviour for both multilayer systems, i.e. long chains and short chains PEMs via the dissipation (ΔD) and frequency (Δf) changes. A link between energy dissipation and roughness, surface hydrophobicity and amount of adsorbed water are elaborated to explain the differences between the two systems.

6.1 Introduction

Polyelectrolyte multilayers (PEMs) are self-assembled systems built up by the subsequential deposition of oppositely charged polymers, known as the Layer-by-Layer (LbL)

---

[1]Similar content is included in: *Long chains versus short chains polyelectrolyte multilayers: a comparison of structural and dynamic properties*, S. Dodoo, S. Micciulla, C. Chevigny, A. Laschewsky, and R. v. Klitzing, *in preparation.*

64

Chapter 6 Long chains versus short chains polyelectrolyte multilayers: a comparison of structural and dynamic properties

method.[2,3] Since two decades PEMs have attracted increasing interest, both from a fundamental and an applied point of view, due to the advantages they offer: simple preparation and wide versatility. They find many applications, ranging from biosensing[11] and biomedicine[131] to optical devices,[10] coating of flat surfaces,[7] surface functionalization,[132,133] colloidal particles or even hollow capsules[13,134] for controlled delivery. Their structure and properties have been extensively studied as a function of different parameters: polyelectrolytes type, ionic strength or counterions, pH or temperature.[28,45,73,98,109] These parameters are known to have major effects on structure, type of growth (linear or exponential) or functionalities (swelling in water, chain mobility, elasticity). Besides these investigations, studies have been directed in understanding the features of adsorption of polymers making thin films.[101,135–138]

Lösche et al.,[40] who investigated the internal structure of PEMs with Neutron Reflectivity, were the first to look at the chain length influence. Working with PSS chain lengths ranging from 400 to over 5000 monomers/chain, combined with 650 monomers/chain PAH, they did not notice any substantial effect in the films structure. But the use of chains shorter than the average (below 300 monomers/chain and down close to the oligomer limit) will significantly change the PEMs features, already from the formation process. The fabrication of multilayers by adsorbing low molecular weight (LMW) polyelectrolytes is a challenge already from this first deposition step: reaching an efficient multilayer growth. As discussed by Sui et al.,[139] the combination of long and short chain polyelectrolytes for the preparation of multilayers leads to the decrease of growth efficiency, and even no overall growth is observed if short chain compounds are used both as polyanion and polycation. This behavior was explained by kinetics considerations: thermodynamically, the most stable conformation for oppositely charged polyelectrolytes in solution is to form complexes, whatever their chain length. But in the case of high molecular weight compounds, adsorption of the chains on a surface is kinetically irreversible in the time frame of a deposition cycle. While for low molecular weight compounds, redissolution of the adsorbed chains will occur during the same time frame, because of weaker interactions between the surface and the polyelectrolytes, the shorter chains being less eager to interdigitate with the already existing multilayer and having less charges pro chain. The screening of electrostatic interactions via increase of ionic strength will also favor the complexes formation, for all chain lengths. More recent investigations were done on the behaviour of short chain or low molecular weight polyelectrolytes on complexes or multilayers,[140–143] always focusing on the formation parameters. Also mentioned are studies on the interaction between polymers and low molecular weight dyes,[144,145] whose results have shown that the adsorption of polymer enters in competition with the desorption of previously adsorbed dyes.

Chapter 6 Long chains versus short chains polyelectrolyte multilayers: a comparison of structural and dynamic properties

65

This chapter present a complete study of the structure and properties of PSS/PDADMAC multilayers formed with two molecular weight ranges: the "standard" High-Molecular Weight (HMW) system (PSS 340 monomers/chain, PDADMAC 840 monomers/chain), and a second system with shorter chains (LMW), close to the oligomer limit (PSS 32 monomers/chain, PDADMAC 31 monomers/chain). After the development of a dipping process which allows the reproducible synthesis of short-chains films, first the structure of the films, obtained by a combination of ellipsometry and AFM will be presented. Then the behaviour in water was investigated (contact-angle measurements and swelling behaviour). Finally, QCM-D was used to unify all the previous results via mass and viscoelasticity monitoring, and get hints on the kinetics of formation of each system. Knowing that the QCM is an improved method for studying the viscoelastic behaviour of polymers,[146–149] and the fact that dissipation change during the adsorption of PEM is influenced by surface roughness of the film, the wetting properties of the film, and the amount of water trapped in the pores or voids in the film,[101,136] these helpful informations about the properties of the film are used to understanding the kinetic behaviour of short and long chains PEMs. Previous studies on the swelling behaviour of PEM showed that aside the swelling water PEM can trap up to 20% void water when swollen. This trapped water is likely to be sensed by the quartz crystal as added mass which is related to the frequency change. Such difficulties which arises in the interpretation of the QCM data can only be overcome by having supporting measurements using techniques like Ellipsometry, AFM and Contact Angle measurements.

LMW polyelectrolytes: The linear polymer PDADMAC (M_n 5,000 g/mol) was synthesized by free radical polymerization in Fraunhofer Institute (Potsdam, Germany). The PEI ($50\%_w$ solution in water, M_w 1,300 g/mol) was purchased by Sigma-Aldrich (Steinheim, Germany) and the PSS (M_n 6,520 g/mol, M_w/M_n<1.2) was obtained from Polymer Standard Service (Mainz, Germany). All the reagents are used without further purification. The LMW PEM is prepared the same way as the HMW PEM, except the dipping time is 5 minutes.

6.2 Results

In this section, the results obtained from the investigation of HMW and LWM PEM are presented. The experimental data are divided into sections which refers to each specific measurement, differences and analogies between the two systems are highlighted with the aim of giving a general overview of the work. A link between the experimental data

66

Chapter 6 Long chains versus short chains polyelectrolyte multilayers: a comparison of structural and dynamic properties

is presented in the discussion, where also further considerations on kinetic aspects are presented.

6.2.1 Multilayer growth

The thickness as a function of number of double layers of PSS/PDADMAC polyelectrolyte multilayers on Si/PEI are shown in Figure 6.1. The long chain (HMW) system form thicker layers compared to short chain equivalent. This feature is confirmed by the values of relative growth, shown in Table 6.1. The growth of each layer is estimated in relation to the thickness of the previous one.
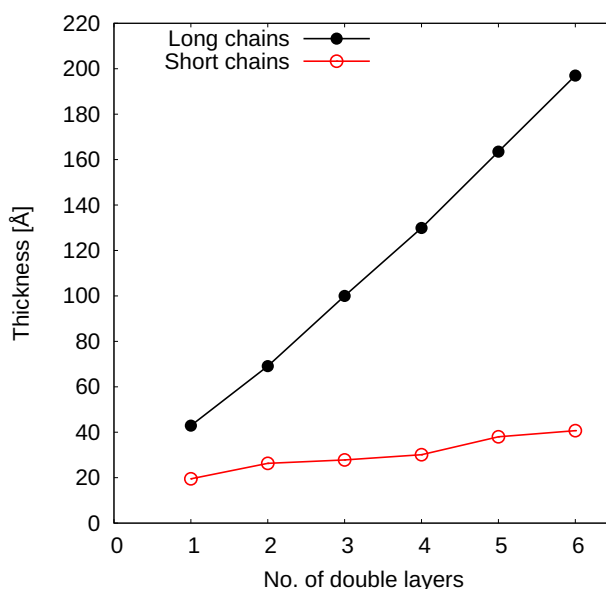
Figure 6.1: *HMW and LMW multilayers of PEI/(PSS/PDADMAC)$_n$, prepared in 0.1 M NaCl aqueous solution. Data points represent the PDADMAC outer layer. Thickness against number of double layers. Measurements are made on dry films, against air.*

Number of double layers	Relative growth [%]	
	Long chains	Short chains
1	95	22
2	61	35
3	45	6
4	30	8
5	26	26
6	20	7

Table 6.1: *Relative growth of thickness of PEI/(PSS/PDADMAC)$_n$ multilayers for HMW and LMW systems. The values are calculated by comparing the increase of thickness of each layer with the thickness of the previous one.*

Chapter 6 Long chains versus short chains polyelectrolyte multilayers: a comparison of structural and dynamic properties

67

6.2.2 Surface morphology

The surface morphology of PEI(PSS/PDADMAC)$_6$ PEM from high and low molecular weight polyelectrolytes are shown in Figure 6.2.

(a)   (b)
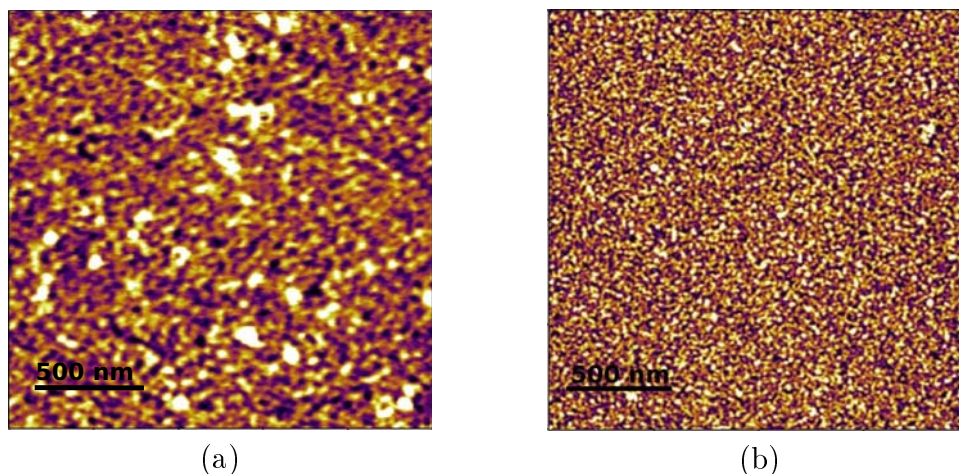
Figure 6.2: *AFM images of PEI/(PSS/PDADMAC)$_6$ multilayers of (a) long chains (PSS ~340 monomers/chain, PDADMAC ~840 monomers/chain) and (b) short chains (PSS ~32 monomers/chain, PDADMAC ~31 monomers/chain) polyelectrolytes prepared from 0.1 M NaCl aqueous solution. The scans which are performed in ambient conditions have size of 2 μm x 2 μm.*
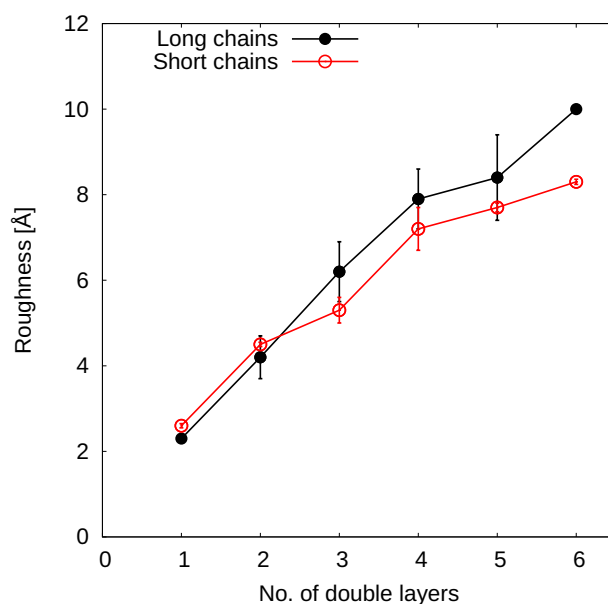
Figure 6.3: *Roughness versus number of double layers for HMW and LMW multilayers of PEI/(PSS/PDADMAC)$_n$, prepared in 0.1 M NaCl aqueous solution. The values reported here are calculated as root mean square roughness of AFM images scanned in ambient conditions.*

68

Chapter 6 Long chains versus short chains polyelectrolyte multilayers: a comparison of structural and dynamic properties

The roughness, extracted from the AFM scan by imaging elaboration, in dependence of the number of double layers are shown in Figure 6.3. Larger aggregates can be noticed for the long chain system. Nevertheless, from Figure 6.3 it is evident that the increase in roughness for both long chain and short chain multilayers proceeds in the same range of values.

6.2.3 Hydrophilicity of the surface: contact angle measurements
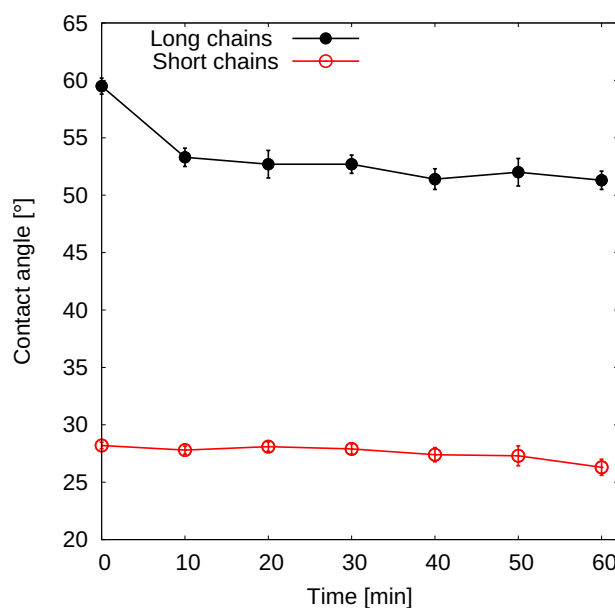
Figure 6.4: *Water contact angle measurements in a saturated vapour cell on polyelectrolyte multilayers PEI/(PSS/PDADMAC)$_6$ prepared from HMW (PSS ∼340 monomers/chain, PDADMAC ∼840 monomers/chain) and LMW (PSS ∼32 monomers/chain, PDADMAC ∼31 monomers/chain) polyelectrolytes from aqueous solutions of 0.1 M NaCl.*

The time-dependent contact angle measurements performed on PEI/(PSS/PDADMAC)$_6$ multilayers after 15 min equilibration are shown in Figure 6.4. For the high molecular weight PEM, after an initial equilibration period, the contact angle levels around 52° (mean value: 52.2°). For the low molecular weight multilayer, the value remains stable around 28° (mean value: 27.6°). The lower contact angle for the short chain multilayer (outermost layer is PDADMAC) indicates higher hydrophilicity compared to the surface of the long chain system.

6.2.4 Multilayer response to water vapour

Figure 6.5a shows the thickness evolution for PEI/(PSS/PDADMAC)$_6$ multilayers of high and low MW polyelectrolytes under increasing relative humidities. In both cases, an

Chapter 6 Long chains versus short chains polyelectrolyte multilayers: a comparison of structural and dynamic properties

69

(a)

(b)
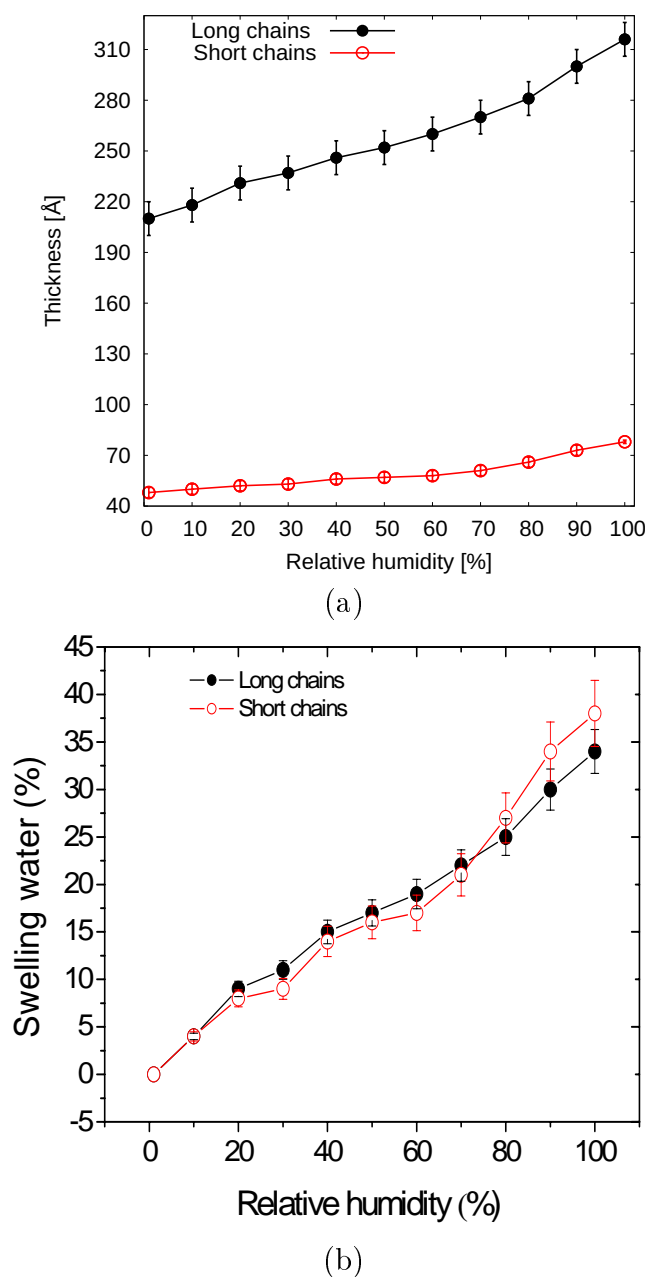
Figure 6.5: *Swelling behavior of PEI(PSS/PDADMAC)$_6$ multilayers prepared from HMW (PSS ~340 monomers/chain, PDADMAC ~840 monomers/chain) and LMW (PSS ~32 monomers/chain, PDADMAC ~31 monomers/chain) polyelectrolytes. Thickness (a) and swelling water (b) versus relative humidity. Filled symbols represent high MW compounds, open symbols represent low MW equivalents.*

increase in thickness with increasing relative humidity of the environment is observed, which represents the swelling of the multilayers as they soak water vapour from the atmosphere like a sponge. As the absolute thicknesses are much larger for the HMW system, it is convenient for a better comparison of the swelling behaviour of the two systems to extract the relative thickness increase between dry and swollen state, which is

70

Chapter 6 Long chains versus short chains polyelectrolyte multilayers: a comparison of structural and dynamic properties

a measurement of the amount of swelling water: $\phi_{swell} = \frac{d_{swollen} - d_{dry}}{d_{swollen}} \times 100$.

From Figure 6.5, it is clear that the swelling behaviour is the same and independent of the chains length. The amount of water in the films increases with increasing humidity, up to about 35 % when fully swollen in water for both HMW and LMW multilayers. This result is in agreement with our previous works,[75,129] as well as with other measurements on the PSS/PDADMAC system.[150]

6.2.5 Layer deposition and viscoelastic properties

Figure 6.6 shows the data of frequency, dissipation and mass adsorbed obtained from QCM-D measurements during the preparation of $PEI(PSS/PDADMAC)_6$, for both HMW and LMW polyelectrolytes. Mass is obtained directly from the frequency change via the Sauerbrey formula, equation 3.31. The Sauerbrey mass is used because the overtones in the measured signals are close to each other (as shown in Figure 6.9) which justifies the Sauerbrey equation. In case of long chains (Figure 6.6a), a regular cycle is observed during the multilayer preparation on the quartz crystal, consisting in two steps : first an adsorption plateau, then a loss of material during water rinsing. The dissipation maintains an overall constant value, but sharp peaks in the signal are registered corresponding to the rinsing steps: an increase after PDADMAC adsorption and a lower increase after PSS adsorption, respectively. It can be noticed that the dissipation values after rinsing increases with increasing number of adsorbed layers, before dropping to its constant value during adsorption.

Figure 6.6b present the results of the short-chains system for QCM-D with water rinse. The first important observation is the loss of mass during the polyelectrolytes adsorption step: this occurs during each PDADMAC deposition and becomes stronger after each cycle. It is however, not observed for the adsorption of PSS. As for the HMW system, the overall dissipation values are constant, but sharp-peaks are observed during the rinsing steps. Rinsing after PDADMAC results in a large increase of dissipation, larger with the number of adsorbed layers, exactly as was observed for the HMW system. On the contrary, rinsing after PSS results in a decrease of the dissipation to almost zero, irrespective of the number of adsorbed layers. The absolute values of dissipation and mass uptake are always significantly lower for the LMW system than for the HMW system.

To check the effect of the change of ionic strength due to the rinse with pure water, the same QCM-D experiments are made by using a solution of 0.1 M NaCl for the rinsing step. The Figure 6.7 shows the data of frequency shift, dissipation and mass change (obtained via Sauerbrey formula, equation 3.31) for the two systems.

(a)

(b)
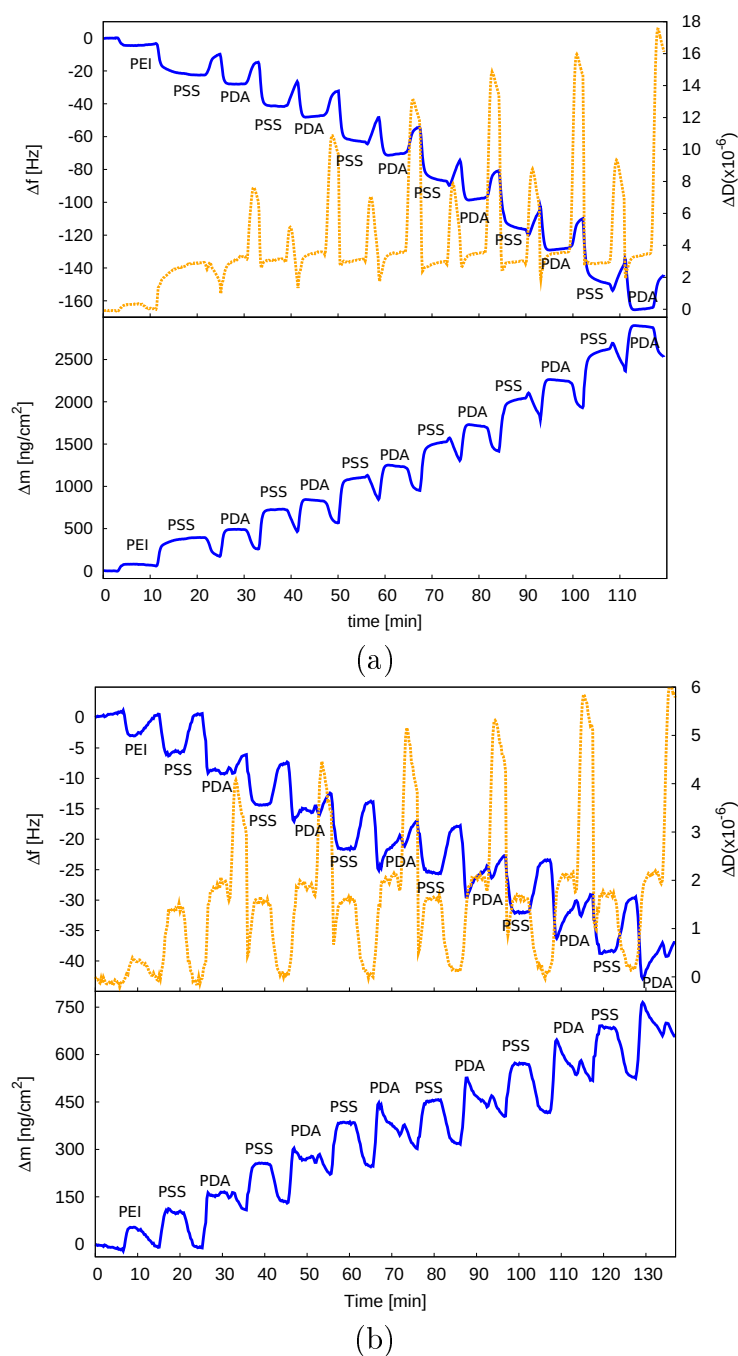
Figure 6.6: *QCM-D data of PEI(PSS/PDADMAC)$_n$ multilayers from (a) HMW (PSS ~340 monomers/chain, PDADMAC ~840 monomers/chain) and (b) LMW (PSS ~32 monomers/chain , PDADMAC ~31 monomers/chain) polyelectrolytes deposited on gold quartz crystal. After each deposition, **Milli-Q water is used for rinsing**. Upper plot: Frequency shift and dissipation, lower plot: change of mass calculated by the Sauerbrey equation. Polyelectrolyte solution contains 0.1 M NaCl; both adsorption and rinsing time are 5 min at constant flow rate of 0.3 mL/min.*

The first remarkable observation concerns the mass uptake: for all chain lengths, it is higher than with pure water rinse, as highlighted in Figure 6.8. But the overall linear

72

Chapter 6 Long chains versus short chains polyelectrolyte multilayers: a comparison of structural and dynamic properties

(a)

(b)
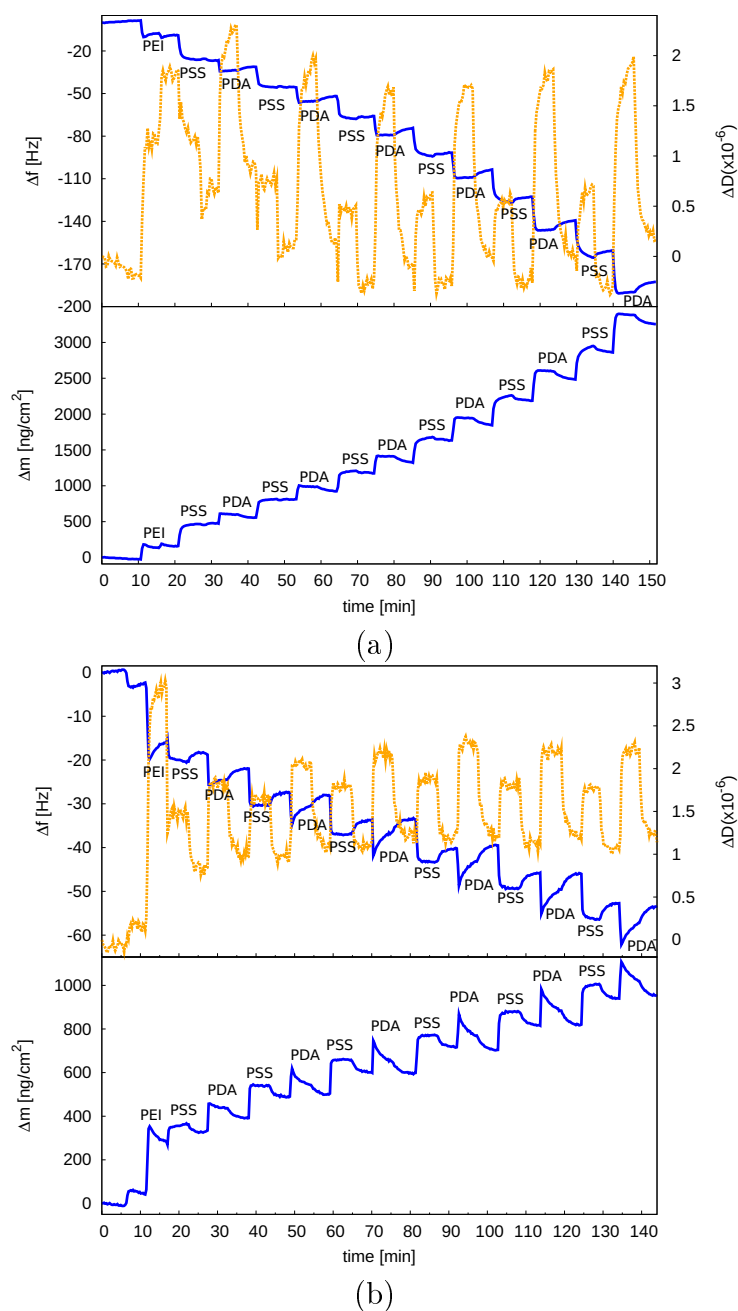
Figure 6.7: *QCM-D data of PEI(PSS/PDADMAC)$_n$ multilayers from (a) HMW (PSS ∼340 monomers/chain, PDADMAC ∼840 monomers/chain) and (b) LMW (PSS ∼32 monomers/chain , PDADMAC ∼31 monomers/chain) polyelectrolytes deposited on gold quartz crystal. After each deposition, **0.1 M NaCl aqueous solution is used for rinsing**. Upper plot: Frequency shift and dissipation, lower plot: change of mass calculated by the Sauerbrey equation. Polyelectrolyte solution contains 0.1 M NaCl; both adsorption and rinsing time are 5 min at constant flow rate of 0.3 mL/min.*

growth is not changed by this new rinsing medium. It is particularly obvious for the HMW system, where the salty water rinsing step induces almost no loss of material irrespective of the outermost polyelectrolyte. Concerning the LMW system, while the loss decreased

Chapter 6 Long chains versus short chains polyelectrolyte multilayers: a comparison of structural and dynamic properties

73
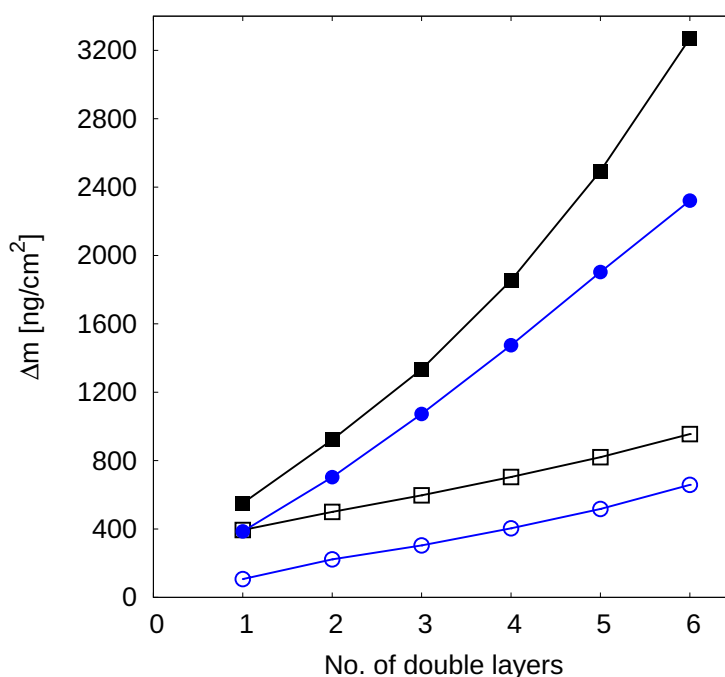
Figure 6.8: *Adsorbed mass versus number of double layers (PDADMAC outer-layer) registered after rinsing with Milli-Q water or 0.1 M NaCl solution subsequent to each PDADMAC deposition. Filled symbols represent high MW system, open symbols represent the low MW equivalent. Cubes for rinsing with 0.1 M NaCl, circles for rinsing with Milli-Q water.*

after PSS adsorption compared to pure water rinse, no changes are observed for the PDADMAC adsorption: the loss during the adsorption steps and the rinsing steps are still observed.

The overall values of dissipation are, as for water rinse, still constant irrespective of the chain length. Differences are noticeable in each adsorption cycle and the most striking being the sharp dissipation peaks. This is observed during the rinsing step following PDADMAC adsorption but vanishes when rinsed with salty water. The dissipation characteristics of one cycle (PSS-adsorption, PSS-rinse, PDADMAC-adsorption, PDADMAC-rinse) are in this case similar for both HMW and LMW multilayers. Always, adsorption of a polyelectrolyte induces an increase in dissipation, higher when this polyelectrolyte is PDADMAC. On the contrary, all rinsing steps are characterized by a dissipation decrease to a constant low value, close to zero. The overall range of the dissipation values is higher in the case of HMW.

To sum-up, single adsorption cycles from the plots in Figures 6.6 and 6.7 are plotted in Figure 6.9 and the differences are:

- For the short-chains system, irrespective of the rinsing media, the PDADMAC ad-
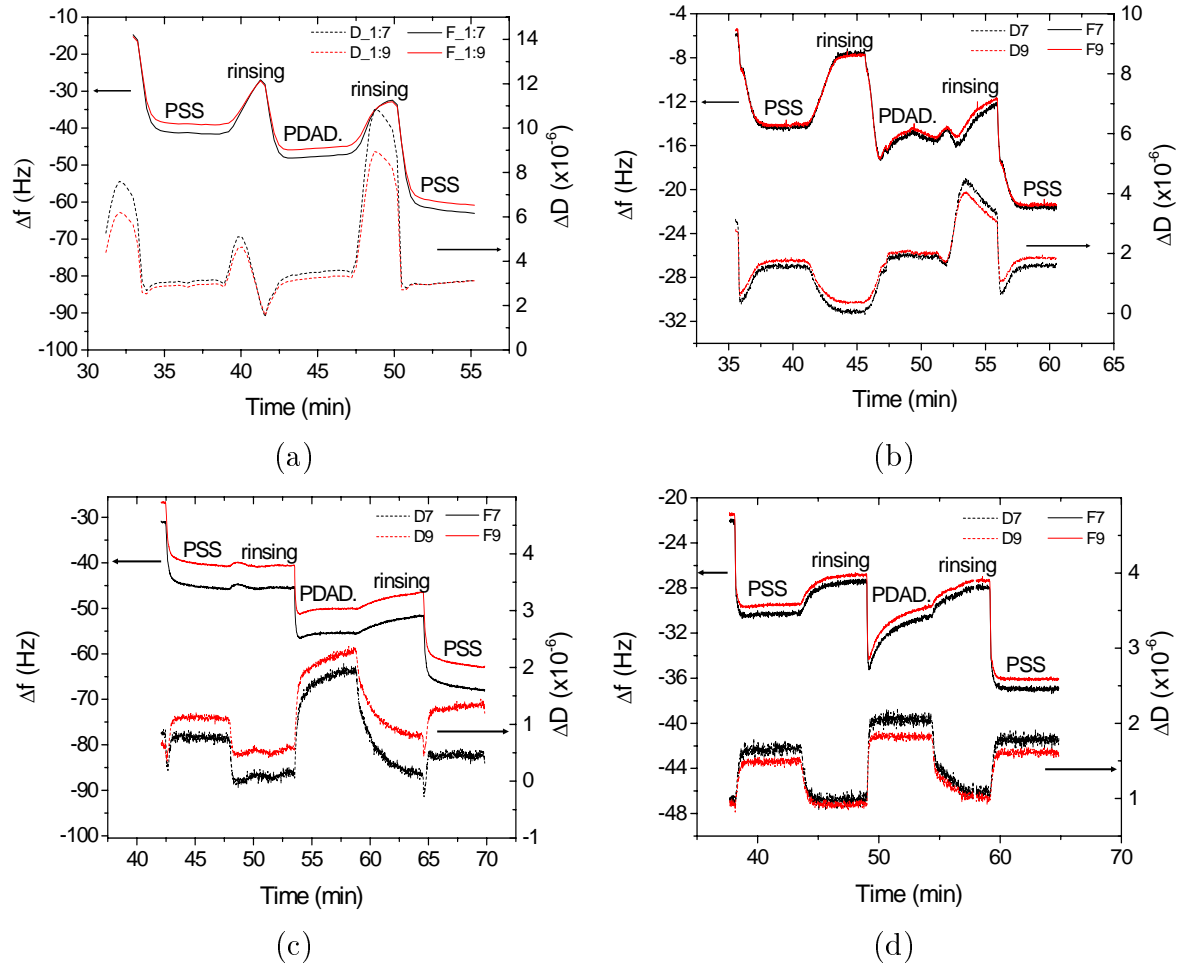
Figure 6.9: *QCM-D data of PEI/(PSS/PDADMAC)$_n$ multilayers. Each plot represent single adsorption cycle in Figures 6.6 and 6.7, respectively. (a) HMW, water rinsing, (b) LMW, water rinsing, (c) HMW, 0.1 M NaCl solution rinsing and (d) LMW, 0.1 M NaCl solution rinsing.*

sorption step is characterized by a loss of material: after a steep mass uptake during the first minute, the adsorbed mass regularly decreases for the next 4 minutes. This is not observed with PSS, and not observed for the HMW multilayers.

- Whatever the chain length is, every rinsing step with pure water induces a mass loss.

- Rinsing with 0.1 M NaCl solution decreases significantly this loss for PSS and PDADMAC in the HMW system, but for the LMW system only for PSS.

- Overall dissipation values are in every case constant, but undergo important sharp rising-and-falling in a cycle.

Chapter 6 Long chains versus short chains polyelectrolyte multilayers: a comparison of structural and dynamic properties

75

- For water-rinse-experiments, rinsing steps after PDADMAC adsorption presents a high increase of the dissipation regardless of the chain length, increasing also with the number of adsorbed layers. This is characteristic of increased flexibility of the film. In the case of HMW multilayers, this is also observed after PSS adsorption.

- On the contrary, every PDADMAC adsorption step induces decrease of dissipation, and this is also observed for PSS adsorption in the HMW system, indicating increased rigidity.

- For the LMW system, rinsing with pure water after PSS adsorption induces a steep decrease of dissipation to almost zero, while PSS adsorption increases the dissipation.

- When rinsing with 0.1 M NaCl solution, regardless of the chain length, adsorption steps are characterized by increased dissipation (flexibility) and rinsing steps by decreased dissipation (rigidity).

6.3 Discussion

6.3.1 Multilayer growth: stripping versus sticking

For the multilayers preparation, different adsorption times are used: 20 minutes for the HMW system, reduced to 5 minutes for the LMW system. The choice of reducing the adsorption time for the LMW system is due to the observation of a continuous and reproducible growth in this case, while no overall thickness increase or reproducibility was accessible with higher dipping times. Sui et al.[139] observed no overall growth when using short chain compounds both as polyanion and polycation. This behavior was explained by kinetics considerations: at first the polyelectrolytes will adsorb on the surface, but thermodynamically, the most stable conformation for oppositely charged polyelectrolytes in solution is to form complexes, regardless of their chain length. In the case of high molecular weight compounds, adsorption of the chains on a surface is kinetically irreversible in the time frame of a deposition cycle, because of strong interdigitation and electrostatic interactions. While for low molecular weight compounds, redissolution of the adsorbed chains will occur during the same time frame, because of weaker interactions between the surface and the polyelectrolytes, the shorter chains being less eager to interdigitate with the already existing multilayer (being more rigid) and having less charges per chain (being shorter). This is indeed observed with QCM: for the short chains, during each PDADMAC adsorption step, after a steep mass uptake (corresponding to the adsorption

76

Chapter 6 Long chains versus short chains polyelectrolyte multilayers: a comparison of structural and dynamic properties

on the multilayer surface, i.e. "sticking"), the adsorbed mass was constantly decreasing (corresponding to complexes formation in solution, i.e. "stripping"). But in 5 minutes, this mass loss was still smaller than the mass uptake taking place at the beginning.

If this "stripping-vs-sticking" kinetic explanation of the short chains behaviour can justify the 20-min-dipping-time results (no multilayer formation for shorter chains), it has to be adapted to understand why growing short-chains multilayers was successful when decreasing the dipping time down to the value used by Sui et al. (5 minutes). Here it should be noticed that these previous observations are made on a PSS/PAH system, the polycation PAH being less rigid (smaller persistence length) than PDADMAC. Because of that, PDADMAC have less binding points available to connect with the previous layer, which makes it more mobile and more eager to interdigitate with previous layers than PAH.[74] The redissolution kinetics is then slower than for PAH, because PDADMAC is more deeply entangled with previous layers, which explains why in 5 minutes stable multilayers of PSS/PDADMAC can be formed while it is impossible to form PSS/PAH multilayers. One could argue that the slightly higher charge density of PAH would create a stronger bond, but at 0.1 M NaCl the influence of this small difference must be screened.

6.3.2 Surface morphology and roughness

The larger aggregates observed in the case of the HMW PEM (Figure 6.2a) is due to higher flexibility of the long chains and higher degree of freedom to form loops which favours coil conformation of the chains on the substrate during adsorption and hence higher roughness (Figure 6.3). Short chains remain stiffer and form thinner and low-roughness films, due to flat conformation during adsorption. Due to their short chain length, a very low degree of chain interpenetration, which leads to poor efficiency for polymer adsorption and that accounts for the lower aggregates observed in the image (Figure 6.2b) as well as the lower surface roughness (Figure 6.3).

6.3.3 wettability

The results from contact angle measurements show difference in hydrophilicity between HMW and LMW PEMs. The reason for the lower contact angle (28°) in the case of LMW PEM is the fewer number of hydrogen atoms in the backbone of the chain. In addition, short chain system can be related to the different surface morphology having smaller aggregates at the surface (Figure 6.2). On the other hand, the long chain system (Figure

Chapter 6 Long chains versus short chains polyelectrolyte multilayers: a comparison of structural and dynamic properties

77

6.2a) has larger homogeneous area, ascribable to the polymer backbone, i.e. hydrophobic parts and hence the higher water contact angle of 52°.

6.3.4 Swelling behaviour

From chapter 4,[75] it has been established that the total amount of water content in a swollen multilayer comes from the void water and the swelling water. From the results in Figure 6.5 which show equal amount of swelling water (35% at 100% r.h.) for both long and short chains PEM, it implies that the difference in dissipation between the two systems could come from the different amount of void water that might be trapped in the film which can not be estimated for, by the present technique. However, the effective density can be estimated from the thickness and the mass per unit area. From the density one can tell if the multilayer structure is closed packed or loosely pack. A denser film implies the multilayer is ridig and chains are less mobile while less dense film implies a flexible multilaye and the chains are very mobile. Since the density is inversely proportional to the
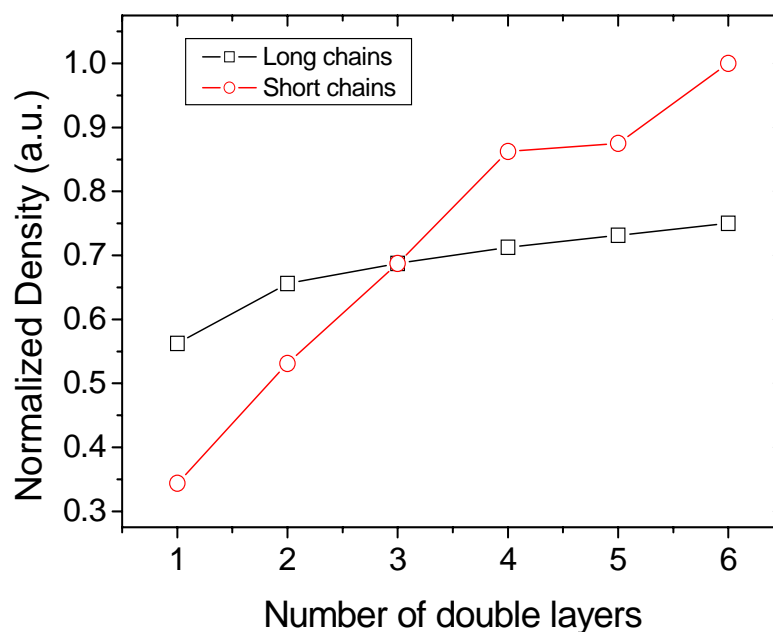
Figure 6.10: *Normalized density versus number of double layers on polyelectrolyte multilayers PEI/(PSS/PDADMAC)$_n$ prepared from high (PSS 70,000 g/mol, PDADMAC 135,000 g/mol) and low (PSS 6,520 g/mol, PDADMAC 5,000 g/mol) molecular weight polyelectrolytes from aqueous solutions of 0.1 M NaCl. Each data point represents PDADMAC outer layer. The density is normalized to 1 by dividing by the highest value. This way the swelling water in the system is eliminated.*

volume, it can be inferred from Figure 6.10 that at the first double layer the density of the

short chains is lower than the long chains which is an indication that there are more voids in the short chains than the long chains. By the third double layer, both the long chains and the short chains PEM have the same density (same amount of voids). After the third double layer, the short chains PEM becomes denser than the long chain PEM indicating compact film structure where the chains are less mobile for the short chains PEM. At this point the voids in the long chains PEM are more than those in the short chain PEM. A reason for this density change can be attributed to rearrangement of chains as the number of adsorption cycles increases. This confirms the expectation that, as the number of layers increases the long chains will have better interdigitation than the short chains and also the long chains will form more coils in their conformation during the adsorption thereby decreasing in layer density. Neutron reflectivity studies have shown that up to 8 vol.% void water exist in the swollen long chains PEM prepared from aqueous solution of 0.1 M NaCl.[75] Therefore the percentage void water in the short chain equivalent is expected to be lower than 8 vol.%.

6.3.5 Adsorption kinetics

Using QCM in the liquid phase to study the structural behaviour of flexible and non-flexible polyelectrolytes reveals interesting experimental results. The dissipation channels of the QCM records the dynamics of the chains or the viscoelastic behaviour of the multilayer during the adsorption process. From the dissipation signal, the structural behaviour of the outer layer as well as the cumulative behaviour of the entire multilayer can be interpreted. The high dissipation peaks observed during rinsing with pure water after polyelectrolyte adsorption in both short and long chain systems indicate the sensitivity of the chains to changes in the aqueous surroundings. Increasing dissipation means increasing flexibility or unfolding of the chains and decreasing dissipation means increasing rigidity related to a stronger folding of the chains and for lower water content. There is difficulty regarding the interpretation of the QCM response. The flexible nature of polyelectrolytes actually implies that the energy dissipation of the system may be affected. Therefore a better way to evaluate the data is to consider $\Delta D/\Delta f$ which gives information about much dissipation that is caused by a unit frequency (mass) change. This method of QCM data evaluation does not only eliminate time as an explicit parameter but also reveals whether the adsorption is purely kinetically controlled or affected by transport (diffusion) limitation.[101] It can also be used as a quantitative measure about when the Sauerbrey relation may be justified.

The Figure 6.11 shows plots of $\Delta D/\Delta f$ of single adsorption cycles (PSS adsorption and

Chapter 6 Long chains versus short chains polyelectrolyte multilayers: a comparison of structural and dynamic properties

79
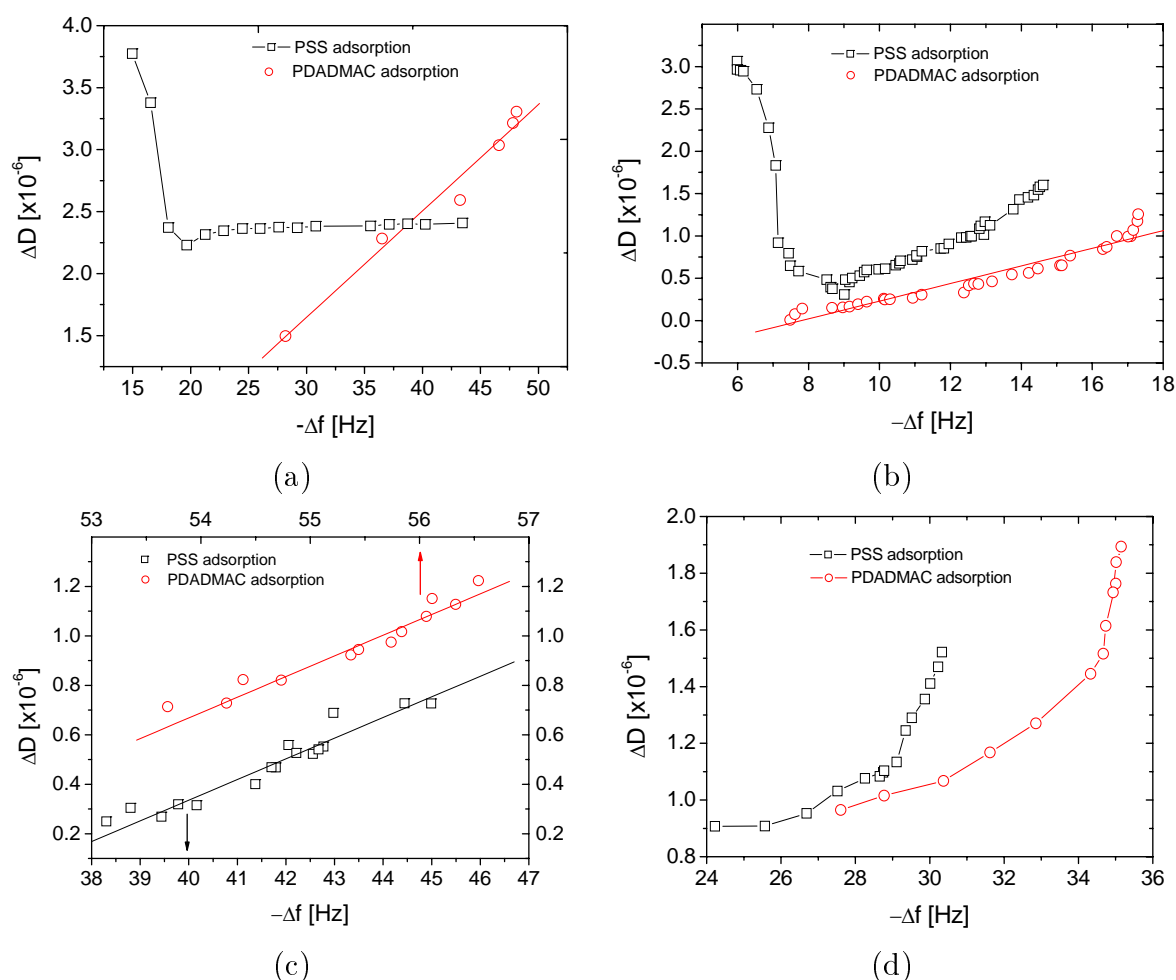
Figure 6.11: ΔD *vs* $-\Delta f$ *for the adsorption of* $PEI/(PSS/PDADMAC)_n$ *multilayers of long chains (PSS 70,000 g/mol, PDADMAC 135,000 g/mol) and short chains (PSS 6,520 g/mol, PDADMAC 5,000 g/mol) polyelectrolytes in 0.1 M NaCl aqueous solution. (a) HMW, water rinsing, (b) LMW, water rinsing, (c) HMW, 0.1 M NaCl solution rinsing and (d) LMW, 0.1 M NaCl solution rinsing. The plots show the different adsorption kinetics of HMW and LMW PEMs in different rinsing media. The data is taken from the single adsorption cycles of PSS/PDADMAC presented in Figure 6.9. The straight lines are guide to the eyes. Note that the density of data points-equispaced in time-become more distant the faster the kinetics in this type of plot. That explains the scarcity of data points at areas where the kinetics is fast.*

PDADMAC adsorption) of the HMW and LMW PEMs. Note that the density of data points (equispaced in time) become more distant the faster the kinetics in this type of plot. That explains the scarcity of data points at areas where the kinetics is fast. The fast and slow phases of the adsorption cause different relative dissipation per unit frequency shift (mass adsorbed), i.e. ΔD and Δf measure different properties of the adsorption kinetics. An indication that the adsorbed polyelectrolyte have different viscoelastic properties depending on the interaction with the solid surface and or with other polyelectrolytes.[136]

80

Chapter 6 Long chains versus short chains polyelectrolyte multilayers: a comparison of structural and dynamic properties

From Figure 6.11 (a) and (b), a fast kinetics is recorded at the onset of PSS adsorption after water rinsing for both HMW and LMW multilayers in terms of large change in dissipation corresponding to a small mass adsorbed. This phenomenon is caused by the rearrangement of the chains and change in conformation leading to folding of the multilayer and pressing of water out of the multilayer. The structure of the multilayer becomes dense and compact at this point. Thereafter, the system either maintains a constant energy dissipation (saturation plateau) in the case of the long chains or slow dissipation increase in the case of the short chains during subsequent mass adsorption. However, PDADMAC exhibits a different kinetics during adsorption after pure water rinse. The dissipation per unit frequency change, takes a linear dependence during the adsorption. In which case a faster adsorption for long chains than short chains is revealed by the steep $\Delta D/\Delta f$ slope for the long chains. Figure 6.11 (c) and (d) are the kinetics for the adsorption after salt rinse. It is remarkable to note that both PSS and PDADMAC adsorption after salt rinse for long chains, have similar linear dependence of $\Delta D/\Delta f$ (c). The short chains also have a similar behaviour but a non-linear dependence on $\Delta D/\Delta f$ (d).

So far only the kinetics of single adsorption cycles have been discussed but it is also interesting and necessary to consider the kinetics of the entire multilayer from the initial rinsing step to the final rinsing step after adsorption of the last PDADMAC layer. In order to do this, $\Delta D/\Delta f$ plots of the whole adsorption steps are plotted in Figure 6.12 for (a) long chain multilayers and (b) short chain multilayers with pure water as the rinsing medium. Though the plots contain a lot of data points which might be a bit confusing, it is however important to notice the different adsorption kinetics between the long and short chains multilayers. The PSS and PDADMAC adsorptions are marked with PSS and PDAD, respectively. The rinsing step are also marked as follows: **r-PSS** for rinsing after PSS adsorption, and **r-PDA** for rinsing after PDADMAC adsorption.

The first important observation from these plots is the position of the adsorption line on the dissipation axis. For the long chains ΔD is about (3×10^{-6}) and for short chains about $(1.5\text{-}2 \times 10^{-6})$. While the dissipation during adsorption is below the dissipation for **r-PSS** and **r-PDA** in the case of the long chains, it is however between the dissipation for **r-PSS** and **r-PDA** in the case of the short chains. During rinsing after PSS adsorption (**r-PSS**), short chains, the dissipation drops to zero. For both long chains Figure 6.12(a) and short chains Figure 6.12(b), the dissipation during rinsing after PDADMAC adsorption (**r-PDA**) increases with increasing number of adsorption steps. An indication of a flexible adsorbed PDADMAC layer to the multilayer matrix, which is weakly coupled to the multilayer and causes a phase shift in following the oscillation of the quartz crystal.

Chapter 6 Long chains versus short chains polyelectrolyte multilayers: a comparison of structural and dynamic properties

81

(a)

(b)
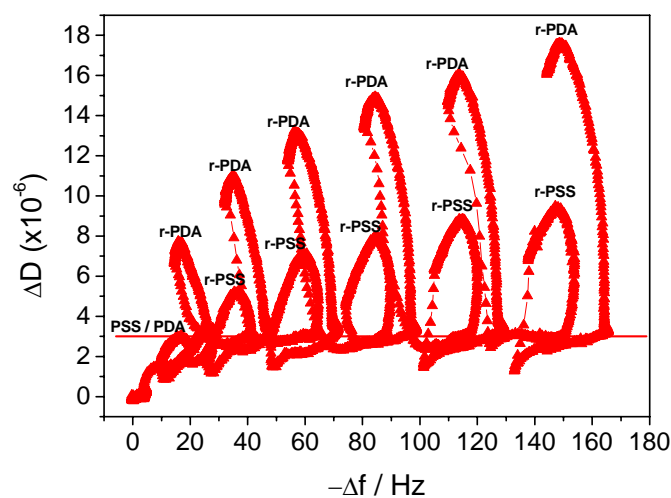
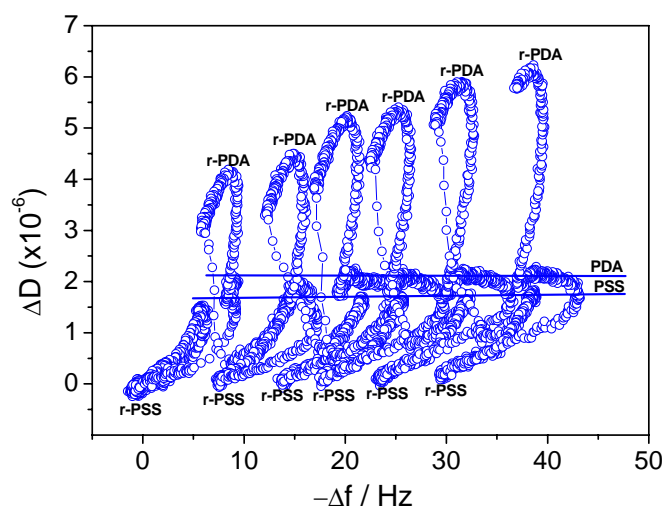**Figure 6.12:** ΔD *vs* Δf *for the adsorption of PEI/(PSS/PDADMAC)$_n$ multilayers of (a) long chains (PSS 70,000 g/mol, PDADMAC 135,000 g/mol) and (b) short chains (PSS 6,520 g/mol, PDADMAC 5,000 g/mol) polyelectrolytes in 0.1 M NaCl aqueous solution. The D and f data in Figure 6.6 with Milli-Q water as rinsing water, are used for the $\Delta D/\Delta f$ plot. On the plot,* **PSS** *and* **PDA** *denote PSS and PDADMAC adsorptions respectively. Also, rinsing after PSS and PDADMAC adsorptions are denoted by* **r-PSS** *and* **r-PDA** *respectively. The straight lines are guide to the eyes just to differentiate between adsorption and rinsing.*

The flexibility of outer layers due to decrease of ionic strength of the rinsing water is in agreement with Feldötö et. al.[151] As a measure of the energy dissipated by the system when it follows the oscillation of the vibrating crystal, the contribution to the dissipation

comes from two interfaces: the substrate-PEM substrate and the aqueous medium-PEM interfaces. At the contact with the substrate, the PEM dissipates energy when it vibrates due to the slippage on the gold resonator.[152] Assuming that the amount of dissipated energy at this interface is constant or minimal[153] during the preparation of the whole multilayer, part of the sharp dissipation peaks could come from the second interface (PEM-aqueous environment).[154,155]

Friction between the multilayer and the surrounding liquid environment can also influence ΔD.[136] Surface roughness of the adsorbed layer is another contributing factor. The higher the surface roughness, the higher the friction between them, since the coupling of the two systems is reduced. The increase of dissipation after subsequent layer deposition (for instance in Figure 6.12a, PDADMAC: from $(8 - 18) \times 10^{-6}$) could be related to the increase of roughness of the multilayer surface.[154,155] Figure 6.3 shows an increase in roughness with increasing number of double layers (long chains: 2.5 Å - 10 Å, short chains: 2.6 Å - 8.4 Å), element which is found also in the increasing of dissipation when the system reacts to changes in the surrounding medium. Longer backbones might wrap around the charged groups which are directed to the inner part of the film, in the side chains, while a short backbone cannot do that in a such efficient way.

Another candidate of ΔD from the polyelectrolyte - liquid interface is the wettability of the PEM surface. From the contact angle measurement in Figure 6.4, water wets the surface of the short chains PEM (CA = 28°) better than long chains PEM (CA = 52°). This partly explains why the maximum ΔD (6.5×10^{-6}) for short chains is less than the maximum ΔD (18×10^{-6}) for longs chains in Figure 6.12.

However interfacial processes and roughness effects are known not to be the dominant mechanism in D shift.[154,156] Dynamic conformational changes in the structure of the polyelectrolytes have been reported[101] to cause dissipational losses in the adsorbed polyelectrolyte multilayers as a result of periodic shear motion of the crystal. Hydration layer might also induce dissipational changes.[157,158] Polyelectrolyte multilayers interdigitate during adsorption and this creates voids in the multilayer. Trapped voids and intralayer water may influence the ΔD. Structural deformation of the adsorbed multilayer caused by the oscillation of the crystal can change the size and shape of the voids forcing the void water to move within or in and out of the multilayer. The movement of the void water can generate dissipative losses.

Chapter 6 Long chains versus short chains polyelectrolyte multilayers: a comparison of structural and dynamic properties

83

6.4 Conclusion

In conclusion, this study shows that structural properties of polyelectrolyte multilayers are strongly affected by the chain lengths. Short chains and long chains PEM require different preparation protocol for stable multilayer formation. Probing the surfaces of the long and short chains multilayers revealed increasing roughness with increasing number of layers. Contact angle measurements confirmed the hydrophilicity of the short chains PEM giving it better wettability at the interface with water. Other structural similarities between the two systems are swelling behaviour in water vapour and equal amount of swelling water.

Structural differences however, include flexibility of the outer PDADMAC layer during rinsing with water and also the different adsorption kinetics between long and short chains PEM. The two systems also have different viscoelastic behaviour in terms of rearrangement of chains in an entropic favorable state. The time resolved dissipation shift indicates their viscoelastic behaviour of the PEM during adsorption and rinsing. The latter is responsible for the quick reversible conformational change of the adsorbed PDADMAC layer when the rinsing medium is of lower ionic strength as the polyelectrolyte solution. Whereas rinsing with water after PSS adsorption leads to flexibility of the multilayer (increasing D) in the case of long chains PEM, it leads to an increase in rigidity of the multilayer (decreasing D) in the case of short chains PEM. Three possible contributions to ΔD during multilayer deposition in the liquid phase are dissipation at the substrate - polyelectrolyte interface, polyelectrolyte - liquid interface, including effects of roughness and hydrophilicity of the surface, and amount of swelling water and void water trapped within the polyelectrolyte multilayers.

Chapter 7

Types of multilayer growth

Abstract

Type of growth of polyelectrolyte multilayers (PEM) namely linear, exponential and unstable growth, has been investigated as a function of different polyelectrolyte pairs, type of salt, amount of salt and degree of charge of the polycation using complementary techniques such as Neutron Reflectometry, Ellipsometry, Contact Angle measurements, Quartz Crystal Microbalance (QCM) and Fluorescence Recovery After Photobleaching (FRAP). The different polyelectrolyte pairs investigated include poly(styrene sulfonate) (PSS)/poly(allylamine hydrochloride) (PAH), PSS/ poly[(diallyl dimethyl ammonium chloride)-stat-(N-methy- lactamide)] (PDADMAC-stat-NMVA), Hyaluronic acid (HA)/PAH, and sodium carboxy-methylcellulose (CMC)/PAH. The competition between ion specific effect (NaF, NaCl and NaBr) and electrostatic interactions at 0.1 M, 0.25 M and 0.5 M are considered. Ions with higher polarizability, larger size with smaller hydration shell turns to interact stronger with the polyions thereby forming thicker and rougher multilayers. The same effect is observed for increasing the ionic strength of the dipping solution which in turn increases chain mobility and flexibility thereby leading to adsorption of thicker multilayers. At low ionic strength (below 0.1 M) electrostatic interactions are dominant but above that dispersion forces become very important due to strong screening of charges along the polymer chains. Decreasing polycation degree of charge, increasing ionic strength, increasing chain mobility and preparation from solutions with large ions lead to transition from linear to exponential growth and even further to unstable multilayers.

7.1 Introduction

The self assembly layer-by-layer method[4,159] developed nearly two decades ago makes fabrication of polyelectrolyte multilayers (PEM)[75] very simple. Studies on PEM growth have shown that the thickness of the PEM can be fabricated with Å precision provided the right parameters which determine PEM growth are carefully tuned. This chapter focuses on the different types of PEM growth namely: *linear growth* (constant thickness increment per double layer (DL)), non-linear growth usually called "*exponential growth*" in the literature (increasing increment with increasing number of DL) and *unstable growth*

(alternating adsorption and desorption). The choice of polyelectrolyte pairs determines whether the multilayer will grow linearly, exponentially or if no PEM will be formed. Aside the polyelectrolyte pairs that determines the type of multilayer growth, certain
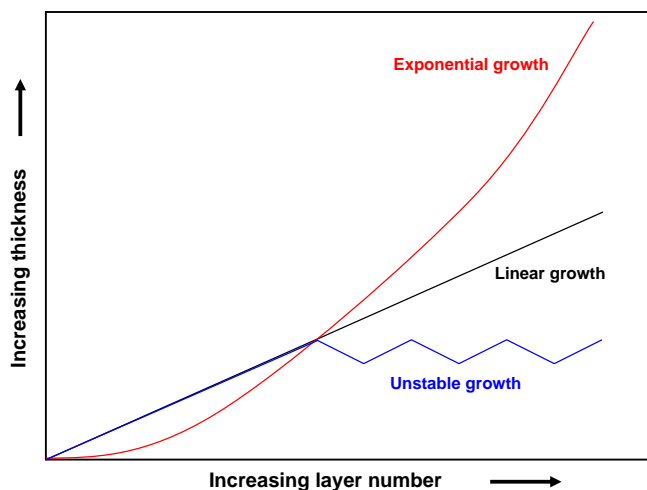
Figure 7.1: *Schematic illustration of different types of polyelectrolyte multilayer growth.*

parameters are also known to influence the type of growth. These parameters include ionic strength, type of ion, polymer charge density (e.g. PDADMAC-stat-NMVA), pH in case of weak polyelectrolytes (e.g. PAA), type of solvent, temperature, adsorption time (short chains PSS/PDADMAC), polymer concentration, and the molecular weight of the polyelectrolytes.

A number of studied multilayers in the literature presented linear growth[79,80,160] including the work of Wong et al.[98] where poly(styrene sulfonate)/poly(allylamine hydrochloride) (PSS/PAH) multilayer studied with ellipsometry exhibited "odd-even effect" in the swollen state but a linear increase with increasing adsorption steps in the dry state. In this case the multilayer structure is said to be flatly conformed at the surface with each adsorbing layer penetrating into only a few previously adsorbed layers.

Examples of multilayers which constitute exponential growth include poly(L-glutamic acid) / poly(L-lysine) (PDA/PLL)[78] or Hyaluronic acid (HA)/PLL.[81] The exponential growth is said to be caused by high polyelectrolyte mobility leading to diffusion of layers deep in and out of the multilayer matrix. This growth type is also attributed to an increase of the film surface roughness with the number of adsorption steps. Garza et al.[161] presented a multilayer which exhibit a combination of exponential (HA/PLL) and linear (PSS/PAH) growth. He studied the multilayer made of several compartments containing "free polyelectrolytes" with Quartz Crystal Microbalance (QCM) and Confocal Laser Scanning Microscopy (CLSM) and showed that the linearly growing multilayer

acts as a barrier preventing polyelectrolyte diffusion from one compartment to another. On the other hand, Kovacevic et al.[162] showed that the stability of poly(acrylic acid) /
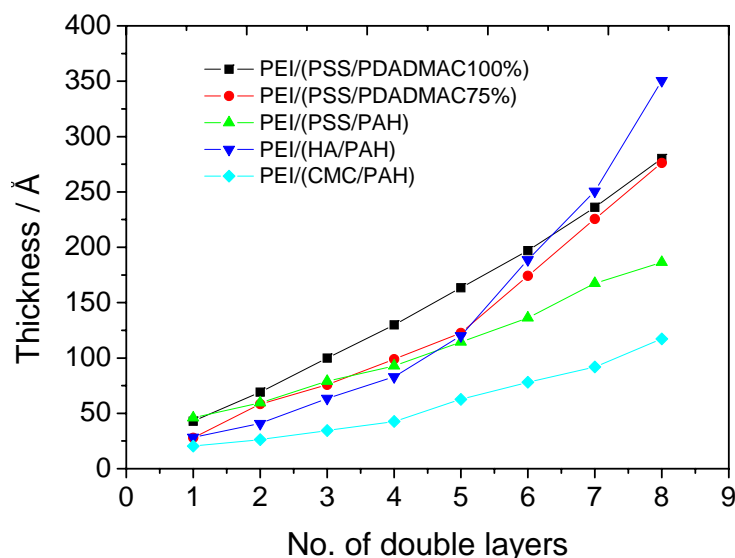
Figure 7.2: *Ellipsometry data on multilayers of different polyelectrolyte pairs prepared from 0.1 M NaCl aqueous solution and measured in ambient conditions (room temperature, 30-50 % relative humidity).*

poly(dimethylaminoethyl methacrylate) (PAA/PAMA) is dependent on the right amount of salt in the aqueous polyelectrolyte solution. It is concluded from the optical reflectometry experiments[162] that the adsorption/redissolution process can be attributed to (i) non-equilibration of the macromolecules during regular multilayer formation, (ii) plasticization of the multilayer by the added salt which causes the molecules to be sufficiently mobile leading to equilibration between the layer and surrounding solution, and (iii) the presence of excess polyelectrolyte brings the system to a one-phase region of the polyelectrolyte complex phase diagram. Despite all these previous studies on PEM growth, the use of different complementary experimental techniques to study the growth behaviour of PEM is still missing. In particular, the use of neutron reflectivity (which probes the internal structure of the films) to investigate the growth behaviour is lacking.

The aim of this work is to use complementary techniques such as Neutron Reflectometry, Ellipsometry, Contact Angle measurements, Quartz Crystal Microbalance (QCM), Atomic Force Microscopy (AFM) and Fluorescence Recovery After Photobleaching (FRAP) to understand the linear, exponential and unstable growth of PEM. The AFM surface roughness of the multilayers are determined as follows: The surface roughness is calculated by root-mean-square (rms) roughness from a (1×1) μm^2 box. This makes data comparison with neutron reflectivity measurements easier since neutrons have μm correlation length. The final value is an average of those calculated at different positions on each image. Different

polyelectrolyte pairs, salts, salt concentrations and degree of charge of PDADMAC are used to determine their effects on the type of growth of polyelectrolyte multilayers.

7.2 Results

Different experimental techniques are employed to study the type of growth of polyelectrolyte multilayers. The results and observations are categorized as follows: (i) Type of polyelectrolyte pairs, (ii) ionic strength, (iii) type of ion and (iv) degree of charge.

7.2.1 Multilayer growth as influenced by polyelectrolyte pairs

The type of polyelectrolyte pairs used during multilayer preparation can strongly affect the type of growth of the multilayer during preparation, i.e. whether the multilayer will grow linearly, exponentially or unstable growth due to redissolution.

In other to investigate this effect, specific polyelectrolyte pairs are chosen for the multilayer formation and the thickness measured with Ellipsometer. These polyelectrolyte pairs are: $PEI/(PSS/PDADMAC100\%)_n$, $PEI/(PSS/PDADMAC75\%)_n$, $PEI/(PSS/PAH)_n$, $PEI/(HA/PAH)_n$ and $PEI/(CMC/PAH)_n$ where n represents the number of double layers. The polyelectrolyte concentration during the preparation is 10^{-2} M (concentration of monomer units) and the salt concentration of the aqueous medium is 0.1 M NaCl. Figure 7.2 shows the thickness of the multilayer plotted against the number of double layers. The different growth patterns are seen by the different multilayer pairs. HA/PAH multilayer exhibits exponential growth where the multilayer thickness increases gradually from the first double layer up to the fifth double layer then a rapid increase in thickness after the fifth double layer. PSS/PDADMAC75% multilayer also grows exponentially but not as thick as the HA/PAH multilayer. PSS/PDADMAC100% and PSS/PAH multilayers grow linearly at low ionic strength such as 0.1 M NaCl.

On the other hand, CMC/PAH multilayer showed very thin increment per double layer which accounts for the low multilayer thickness of 120 Å after 8 double layers. PSS/PDADMAC100% and PSS/PDADMAC75% are both 275 Å thick. Although the multilayers have the same thickness the different growth types between them is seen from the shape of the growth curves. However, the difference is clearly seen at higher ionic strength (0.25 M NaCl) as will be shown later. This observation is in agreement with the work of Voigt et al.[110] where at low ionic strength of 0.1 M NaCl, six double layers of both PSS/PDADMAC100% and PSS/PDADMAC75% are about 200 Å thick.

Polyelectrolyte Pairs	Ionic cond. Preparation	Ionic cond. Treatment	Diff. coeff. (cm^2/sec)	Nom. charge distance (Å)
CMC/PAH	0.5 M NaCl	0.1 M NaCl	$< 10^{-15}$	10/2.5
PSS/PAH	0.5 M NaCl	0.1 M NaCl	$(2.0 \pm 1.0) \times 10^{-15}$	2.5/2.5
PSS/PDAD.100%	0.1 M NaCl	0.1 M NaCl	$(1.4 \pm 1.0) \times 10^{-14}$	2.5/3.6
PSS/PDAD.75%	0.1 M NaCl	0.1 M NaCl	$(9.0 \pm 2.3) \times 10^{-14}$	2.5/4.8
HA/PAH	0.1 M NaCl	0.1 M NaCl	$(7.5 \pm 2.0) \times 10^{-12}$	10/2.5

Table 7.1: *Diffusion coefficient of the FITC-PAH layer (0.5 M NaCl) adsorbed on top of different polyelectrolyte pairs as obtained from FRAP measurement. The multilayers are prepared from 0.1 M NaCl except for CMC/PAH and PSS/PAH which are prepared from 0.5 M NaCl solution to increase their mobility since they are much rigid and glassy. After the preparation the multilayers are treated in 0.1 M NaCl solution for 24 h before measurement.*

Since the mobility of the polyelectrolyte pairs affects the type of growth, FRAP measurement is performed to support the results of the ellipsometry in order to draw convincing conclusions. The diffusion coefficient of each polyelectrolyte pair is calculated from the lateral mobility of FITC labelled PAH layer into a bleached spot. The FITC-PAH, CMC/PAH and PSS/PAH are prepared from 0.5 M NaCl and the rest are prepared from 0.1 M NaCl. The multilayers are treated in 0.1 M NaCl solution for 24 h to enhance the mobility of the chains before measurement. The diffusion coefficient is calculated using equation 3.33. The results which are shown in Table 7.1 show that the order of increasing diffusion coefficients correspond to the order of increasing multilayer thickness obtained from ellipsometry. The order of increasing mobility correlates with the charge density (norminal charge distance divided by the Bjerrum length in water (7.12 Å)) of the Polyelectrolyte pairs except for CMC/PAH. Although CMC and HA have the same charge density (1.4), it is not clear why the multilayers of CMC/PAH are exceptionally thin. The experiment is repeated but the same result is obtained.

7.2.2 Effect of ionic strength on type of growth

QCM data obtained from in-situ monitoring of multilayer growth shows that the growth type can be influenced by the ionic strength of the aqueous solution. Figure 7.3 shows the frequency shift and the corresponding adsorbed mass as a function of number of layers of PSS/PDADMAC100% multilayer prepared from different ionic strength of NaCl and NaBr. The adsorbed mass increases with increasing number of layers. As the ionic strength increases from 0.1 M to 0.25 M the multilayer growth changes from linear growth to exponential growth for both ion types. At 0.5 M the exponential growth becomes
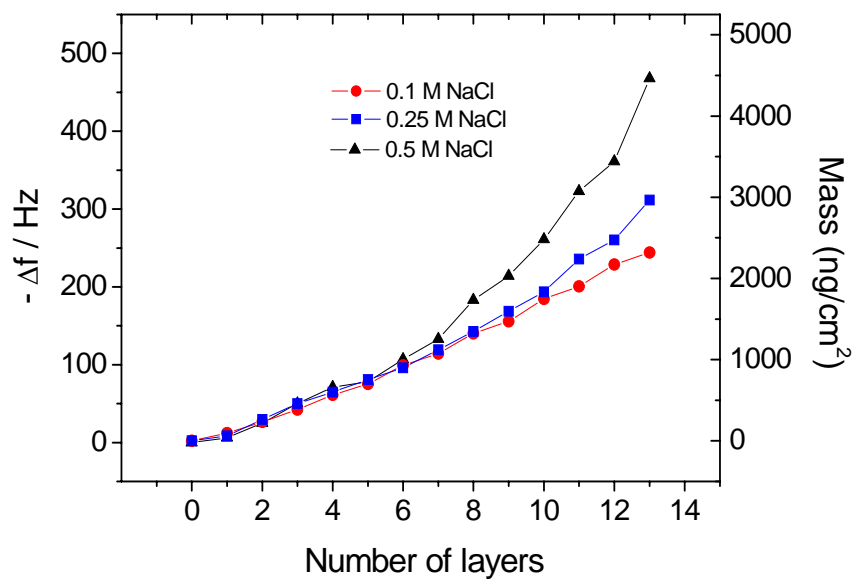
(a)
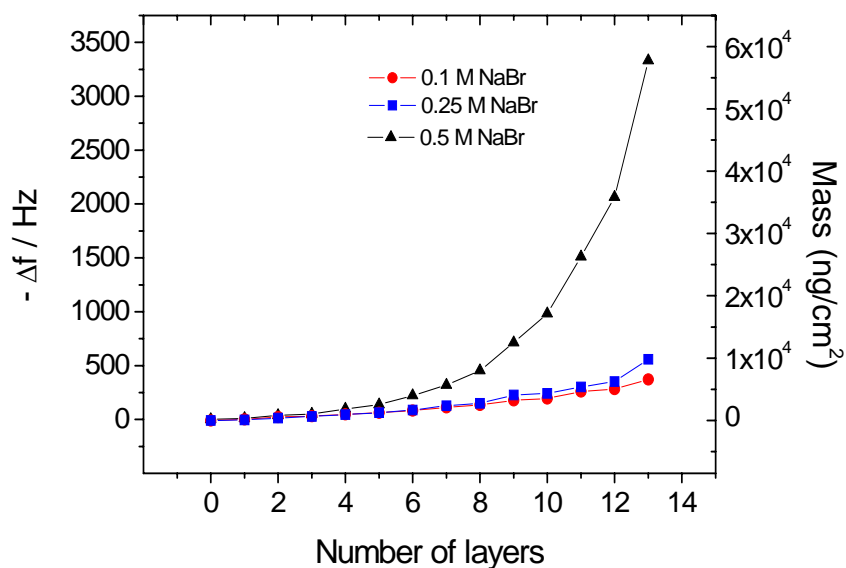
(b)

Figure 7.3: *QCM data on PSS/PDADMAC100% multilayer showing change in frequency and the corresponding adsorbed mass with increasing layer number. (a) Multilayers prepared from different NaCl concentrations, and (b) different NaBr concentrations. X-axis: Even and odd numbers represent PSS and PDADMAC adsorption respectively except number 1 which represents PEI adsorption.*

very pronounced due to effective screening of the charges along the polyelectrolyte chain as a result of the high amount of counterions in the solution. The effective screening

of the charges leads to a rearrangement of the chains from flat conformation to coiled conformation and hence the higher adsorbed mass. The Sauerbrey relation, equation 3.31 is used to calculate the mass per unit area. To justify the Sauerbrey relation, the data is further analyzed using the Voigt model. Comparing the two models showed no significant difference because the frequency overtones are closed to each other. Moreover the energy dissipated during the vibration of the quartz crystal is not too high.

7.2.3 Effect of type of ion

Figure 7.4 shows PSS/PDADMAC multilayers prepared from 0.5 M concentration of NaF, NaCl and NaBr.
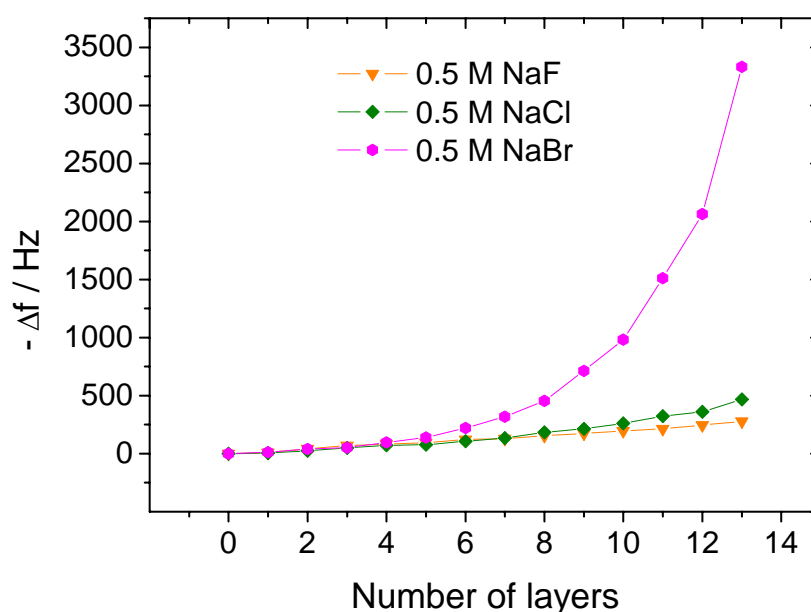
Figure 7.4: *Frequency shift versus number of layers of PSS/PDADMAC100% multilayers prepared from aqueous solution of 0.5 M NaF, NaCl and NaBr. X-axis: Even and odd numbers represent PSS and PDADMAC adsorption respectively except number 1 which represents PEI adsorption.*

The multilayer prepared from NaBr has the highest frequency shift, followed by NaCl and then NaF. The frequency shift is directly proportional to the adsorbed mass per unit area as observed in Figure 7.3. The increasing order NaF<NaCl<NaBr, is due to the ion specific effect as explained in Chapter 4. Among the three type of ions, NaBr multilayer grows exponentially while NaCl and NaF multilayers grow linearly.

7.2.4 Effect of degree of charge

Multilayers prepared from PSS/PDADMAC75% at certain ionic strength and ion type causes the multilayer growth to become unstable.
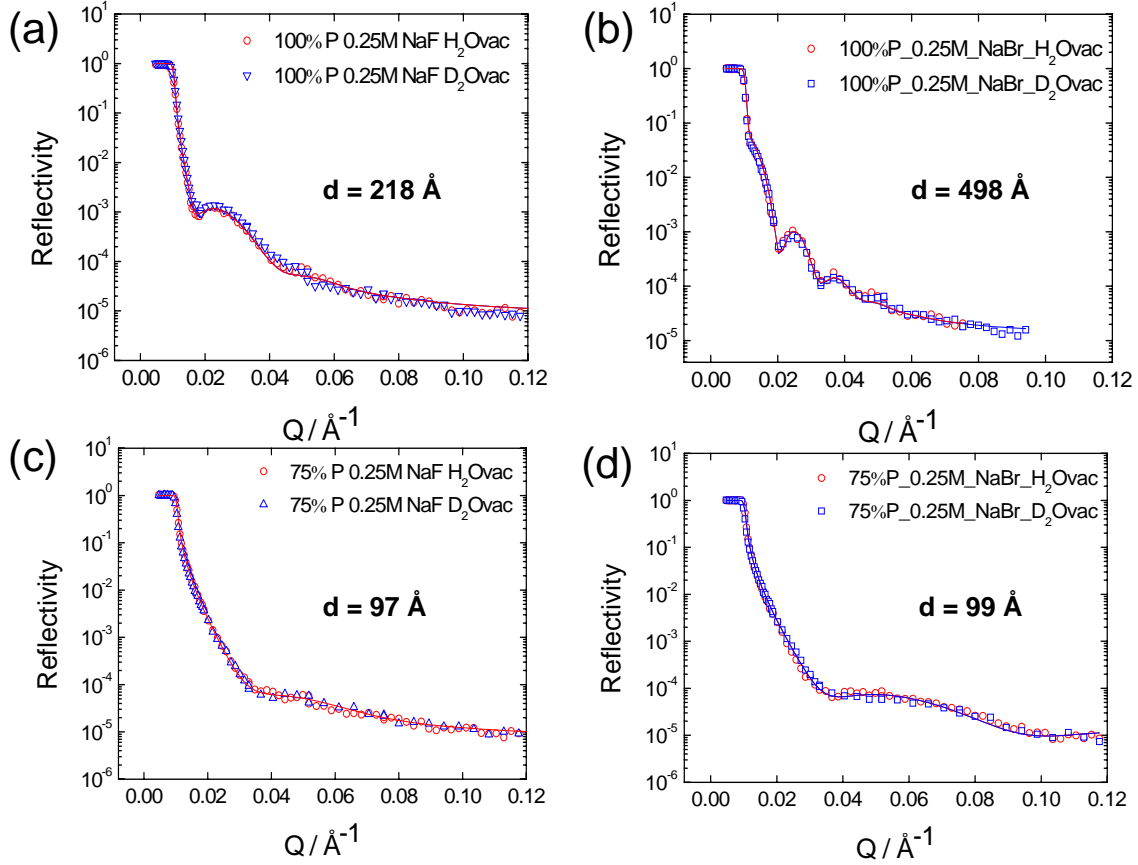
Figure 7.5: *Neutron reflectivity of PSS/PDADMAC100% (100%P) and PSS/PDAD-MAC75% (75%P) prepared from 0.25 M NaF or NaBr. H_2Ovac and D_2Ovac indicate measurement against vacuum after exposure to either H_2O liquid or D_2O liquid respectively. Open symbols represent data points and solid lines represent best fit. Data from both H_2Ovac and D_2Ovac are presented to show that both water isotopes produce identical reflectivity curves. This observation is explained as no displacement of hydration water or exchange of H by D in the water molecules even after eight hours of exposure to D_2O liquid.*

This unstable growth is observed in the multilayers of PSS/PDADMAC75% - NaF: 0.5 M, NaCl: 0.5 M and NaBr: 0.25 M and 0.5 M. Figure 7.5 shows neutron reflectivity data of six double layers of PSS/PDADMAC100% and PSS/PDADMAC75% prepared from 0.25 M aqueous solution of NaF or NaBr. PSS/PDADMAC100% multilayers prepared from 0.25 M NaF and 0.25 M NaBr are stable as can be seen from the multilayer thicknesses i.e. 218 Å and 498 Å for NaF and NaBr, respectively. However, the multilayers of

PSS/PDADMAC75% prepared from the same amount NaF and NaBr showed NaF PEM to be very thin (only 97 Å thick) and NaBr PEM to be unstable (99 Å thick). The results are in good agreement with literature,[73] where PSS/PDADMAC75% prepared at 0.25 M NaBr showed unstable (zig-zag) growth.
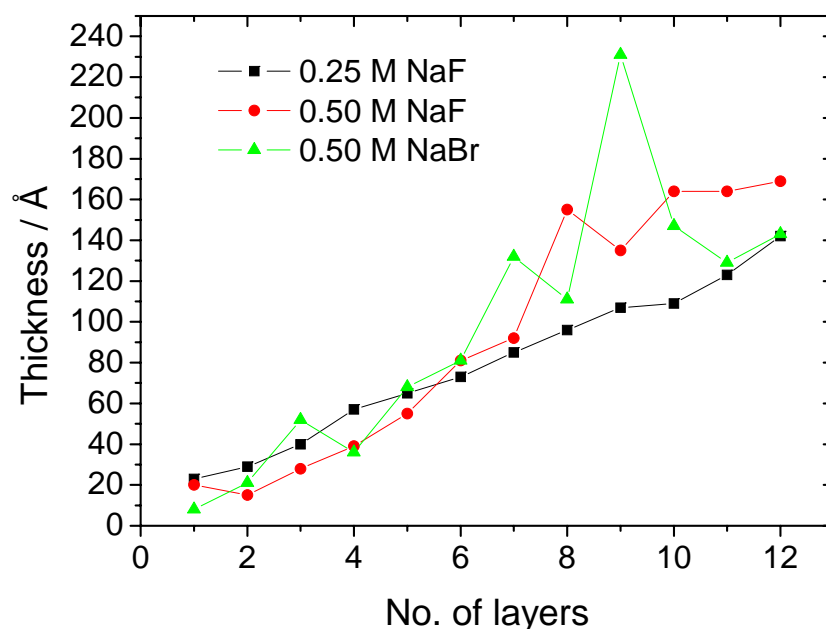
Figure 7.6: *Ellipsometry data on (PSS/PDADMAC75%)$_6$ multilayer prepared from aqueous solution of 0.25 M NaF, 0.50 M NaF and 0.50 M NaBr, measured at ambient conditions.*

In the same literature reference,[73] it is reported that PSS/PDADMAC75% multilayer becomes unstable at 0.5 M NaCl. To confirm whether the multilayers of 0.25 M NaF, 0.5 M NaF and 0.5 M NaBr are just too thin or unstable the thickness of the same multilayers are measured by ellipsometry where the layer-by-layer thickness can be determined. The result is presented in Figure 7.6. A summary of results obtained from the different ion types, ionic strength and degree of charge are shown in Tables 7.2 and 7.3. Deducing from the total multilayer thickness as seen in the table, PDADMAC100% multilayer grows linear when prepared from 0.25 M NaF but grows exponentially when prepared from 0.25 M NaBr. However the multilayer of PDADMAC75% becomes very thin when prepared from 0.25 M NaF and unstable when prepared from 0.5 M NaF and 0.25 M NaBr. Another observation is that, at lower ionic strength of 0.1 M NaBr PDADMAC75% multilayer is stable but become unstable at concentrations higher than 0.1 M NaBr.

Ion type &	(PSS/PDADMAC100%)$_6$			(PSS/PDADMAC75%)$_6$		
Ionic strength	d / Å	ρ (10^{-6} Å^{-2})	σ / Å	d / Å	ρ (10^{-6} Å^{-2})	σ / Å
0.10 M NaCl	144 ± 1	1.33 ± 0.02	10 ± 4	142 ± 3	1.33 ± 0.04	11 ± 5
0.10 M NaBr	229 ± 5	1.04 ± 0.02	23 ± 4	209 ± 5	1.02 ± 0.03	39 ± 5
0.25 M NaF	218 ± 3	0.95 ± 0.02	25 ± 5	97 ± 3	0.95 ± 0.03	32 ± 7
0.25 M NaCl	267 ± 6	1.34 ± 0.03	11 ± 4	306 ± 5	0.99 ± 0.04	27 ± 6
0.25 M NaBr	498 ± 4	1.05 ± 0.02	50 ± 8	99 ± 4	0.70 ± 0.03	60 ± 8
0.50 M NaF	300 ± 5	1.20 ± 0.03	34 ± 6	76 ± 4	0.65 ± 0.02	37 ± 4

Table 7.2: *Parameters extracted from Neutron reflectivity data with Parratt's dynamic approach[96] using the Parratt32 fitting software (provided by HZB). d, ρ and σ stand for thickness, scattering length density and roughness respectively.*

	(PSS/PDADMAC100%)$_6$					
	dry	swollen	dry	swollen	dry	swollen
Ionic strength	d / Å	d / Å	σ / Å	σ / Å	ρ (10^{-5} Å^{-2})	ρ (10^{-5} Å^{-2})
0.10 M NaCl	160 ±2	226 ±3	11 ±1	24 ±2	1.16 ±0.02	1.28 ±0.03
0.25 M NaCl	297 ±4	428 ±5	12 ±1	32 ±6	1.27 ±0.02	1.29 ±0.03
0.50 M NaCl	507 ±9	757 ±6	21 ±4	42 ±7	1.15 ±0.02	1.17 ±0.04
PDADMAC75%						
0.10 M NaCl	140 ±2	207 ±2	13 ±2	25 ±3	1.16 ±0.02	1.27 ±0.02

Table 7.3: *Parameters extracted from X-ray reflectivity data with Parratt's dynamic approach[96] using the Parratt32 fitting software (provided by HZB). d, ρ and σ stand for thickness, electron density and roughness respectively. For the dry thickness the film is measured against P_2O_5 dry powder and for the swollen thickness the film is measured against H_2O vapour. (PSS/PDADMAC75%)$_6$ is represented by PDADMAC75%.*

7.3 Discussion

The results presented that the type of growth of polyelectrolyte multilayers can be tuned by the preparation conditions: ionic strength, type of ion, type of polyelectrolyte pair and charge density. All three types of growth can be achieved.

7.3.1 Effect of polyelectrolyte pairs

The linearly growing PSS/PAH and PSS/PDADMAC100% multilayers are a result of charge overcompensation which is required for multilayer formation. In this case intrinsic and extrinsic complex formation in the solution leads to equal adsorbed amount per deposition cycle.

The mechanism that leads to the exponential growth is well investigated by the use of proteins such as polypeptides and polysaccharides,[78,83,163] where the polyelectrolytes (e.g. PLL or HA) are mobile. Lavalle et al.[78,164] explained that in the exponential growth mode, chains which have not formed complex, diffuse into the multilayer matrix[9] and diffuse back to the surface. At the surface, this mobile chain forms complex with another oppositely charged polyelectrolyte. In this case additional complexes are formed between polyelectrolytes of opposite charges at the multilayer surface, aside the regular intrinsic and extrinsic complexes already taking place. The additional complex formation leads to mass gain by the multilayer. The results of the FRAP measurement as shown in Table 7.1,
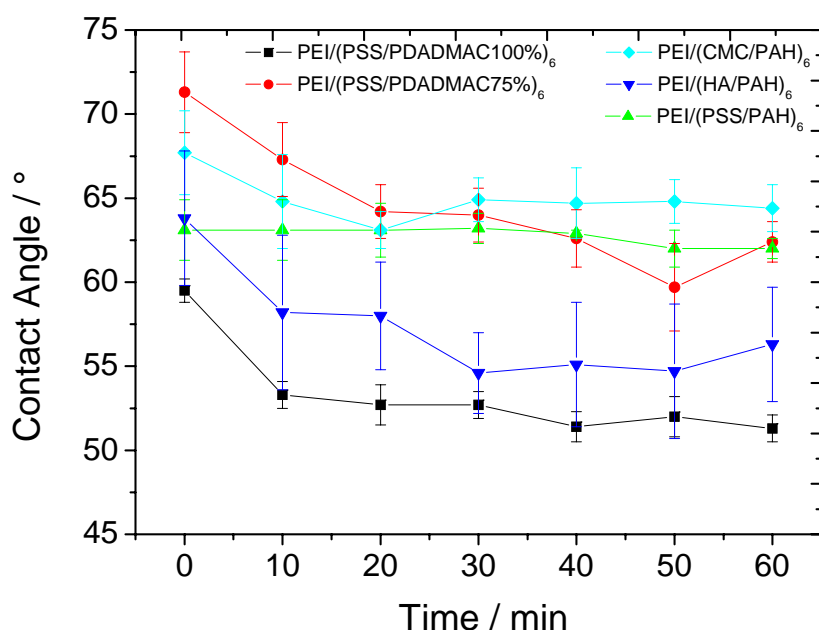
Figure 7.7: *Contact angles versus time for various polyelectrolyte pairs measured against saturated water vapour in a cell. The humidity cell is chosen to prevent evaporation of the water droplet from the surface of the multilayer. The multilayers are allowed 15 minutes saturation time to ensure equilibrium conditions.*

confirm the exponential growth of HA/PAH and PSS/PDADMAC75% multilayers. This is due to their higher diffusion coefficient compared to the linearly growing multilayers. The diffusion coefficient increases in the order PSS/PAH < PSS/PDADMAC100% < PSS/PDADMAC75% < HA/PAH.

The unexpectedly thin multilayer growth observed by CMC/PAH can be due to either too long dipping time or inadequate balance of counterions because of the presences of at least one weak polyelectrolyte (PAH). In such polyelectrolyte pairs the dipping time is very critical since after some time the polyelectrolyte complexes become soluble and the multilayer is destroyed.[162] The behaviour of such polyelectrolyte pairs can be well

explained by the stability diagram of an adsorbed multilayer consisting of oppositely charged polyelectrolytes reported by Kovacevic et al.[162]

In some cases the type of growth can be correlated with certain structural properties of the multilayer. However, there is no correlation observed between the type of growth and the hydrophobicity of the multilayer surface. Figure 7.7 exhibits the water contact angle against time for PSS/PAH, PSS/PDADMAC100%, PSS/PDADMAC75%, HA/PAH, and CMC/PAH multilayers. The water contact angle of the multilayers in this plot are unusully high. The reaseon could be the age of the films before measurement (measured 48 hours after preparation)

7.3.2 Effect of ion type and ionic strength

The type of ion and the ionic strength influence the type of growth of polyelectrolyte multilayers in terms of thickness and roughness. Type of ion and ionic strength increases the vertical mobility of the polyelectrolyte chains which is a requisite for the transition from linear to exponential growth. Summary of these two effects can be seen in Figure 7.8(a) where the ellipsometric thickness of (PSS/PDADMAC100%)$_6$ multilayers prepared from NaF, NaCl and NaBr are plotted aagainst the ionic strength of the aqueous solution. The plot shows transition from linear growth to exponential growth and vice versa depending on the type of ion and the ionic strength of the dipping solution. As one moves from NaF to NaCl and to NaBr, the slope gets steeper or the gradient of the slope increases. The same is observed for increasing the ionic strength of the dipping solution.

Increasing ionic strength increases screening of the charges along the polyelectrolyte chains and increases chain flexibility, this causes more coiling of the polyelectrolyte chains which results in larger thickness and higher roughness of the adsorbed layer.[9] For the linearly growing multilayers the chains are adsorbed with flat conformation while in the exponentially growing multilayers the chains are adsorbed with coil conformation.

The ion specific effect as arranged in the Hofmeister series explains the dependency of the growth type on the type of ion. Among the three anions: F^-, Cl^- and Br^-, the smallest anion (F^-) has the least polarizability, highest electric field at short distances and prefer to keep its water of hydration. In addition, F^- has a well-ordered larger hydration shell than Br^-, which on the other hand, is larger in size with a higher polarizability, a weak electric field and small hydration shell which can be easily removed. The Br^- therefore adapts to the environment (polycation) easily which leads to a stronger interaction between them causing a kind of bridging and/or overlap of hydration shells of counterions and
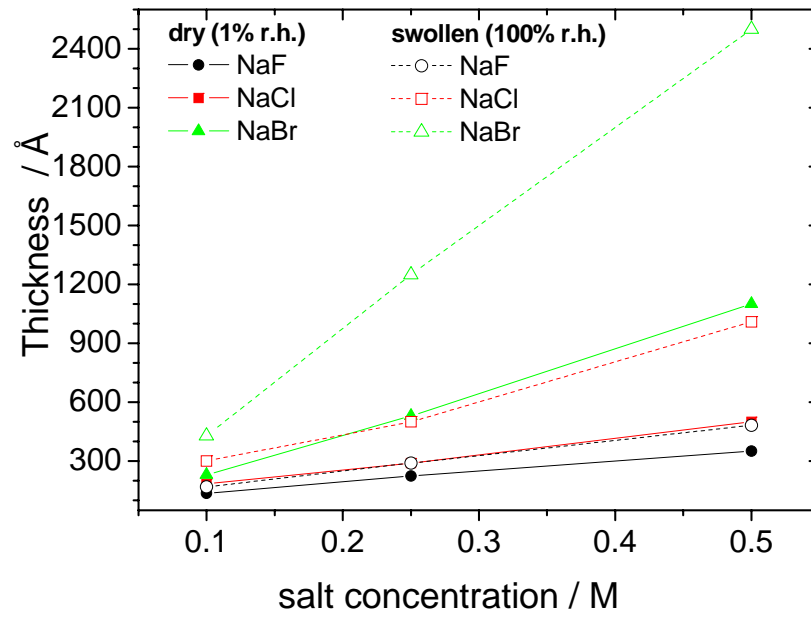
(a)
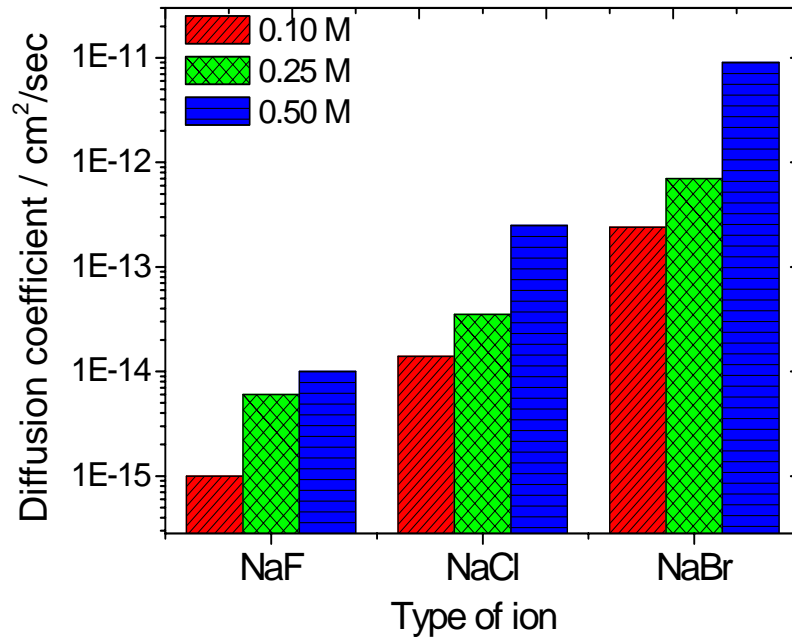
(b)

Figure 7.8: *(a) Ellipsometry data of (PSS/PDADMAC100%)₆ multilayers prepared from NaF, NaCl and NaBr. Dry thickness (closed symbols) and swollen thickness (open symbols). (b) Diffusion coefficient of (PSS/PDADMAC100%)₅/PSS/FITC-PAH as a function of type of ion. Three ionic strengths (0.1 M, 0.25 M and 0.5 M) are used during preparation and for 24 hours treatment 0.1 M NaCl solution is used. The FITC-PAH is prepared from 0.5 M NaCl solution.*

polycations. Consequently the amount of extrinsically compensated polymer charges in
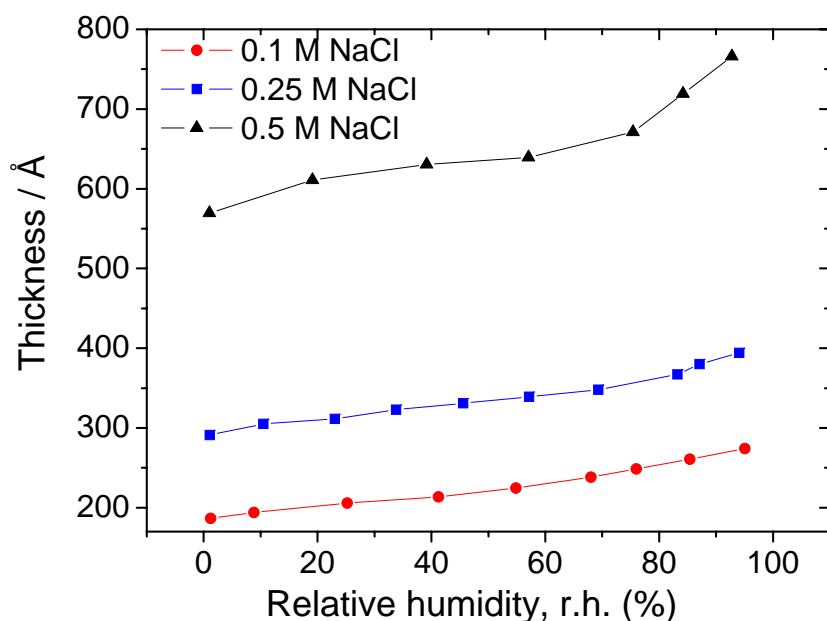
Figure 7.9: *Ellipsometry data of (PSS/PDADMAC100%)$_6$ multilayers prepared from 0.1 M. 0.25 M, 0.5 M NaCl. Thickness plotted as a function of increasing relative humidity. 100% relative humidity means measurement aagainst water.*

the case of Br$^-$ should be higher and the density of complexes lower than in the case of F$^-$. This increases the chain mobility as shown in Figure 7.8(b) which in turn will lead to transition from linear growth to exponential growth. This result is in agreement with literature.[73,120,165]

There is a correlation between the type of growth and the swelling behaviour of the multilayers. Figure 7.8(a) shows that the slope of the swollen thickness is steeper than that of the dry thickness. The same correlation can also be seen in Figure 7.9 where the thickness of (PSS/PDADMAC100%)$_6$ multilayers prepared from 0.1 M. 0.25 M, 0.5 M NaCl, is plotted against changing relative humidity. The multilayer of 0.5 M NaCl swells faster than that of 0.25 M and 0.1 M NaCl.

7.3.3 Effect of degree of charge

The effect of degree of charge on multilayer growth is in two ways: (i) Induces transition from linear growth to exponential growth e.g. from PSS/PDADMAC100% to PSS/P-DADMAC75% at 0.25 M NaCl. This is in agreement with Voigt et al.,[110] where it is shown that the minimum degree of charge of PDADMAC required to form stable PEM
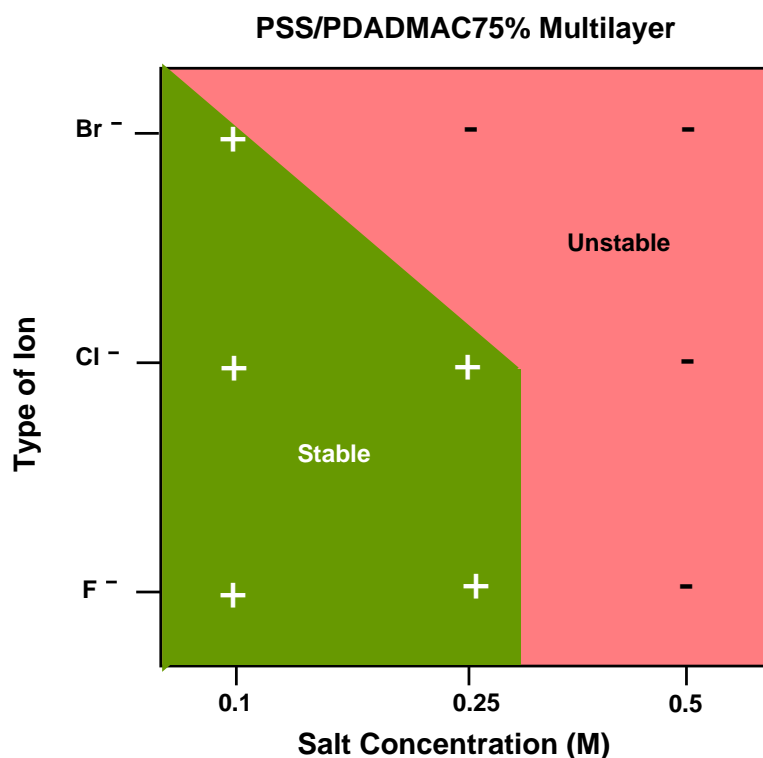
Figure 7.10: *Stability diagram of PSS/PDADMAC75% multilayer showing the effect of degree of charge in combination with ion type and ionic strength. The signs plus (+) and minus (-) stand for stable and unstable growth, respectively. The green zone indicates region of stability and the pink zone indicates region of instability. This sketch is based on complementary data from neutron reflectivity and ellipsometry. The data 0.5 M NaCl is adapted from Wong et al.[73]*

with PSS is 70%. (ii) Produces unstable multilayer at certain concentrations for certain anions as can be seen in Figure 7.10.

The exponential growth of PDADMAC75% over PDADMAC100% at 0.25 M NaCl is due to the charge density of PDADMAC75%. At higher ionic strength of 0.25 M NaCl, more extrinsic complexes are formed in the solution between the counterions and the polyelectrolyte chains. Because of the lower charge density of PDADMAC75% the weak electrostatic repulsion along the polymer backbone favours stronger coiling of the chains than in the case of the fully charge PDADMAC. The coil conformation of PDADMAC75% gives rise to higher adsorbed amount leading to exponential growth. In the case of PDADMAC100%, there is strong electrostatic repulsion between the charges along the polyelectrolyte backbone forcing the the polyelectroyte chains to be extended, stiff and flat conformation.

The multilayer of PDADMAC100% is stable against all three anions (F^-, Cl^-, and Br^-) and for all three concentrations 0.1 M, 0.25 M and 0.5 M, but for PDADMAC75% this
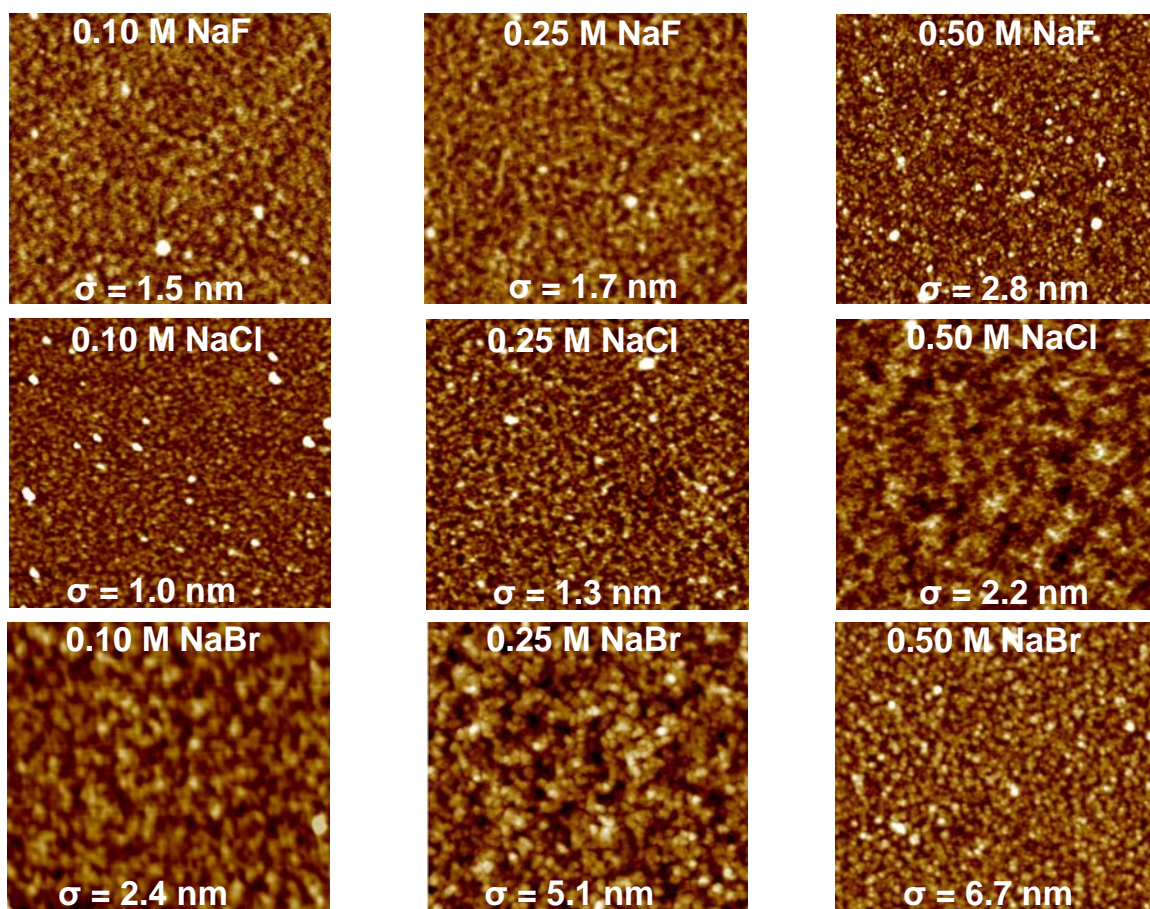
Figure 7.11: *AFM images scanned against air of (PSS/PDADMAC100%)$_6$ multilayer prepared from aqueous solution of NaF, NaCl and NaBr (rows). The columns represent three ionic strengths: 0.10 M, 0.25 M and 0.50 M, respectively. Scan size: 2.5 × 2.5 μm^2.*

is not the case. At lower ionic strength of 0.1 M, electrostatic interactions are dominant and the multilayers of PDADMAC75% are stable. Above ionic strength of 0.1 M, dispersion forces overcome the effect of electrostatic interactions and the multilayer of PDADMAC75% becomes unstable against F$^-$ and Br$^-$ as shown in Figure 7.10. Wong et. al.[73] reported that at 0.5 M NaCl, PDADMAC75% multilayer becomes unstable.

7.3.4 Surface roughness and topology

Figures 7.11 and 7.12 present the AFM images of PEI/(PSS/PDADMAC100%)$_6$ and PEI/(PSS/PDADMAC75%)$_6$ multilayers, respectively. The multilayers are prepared from NaF, NaCl and NaBr (columns) at 0.1 M, 0.25 M and 0.5 M (rows). The images show homogeneously adsorbed PEMs with grain-like morphology. The images have similar surface topology irrespective of salt type and ionic strength. However, increasing ionic strength
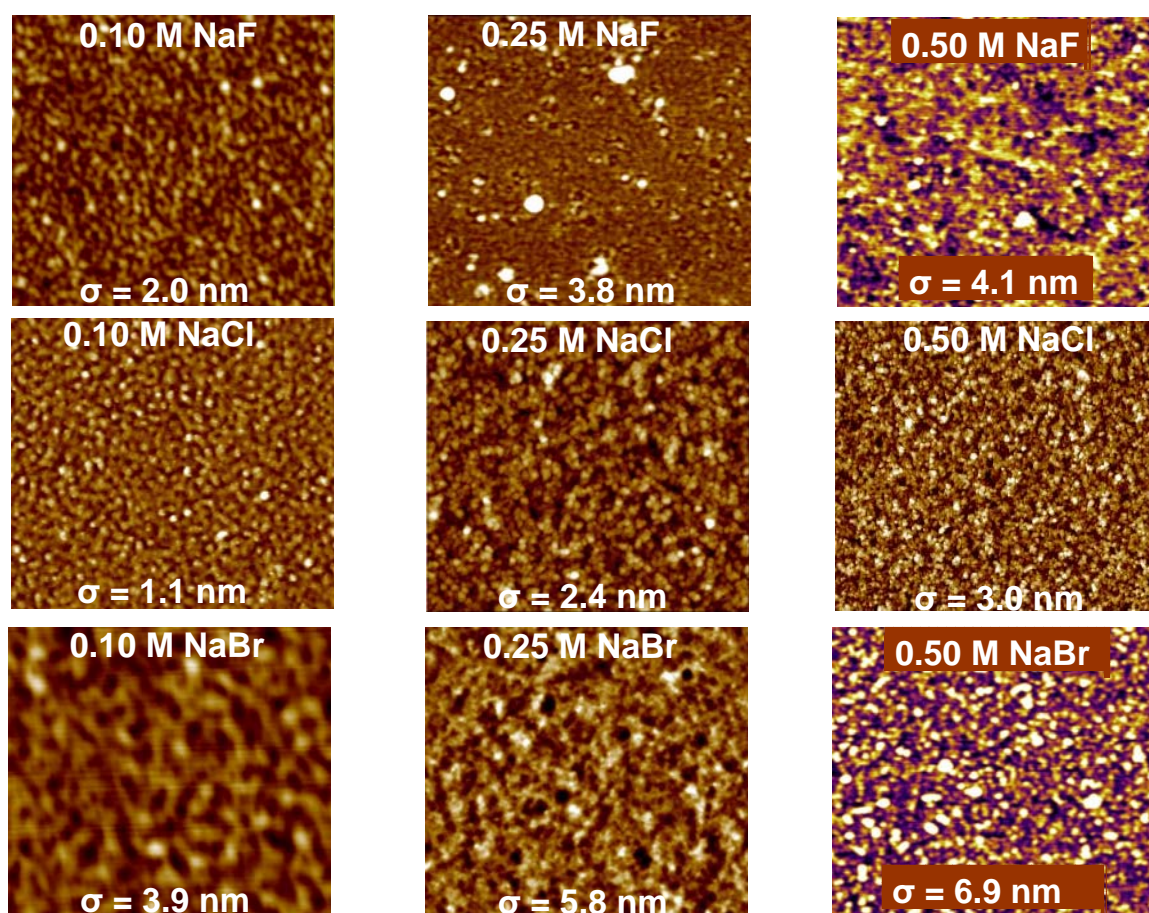
Figure 7.12: *AFM images scanned against air of (PSS/PDADMAC75%)$_6$ multilayer prepared from aqueous solution of NaF, NaCl and NaBr (rows). The columns represent three ionic strengths: 0.10 M, 0.25 M and 0.50 M, respectively. Scan size: $2.5 \times 2.5 \ \mu m^2$.*

increases the surface roughness for each type of salt. Increasing ionic strength increases effective screening of charges along the polyelectrolyte chain thereby reducing the electrostatic attraction between the chain and the multilayer leading to stronger coiling, higher mobility and interdigitation of the chains. This in turn leads to rougher multilayers.

The effect of type of ion on the roughness is different from the effect of ionic strength. The effect of type of ion on roughness does not follow systematically the Hofmeister series. The roughness increases in the order NaCl < NaF < NaBr. In the previous chapters, ion-specific effect is explained as the reason for ions having larger size, higher polarizability and smaller hydration shell to react stronger with polyions leading to stronger coiling of the chains. The increasing coiling of the chains leading to an increasing film thickness has two counteracting effects on the roughness. A slight increasing flexibility of the PDADMAC chains due to a stronger interaction with anions from F^- to Cl^- leads to a stronger ability for rearrangement and therefore to a smoother interface. A further increasing coiling

(from Cl^- to Br^-) leads to rougher surfaces.[9,73,119]

The multilayers of PEI/(PSS/PDADMAC75%) are rougher than the multilayers of PEI/-(PSS/PDADMAC75%) becuase of the lower charge density of PDADMAC75%. This result is in good agreement literature.[110] At higher charge densities, the roughness decreases slightly due to an increase in the electrostatic repulsion between charged segments that makes PDADMAC100% adsorb in a more flat conformation.[74]

7.4 Conclusion

Polyelectrolyte multilayer growth has been investigated by varying preparation conditions like type of polyelectrolyte pairs, type of ion, ionic strength of the dipping solution and the degree of charge of PDADMAC. The experiments which are performed using different techniques such as Ellipsometry, QCM, FRAP, AFM, Neutron and X-ray Reflectometry give complementary results.

Among multilayers of different polyelectrolyte pairs, the polyelectrolyte with higher mobility turns to have exponential growth due to diffusion of free mobile chains in and out of the multilayer matrix thereby forming extra complexes with the adsorbing layer which results in higher adsorbed amounts. The less mobile polyelectrolyte pairs grow linearly with increasing adsorption cycles. Polyelectrolyte pairs containing at least one weak polyelectrolyte turns to have unstable multilayer growth due to inadequate charge distribution along the chains which leads to redissolution of the complex after some time.

The results show that increasing ionic strength and preparing from solution of large highly polarized ions with smaller hydration have similar effect on the mode of growth of the multilayers. The bigger ions interact strongly with charged polyelectrolytes leading to thicker and rougher multilayers. At low ionic strength electrostatic interactions dictate the mode of growth and dispersion forces play a minor role. However, ion specific effects become dominant at elevated ionic strength i.e. 0.25 M and higher, due to strong electrostatic screening of charges along the polyelectrolyte chains. It is therefore concluded that increasing ionic strength, increasing ion size and decreasing polymer charge density (from 100% to 75%) support transition from linear to exponential growth and in some cases unstable multilayers.

Finally, PDADMAC100% multilayer is always stable when prepared from NaF, NaCl and NaBr at 0.1 M, 0.25 M and 0.5 M. The stability of PDADMAC75% critically depends

on the type of ion especially above 0.1 M where dispersion forces dominate electrostatic interactions.

Chapter 8

Summary and Outlook

8.1 Summary

The control of correlation between structure and ion distribution within polyelectrolyte multilayers are investigated. Both sensitivity to external stimuli and the stability of thin film are considered. The properties of the multilayer are scanned in order of layer by layer increase in thickness. Polyelectrolyte multilayers are fabricated by alternate adsorption of polyanions and polycations on a planar substrate. The thesis has addressed the profile of the properties across the polyelectrolyte multilayers as a function of the preparation parameter and the effect of the solid substrate.

In Chapter 4, the thesis addressed the effect of ionic strength and type of ion on the structure and water content of polyelectrolyte multilayers. Polyelectrolyte multilayers of poly(sodium-4 styrene sulfonate) (PSS) and poly(diallyl dimethyl ammonium chloride) (PDADMAC) prepared at different NaF, NaCl and NaBr concentrations, have been investigated by neutron reflectometry against vacuum, H_2O and D_2O. Both thickness and water content of the multilayers increase with increasing ionic strength and increasing ion size. Two types of water are identified, "void water" which fills the voids of the multilayers and does not contribute to swelling but to a change in scattering length density and "swelling water" which directly contributes to swelling of the multilayers. The amount of void water decreases with increasing salt concentration and anion radius while the amount of swelling water increases with salt concentration and anion radius. This is interpreted as a denser structure in the dry state and larger ability to swell in water (sponge) for multilayers prepared from high ionic strengths and/or salt solution of large anions. No exchange of hydration water or replacement of H by D was detected even after eight hours incubation time in water of opposing isotopic composition.

In chapter 5, the swelling behavior of polyelectrolyte multilayers (PEMs) of poly(sodium - 4 styrene sulfonate) (PSS) and poly(diallyl dimethyl ammonium chloride) (PDADMAC) prepared from aqueous solution of 0.1 M and 0.5 M NaCl are investigated by ellipsometry and Atomic Force Microscopy (AFM). The study shows that from 1 double-layer up to 4 double-layers from 0.1 M NaCl, the amount of swelling water in the PEMs decreases with increasing number of adsorbed double layers. This is explained by an increase in polyelectrolyte density as a result of the attraction between the positively charged outermost PDADMAC layer and the Si substrate. From 6 double layers to 30 double layers, the attraction is reduced due to a much larger distance between substrate and outermost

layer leading to a much lower polyelectrolyte density and a higher swelling water. In PEMs prepared from aqueous solution of 0.5 M NaCl the amount of water constantly increases which is related to a monotonically decreasing polyelectrolyte density with increasing number of polyelectrolyte layers. Studies of the surface topology also indicate a transition from a more substrate affected *interphase* behavior to a *continuum* properties of the polyelectrolyte multilayers. It is shown that the threshold for the transition from *interphase* to *continuum* behavior depends on the physical quantity that is investigated.

In chapter 6, structural and viscoelastic properties of high (HMW) and low (LMW) molecular weight polyelectrolyte multilayers (PEM) are investigated by the use of techniques like Ellipsometry, Atomic Force Microscopy (AFM), Contact Angle (CA) and Quartz Crystal Microbalance with Dissipation (QCM-D). The combination of the obtained results has the aim of highlighting analogies and differences between long and short chains poly(sodium styrene sulfonate) PSS / poly(diallyl dimethyl ammonium chloride) PDADMAC multilayers. Starting from different preparation settings, since the 20 minutes dipping time required for long chain systems have to be reduced to 5 minutes in the case of short chain multilayers in order to observe progressive layer-by-layer and reproducible growth, the structure and the response to changes in the external environment are investigated for both systems. A deep analysis of the QCM-D results showed that for both multilayer systems, i.e. long chains (PSS 70,000 g/mol, $\sim$340 monomer/unit; PDADMAC 135,000 g/mol, $\sim$840 monomer/unit) and short chains (PSS 6,520 g/mol, $\sim$32 monomer/unit; PDADMAC 5,000 g/mol, $\sim$31 monomer/unit) PEM, dissipation change (ΔD) and frequency change (Δf) show different adsorption phases. A link between energy dissipation and roughness, surface hydrophobicity and amount of adsorbed water was elaborated to justify the differences between the two systems.

In chapter 7, type of growth of polyelectrolyte multilayers (PEM) namely linear, exponential and unstable growth, has been investigated as a function of different polyelectrolyte pairs, type of salt, amount of salt and degree of charge of the polycation using complementary techniques such as Neutron Reflectometry, Ellipsometry, Contact Angle measurements, Quartz Crystal Microbalance (QCM) and Fluorescence Recovery After Photobleaching (FRAP). The different polyelectrolyte pairs investigated include poly(styrene sulfonate) (PSS)/poly(allylamine hydrochloride) (PAH), PSS/ poly[(diallyl dimethyl ammonium chloride)-stat-(N-methy- lactamide)] (PDADMAC-stat-NMVA), Hyaluronic acid (HA)/PAH, and sodium carboxy-methylcellulose (CMC)/PAH. The competition between ion specific effect (NaF, NaCl and NaBr) and electrostatic interactions at 0.1 M, 0.25 M and 0.5 M are considered. Ions with higher polarizability, larger size with smaller hydration shell turns to interact stronger with the polyions thereby forming thicker and

rougher multilayers. The same effect is observed for increasing the ionic strength of the dipping solution which in turn increases chain mobility and flexibility thereby leading to adsorption of thicker multilayers. At low ionic strength (0.1 M) electrostatic interactions are dominant but above that dispersion forces become very important due to strong screening of charges along the polymer chains. Decreasing polycation degree of charge, increasing ionic strength, increasing chain mobility and preparation from solutions with large ions lead to transition from linear to exponential growth and even further to unstable multilayers.

8.2 Outlook

During the course of the thesis, the quest to find answers to some challenging questions led to new projects which could be further undertaken. The following are some projects which could be done and possible research areas.

For instance, Neutron Reflectivity measurements offer a lot of detail analysis of the internal structure of the multilayers and has advantage over other techniques. The results obtained from Neutron Reflectivity measurements in a saturated vapour atmosphere was performed at the beginning of the thesis but due to inability to control the vapour in the cell, this project could not be completed. If this work is done, one can compare the data from ellipsometry humidity studies to those of neutron reflectometry.

Although much work has been done on different polyelectrolyte systems (mostly PSS/P-DADMAC), there are more which could be done. Due to lack of beam-time not all the analysis on some of the systems could be completed. So far no neutron reflectivity measurements have been performed on PSS/PDADMAC75% multilayers prepared from 0.1 M NaF, 0.5 M NaCl and 0.5 M NaBr. If these measurements are done it will make the knowledge on these systems complete.

The effect of the type of ion on the swelling water is very interesting and more anions must be employed to enlarge the scope of research in this area. So far, only three types of salts (NaF, NaCl and NaBr) have been studied. The effect of cation at higher concentrations is not considered in this work and can be a future project.

Appendix A

AFM Images
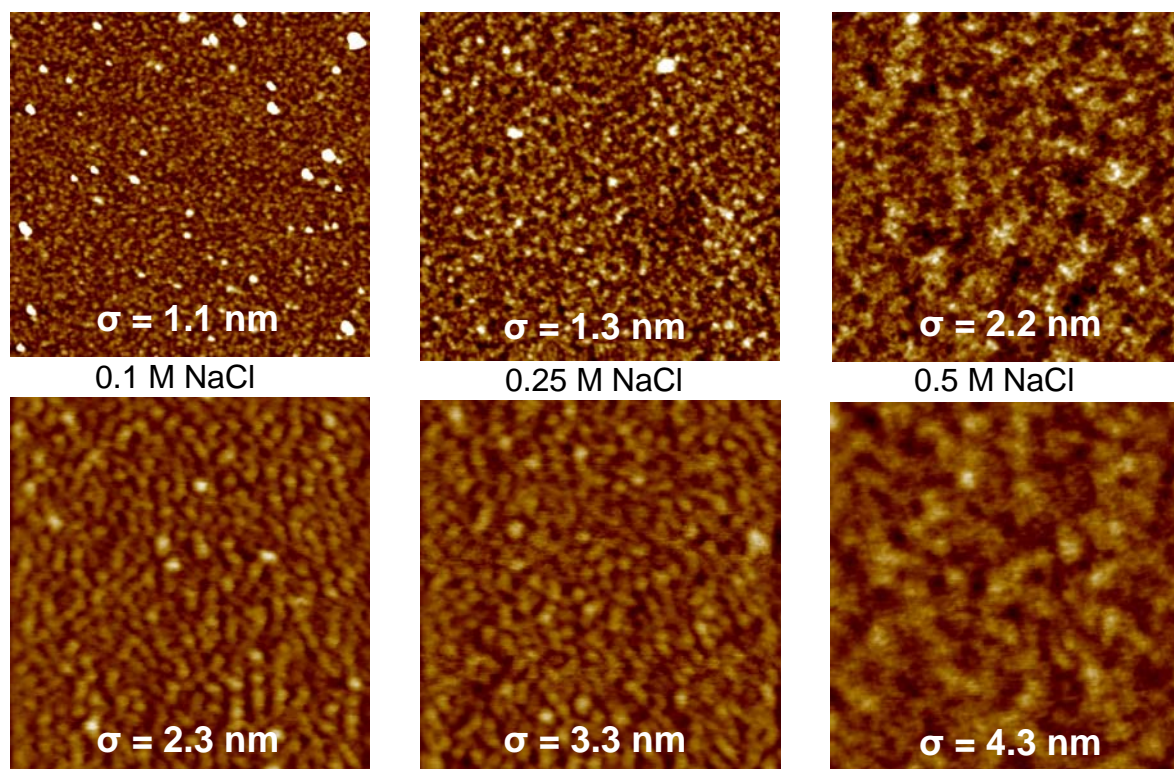
Figure .1: *AFM images of (PSS/PDADMAC100%)$_6$ multilayers against air (top row) and against water (bottom row). Scan size: 2.5×2.5 μm^2.*

PEI/(PSS/PDADMAC100%)$_6$

σ = 2.4 nm

0.1 M NaBr

σ = 1.5 nm

0.1 M NaF

PEI/(PSS/PDADMAC75%)$_6$

σ = 3.9 nm

0.1 M NaBr

σ = 2.0 nm
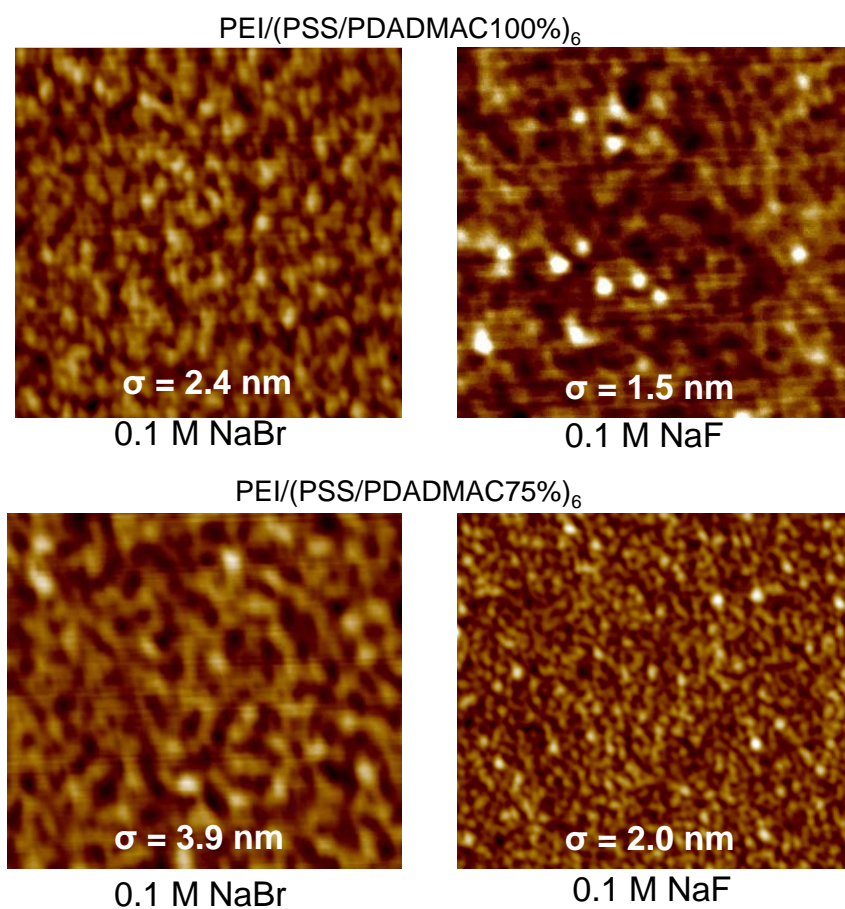
0.1 M NaF

Figure .2: *AFM images scanned against air of (PSS/PDADMAC100%)$_6$ - (top row) and (PSS/PDADMAC75%)$_6$) (bottom row) multilayers prepared from 0.1 M NaF and NaBr solutions. Scan size: 2.5 × 2.5 μm^2.*

Water Content in H$_2$O

Concentration of salt	void water Φ_{void} (%)	swell water Φ_{swell} (%)	total water Φ_{total}(%)
0.25 M NaF	10.6 ± 0.3	26.0 ± 0.8	36.6 ± 0.5
0.5 M NaF	13.2 ± 0.4	38.3 ± 1.0	51.5 ± 0.6
0.1 M NaCl	9.1 ± 0.4	36.2 ± 0.8	45.3 ± 0.5
0.25 M NaCl	7.2 ± 0.7	42.6 ± 1.3	49.8 ± 0.8
0.5 M NaCl	2.7 ± 0.2	53.8 ± 1.3	56.5 ± 1.2
0.1 M NaBr	4.2 ± 0.6	42.1 ± 1.9	46.3 ± 2.1
0.25 M NaBr	2.8 ± 0.2	61.2 ± 1.4	64.0 ± 1.3

Water Content in D$_2$O

Concentration of salt	void water Φ_{void} (%)	swell water Φ_{swell} (%)	total water Φ_{total}(%)
0.25 M NaF	12.6 ± 0.3	26.1 ± 0.8	38.7 ± 3.2
0.5 M NaF	13.3 ± 0.4	38.5 ± 1.0	51.8 ± 0.7
0.1 M NaCl	7.4 ± 0.4	35.8 ± 0.9	43.2 ± 0.5
0.25 M NaCl	7.1 ± 0.7	42.7 ± 1.0	49.8 ± 0.8
0.5 M NaCl	2.8 ± 0.2	56.6 ± 1.1	59.4 ± 1.2
0.1 M NaBr	5.0 ± 0.6	39.2 ± 1.3	44.2 ± 1.8
0.25 M NaBr	3.1 ± 0.4	58.5 ± 2.0	61.6 ± 2.5

Figure .3: *Neutron reflectivity data on (PSS/PDADMAC)$_6$ multilayers. Supporting information to the work in Chapter 4.*

	Ellipsometry: Thickness / nm of PEI/(PSS/PDADMAC)n 0.1 M NaCl							
r.h. %	**n = 1**	**n = 2**	**n = 4**	**n = 6**	**n = 8**	**n = 14**	**n = 20**	**n = 30**
0	3.5	4.4	10.0	21.0	32.4	58.4	102.3	156.7
10	3.6	4.5	10.2	21.8	33.9	61.5	109.0	168.4
20	3.8	4.7	10.3	23.1	35.6	65.0	114.6	177.4
30	3.9	4.8	10.5	23.7	36.7	67.8	121.5	192.8
40	4.1	4.9	10.7	24.6	39.2	72.0	129.6	205.8
50	4.2	5.0	10.9	25.2	40.0	73.9	135.2	215.6
60	4.3	5.1	11.0	26.0	41.0	76.2	141.6	229.4
70	4.4	5.2	11.2	27.0	42.5	80.8	150.9	239.6
80	4.6	5.6	11.6	28.1	44.1	85.2	161.8	262.4
90	4.8	5.8	11.9	30.0	48.4	93.4	175.5	292.3
100	**5.0**	**6.0**	**12.1**	**31.6**	**50.6**	**106.2**	**200.2**	**326.3**

Figure .4: *Parameter values of Figure 4.4a as measured by Ellipsometry. Thicknesses in nm, n represents number of double layers. Supporting information to the work in Chapter 5.*

AFM: PEI/(PSS/PDADMAC)n 0.1 M NaCl							
n = 1		**n = 2**		**n = 4**		**n = 6**	
r.h.%	d / nm	r.h. %	d / nm	r.h. %	d / nm	r.h. %	d / nm
9.9	2.3 ± 0.4	16.4	3.8 ± 0.8	6.4	10.0. ± 0.5	8.0	17.9 ± 2.2
18.8	4.2 ± 0.9	29.0	4.0 ± 0.5	22.3	10.2 ± 1.4	18.6	18.1 ± 1.3
30.5	4.4 ± 0.6	83.4	5.9 ± 0.8	75.6	13.3 ± 1.5	87.1	31.6 ± 3.4
100.0	**5.5 ± 1.3**	**100.0**	**6.7 ± 0.6**	**100.0**	**15.0 ± 1.8**	**100.0**	**30.4 ± 2.4**
n = 8		**n = 14**		**n = 20**		**n = 30**	
r.h.%	d / nm	r.h. %	d / nm	r.h. %	d / nm	r.h. %	d / nm
4.6	26.2 ± 1.6	28.6	61.8 ± 1.3	6.4	95.7 ± 5.7	9.2	198.3 ± 3.4
22.9	27.6 ± 1.6	33.3	68.2 ± 2.7	20.0	97.5 ± 5.2	26.1	199.8 ± 10.2
81.1	32.5 ± 2.0	85.0	87.4 ± 3.2	76.4	164.5 ± 1.2	79.1	395.2 ± 28.9
100.0	**39.3 ± 1.3**	**100.0**	**89.0 ± 3.7**	**100.0**	**174.7 ± 3.6**	**100.0**	**404.3 ± 39.8**

Figure .5: *Parameter values of Figure 4.4c as measured by AFM. Thicknesses in nm, n represents number of double layers. Supporting information to the work in Chapter 5. The measurements are done by Bizan Balzer[129]*

R.H. %	Ellipsometry: Thickness / nm of PEI/(PSS/PDADMAC)n 0.5 M NaCl							
	n = 1	n = 2	n = 4	n = 6	n = 8	n = 14	n = 20	n = 30
0	5.5	12.9	36.1	44.9	64.2	207.6	285.0	439.8
10	5.7	13.4	37.7	47.0	68.2	221.1	305.0	476.1
20	5.8	13.6	38.5	48.2	69.8	230.5	319.0	499.5
30	5.8	14.1	39.0	51.7	74.5	240.6	331.0	522.8
40	6.0	14.2	41.6	53.0	76.4	252.5	358.0	560.2
50	6.1	14.6	42.5	58.6	84.3	275.0	388.0	621.0
60	6.3	15.0	44.2	61.9	90.7	305.0	430.0	704.0
70	6.4	15.6	46.1	67.0	98.9	332.0	470.0	814.8
80	6.5	17.5	52.0	75.6	111.9	380.0	550.0	920.7
90	7.0	19.2	57.3	87.9	129.4	430.0	648.5	1120.0
100	**7.1**	**20.3**	**70.2**	**101.0**	**152.8**	**530.0**	**791.2**	**1337.8**

Figure .6: *Parameter values of Figure 4.4b as measured by Ellipsometry. Thicknesses in nm, n represents number of double layers. Supporting information to the work in Chapter 5.*

AFM: PEI/(PSS/PDADMAC)n 0.5 M NaCl							
n = 1		**n = 2**		**n = 4**		**n = 6**	
r.h.%	d / nm	r.h. %	d / nm	r.h. %	d / nm	r.h. %	d / nm
4.2	7.4 ± 0.9	9.2	16.1 ± 1.7	11.75	30.7 ± 4.9	6.6	46.1 ± 1.4
20.0	7.6 ± 0.8	22.7	17.3 ± 1.9	29.5	34.4 ± 3.2	20.1	46.2 ± 1.9
74.7	7.9 ± 1.1	74.9	21.8 ± 1.6	73.5	50.5 ± 1.2	92.6	61.6 ± 2.5
100.0	**9.7 ± 1.2**	**100.0**	**24.0 ± 0.8**	**100.0**	**55.3 ± 1.9**	**100.0**	**67.3 ± 1.7**
n = 8		**n = 14**		**n = 20**		**n = 30**	
r.h. %	d / nm	r.h. %	d / nm	r.h. %	d / nm	r.h. %	d / nm
5.2	54.6 ± 1.5	9.7	222.2 ± 8.5	5.0	206.2 ± 15.4	7.8	407.7 ± 6.8
20.4	60.4 ± 3.3	22.9	258.5 ± 13.6	19.7	230.8 ± 36.5	25.9	416.9 ± 27.5
81.1	88.0 ± 1.8	76.6	410.2 ± 6.4	89.7	337.4 ± 69.1	92.6	529.1 ± 17.8
100.0	**107.8 ± 3.5**	**100.0**	**632.9 ± 17.9**	**100.0**	**553.0 ± 38.1**	**100.0**	**1068.5 ± 46.6**

Figure .7: *Parameter values of Figure 4.4d as measured by AFM. Thicknesses in nm, n represents number of double layers. Supporting information to the work in Chapter 5. The measurements are done by Bizan Balzer[129]*

Preparation/	Ellipsometry		Neutrons		X-rays	
condition	d_dry/Å	$d_swollen$/Å	d_dry/Å	$d_swollen$/Å	d_dry/Å	$d_swollen$/Å
$(PSS/PDADMAC100\%)_6$						
0.10 M NaF	136	170	-	-	-	-
0.25 M NaF	225	290	218	295	-	-
0.50 M NaF	325	482	300	486	-	-
0.10 M NaCl	185	300	144	226	160	226
0.25 M NaCl	290	500	267	465	297	428
0.50 M NaCl	500	1010	481	1041	507	757
0.10 M NaBr	230	429	229	395	-	-
0.25 M NaBr	530	1250	498	1282	-	-
0.50 M NaBr	1100	2500	-	-	-	-
$(PSS/PDADMAC75\%)_6$						
0.10 M NaF	116	-	-	-	-	-
0.25 M NaF	142	-	97	143	-	-
0.50 M NaF	170	-	76	115	-	-
0.10 M NaCl	180	-	142	219	140	207
0.25 M NaCl	300	-	306	564	-	-
0.50 M NaCl	-	-	-	-	-	-
0.10 M NaBr	217	-	209	325	-	-
0.25 M NaBr	145	-	99	140	-	-
0.50 M NaBr	135	-	-	-	-	-

Table .1: *Measured thickness obtained for PEI/(PSS/PDADMAC100%)$_6$ and PEI/-(PSS/PDADMAC100%)$_6$ multilayers, respectively by Ellipsometry, Neutron and X-ray Reflectometry. The dry thickness is measured at $\approx$ 0% r.h. and the swollen at 100% r.h. (or against water). The error bars are up to a maximum of $\pm$ 10%.*

Preparation/	AFM		Neutrons		X-rays	
condition	$\sigma_d ry$/Å	$\sigma_s wollen$/Å	$\sigma_d ry$/Å	$\sigma_s wollen$/Å	$\sigma_d ry$/Å	$\sigma_s wollen$/Å
(PSS/PDADMAC100%)$_6$						
0.10 M NaF	15	-	-	-	-	-
0.25 M NaF	17	-	25	40	-	-
0.50 M NaF	28	-	34	55	-	-
0.10 M NaCl	11	23	10	27	11	24
0.25 M NaCl	13	33	11	35	12	32
0.50 M NaCl	22	43	22	48	21	42
0.10 M NaBr	24	-	23	36	-	-
0.25 M NaBr	51	-	50	123	-	-
0.50 M NaBr	67	-	-	-	-	-
(PSS/PDADMAC75%)$_6$						
0.10 M NaF	20	-	-	-	-	-
0.25 M NaF	38	-	32	-	-	-
0.50 M NaF	41	-	37	40	-	-
0.10 M NaCl	11	-	11	14	13	25
0.25 M NaCl	24	-	27	44	-	-
0.50 M NaCl	30	-	-	-	-	-
0.10 M NaBr	39	-	39	56	-	-
0.25 M NaBr	58	-	60	-	-	-
0.50 M NaBr	69	-	-	-	-	-

Table .2: *Measured roughness obtained for PEI/(PSS/PDADMAC100%)$_6$ and PEI/-(PSS/PDADMAC100%)$_6$ multilayers, respectively, by AFM, Neutron and X-ray Reflectometry. The dry roughness is measured at ambient conditions (AFM) or at $\approx$ 0% r.h. (reflectometry). the swollen roughness is measured at 100% r.h. (or against water). The error bars are up to a maximum of $\pm$ 10%.*
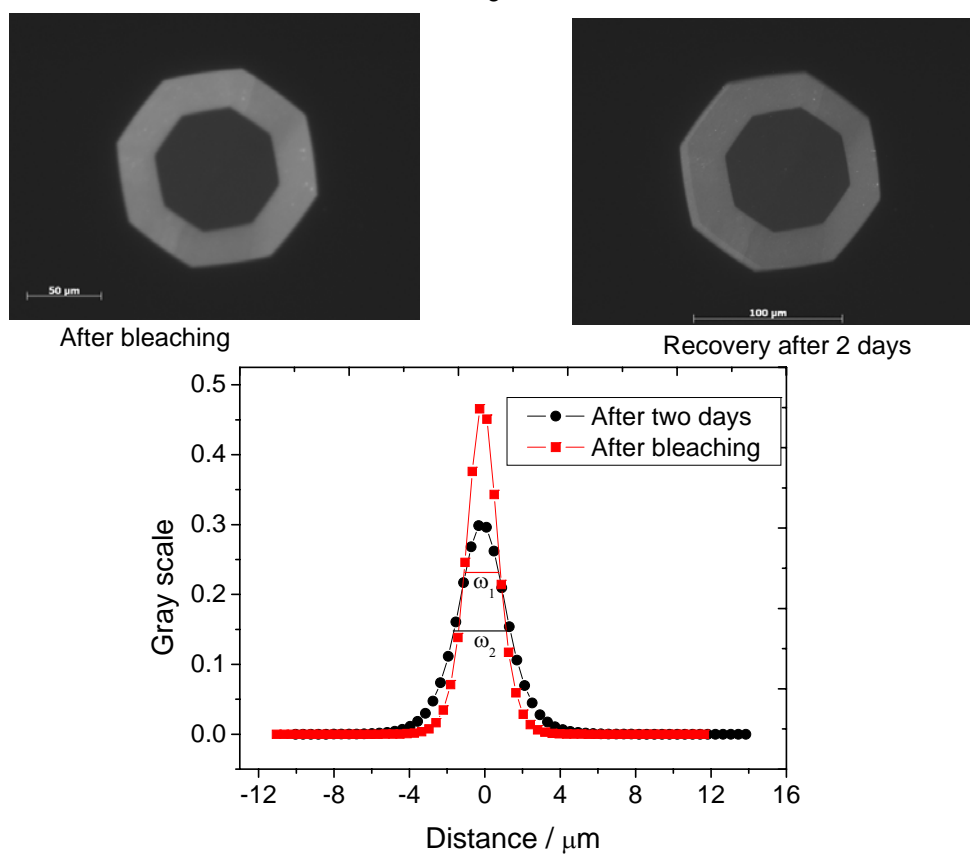
Figure .8: *FRAP of (PSS/PDADMAC100%)$_6$ multilayers prepared from 0.1 M NaBr. Top row: images of the film just after bleaching and after several hours after recovery. Bottom: Gaussian plot representing the diffusion process in a probing layer. Values in the vertical axis show the grey scale values normalized with respect to the highest number.*

Figure .9: *FRAP of (PSS/PDADMAC100%)$_6$ multilayers prepared from 0.25 M NaBr. Top row: images of the film just after bleaching and after several hours after recovery. Bottom: Gaussian plot representing the diffusion process in a probing layer. Values in the vertical axis show the grey scale values normalized with respect to the highest number.*
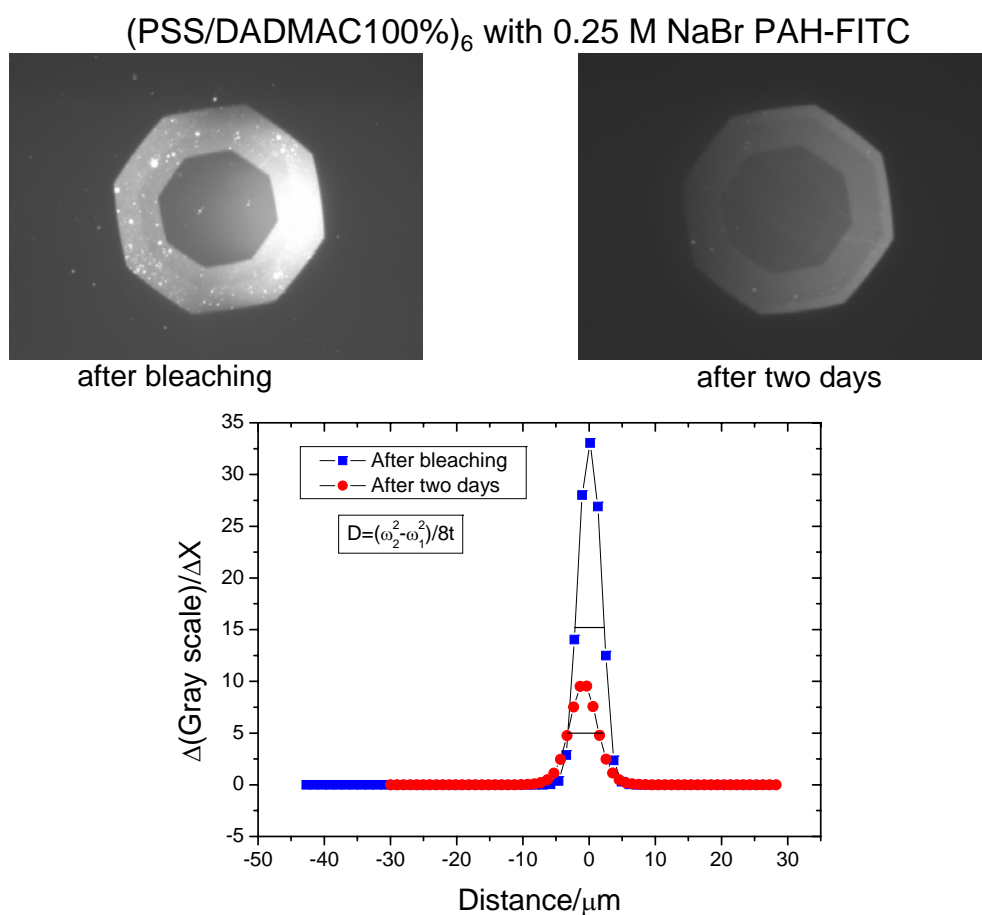
(PSS/PDADMAC100%)$_6$ 0.5 M NaBr PAH-FITC

After bleaching   Recovery after 2 days

$$D=(\omega_2^2-\omega_1^2)/8t$$

Figure .10: *FRAP of (PSS/PDADMAC100%)$_6$ multilayers prepared from 0.5 M NaBr. Top row: images of the film just after bleaching and after several hours after recovery. Bottom: Gaussian plot representing the diffusion process in a probing layer. Values in the vertical axis show the grey scale values normalized with respect to the highest number.*
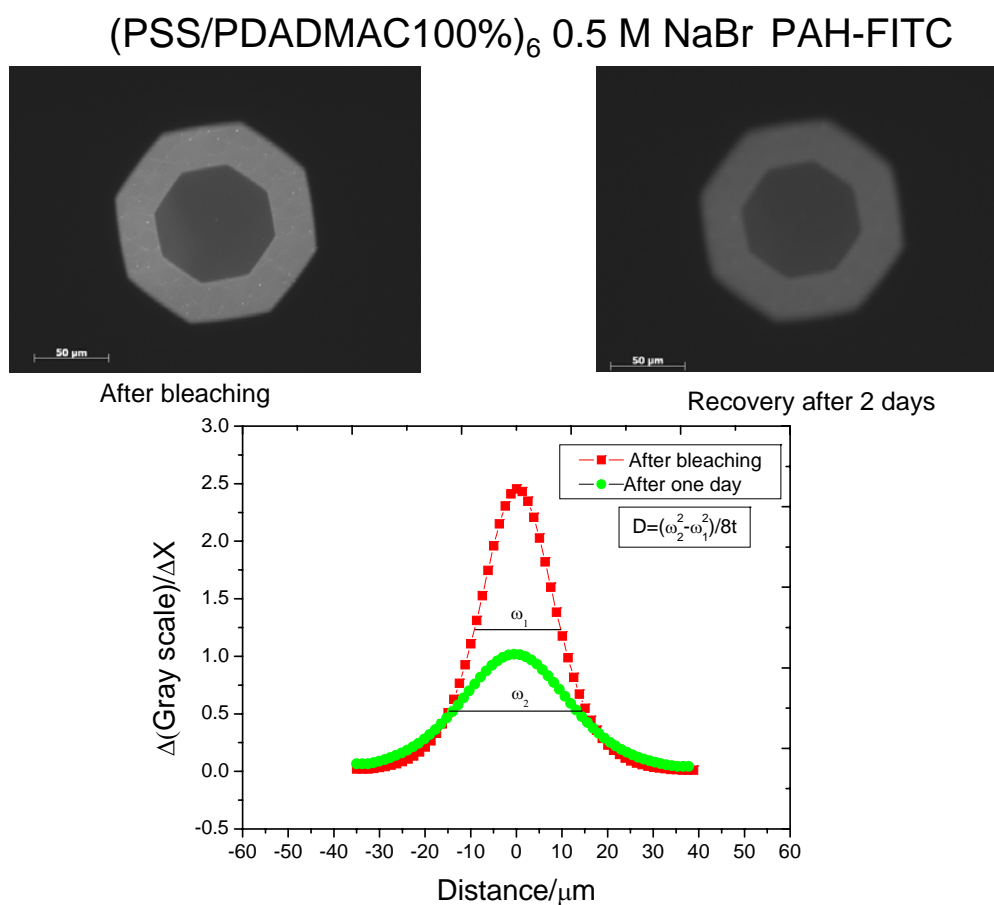
Bibliography

[1] Decher, G.; Hong, J. D. *Makromol. Chem., Macromol. Symp.* **1991**, *46*, 321.

[2] Decher, G.; Hong, J. D.; Schmitt, J. *Thin Solid Films* **1992**, *210*, 831–835.

[3] Decher, G. *Science* **1997**, *277*, 1232.

[4] Decher, G.; Schmitt, J. *Prog. Colloid Polym. Sci.* **1992**, *89*, 160–164.

[5] Iler, R. K. *J. Colloid Interface Sci.* **1996**, *21*, 569.

[6] Hammond, P. *Curr. Opinion Coll. & Interf. Sci.* **2000**, *4*, 430.

[7] Bertrand, P.; Jonas, A.; Laschewsky, A.; Legras, R. *Macromol. Rapid Commun.* **2000**, *21*, 319–348.

[8] Caruso, F. *Adv. Mater.* **2001**, *13*, 11.

[9] von Klitzing, R. *Phys. Chem. Chem. Phys.* **2006**, *8*, 5012–5033.

[10] Wu, A.; Yoo, D.; Lee, J.; Rubner, M. *J. Am. Chem. Soc.* **1999**, *121*, 4883–4891.

[11] Caruso, F.; Furlong, D.; Ariga, K.; Ichinose, I.; Kunitake, T. *Langmuir* **1998**, *14*, 4559–4565.

[12] Sun, Y.; Zhang, X.; Sun, C.; Wang, B.; Shen, J. *Macromol. Chem. Phys.* **1996**, *197*, 147–153.

[13] Donath, E.; Sukhorukov, G.; Caruso, F.; Davis, S.; Mohwald, H. *Angew. Chem., Int. Ed.* **1998**, *37*, 2202–2205.

[14] Sukhorukov, G. B.; Dontah, E.; Lichtenfeld, H.; Knippel, E.; Knippel, M.; Budde, A.; Möhwald, H. *Colloids Surfaces A* **1998**, *137*, 253–266.

[15] Lvov, Y.; Ariga, K.; Onda, M.; Ichinose, I.; Kunitake, T. *Colloids Surf., A* **1999**, *146*, 337–346.

[16] Harris, J.; Bruening, M. *Langmuir* **2000**, *16*, 2006–2013.

[17] Dubas, S.; Farhat, T.; Schlenoff, J. *J. Am. Chem. Soc.* **2001**, *123*, 5368–5369.

[18] Sullivan, D. M.; Bruening, M. L. *J. Membr. Sci.* **2005**, *248*, 161–170.

[19] Lajimi, R.; Ben Abdallah, A.; Ferjani, E.; Roudesli, M.; Deratani, A. *Desalination* **2004**, *163*, 193–202.

[20] Tarabia, M.; Hong, H.; Davidov, D.; Kirstein, S.; Steitz, R.; Neumann, R.; Avny, Y. *J. Appl. Phys.* **1998**, *83*, 725–732.

[21] Stepp, J.; Schlenoff, J. B. *Electrochem. Soc.* **1997**, *144*, L155.

[22] Stroeve, P.; Vasquez, V.; Coelho, M. A. N.; Rabolt, J. F. *Thin Solid Films* **1996**, *284*, 708–712.

[23] Levasalmi, J.; McCarthy, T. J. *Macromolecules* **1997**, *30*, 1752–1757.

[24] Hammond, P. T.; Whitesides, G. M. *Macromolecules* **1995**, *28*, 7569.

[25] Lang, Z. J.; Susha, A. S.; Yu, A. M.; Caruso, F. *Adv. Mater.* **2003**, *15*, 1849–1853.

[26] Mayya, K. S.; Gittins, D. I.; Dibaj, A. M.; Caruso, F. *Nano Lett.* **2001**, *1*, 727–730.

[27] Schmidt, M.; Löwen, H. *Phys. Rev. E* **1997**, *55*, 7228.

[28] Burmistrova, A.; Steitz, R.; von Klitzing, R. *ChemPhysChem* **2010**, *11*, 3571–3579.

[29] Fischer, P.; Laschewsky, A.; Wischerhoff, E.; Arys, X.; Jonas, A.; Legras, R. *Macromol. Symp.* **1999**, *137*, 1–24.

[30] Hong, J. D.; Park, E. S.; Park, A. L. *Langmuir* **1999**, *15*, 6515–6521.

[31] Lvov, Y.; Essler, F.; Decher, G. *J. Phys. Chem.* **1993**, *97*, 13773–13777.

[32] Sukhorukov, G. B.; Möhwald, H.; Decher, G.; Lvov, Y. M. *Thin Solid Films* **1996**, *284/285*, 220–223.

[33] Arys, X.; Laschewsky, A.; Jonas, A. M. *Macromolecules* **2001**, *34*, 3318–3330.

[34] Ott, P.; Gensel, J.; Roesler, S.; Trenkenschuh, K.; Andreeva, D.; Laschewsky, A.; Fery, A. *Chem. Mater.* **2010**, *22*, 3323–3331.

[35] Decher, G.; Hong, J. D.; Schmitt, J. *Thin Solid Films* **1992**, *210/211*, 831–835.

[36] Ahn-Ercan, G.; Krienke, H.; Kunz, W. *Curr. Opinion Coll. & Interf. Sci.* **2004**, *9*, 92–96.

[37] Vlachy, V.; Hribar-Lee, B.; Kalyuzhnyi, Y. V.; Dill, K. A. *Curr. Opinion Coll. & Interf. Sci.* **2004**, *9*, 92–96.

[38] von Klitzing, R.; Wong, J. E.; Jaeger, W.; R., S. *Curr. Opinion Coll. & Interf. Sci.* **2004**, *9*, 158–162.

[39] Salomäki, M.; Tervasmäki, P.; Areva, S.; Kankare, J. *Langmuir* **2004**, *20*, 3679–3683.

[40] Losche, M.; Schmitt, J.; Decher, G.; Bouwman, W. G.; Kjaer, K. *Macromolecules* **1998**, *31*, 8893–8906.

[41] Van der Schee, H. A.; Lyklema, J. *J. Phys. Chem.* **1984**, *88*, 6661–6667.

[42] Bohmer, M. R.; Evers, O. A.; Scheutjens, J. M. *Macromolecules* **1990**, *23*, 2288–2301.

[43] von Klitzing, R.; Mohwald, H. *Macromolecules* **1996**, *29*, 6901–6906.

[44] Decher, G.; Eckle, M.; Schmitt, J.; Struth, B. *Curr. Opinion Coll. & Interf. Sci.* **1998**, *3*, 32–39.

[45] Steitz, R.; Jaeger, W.; von Klitzing, R. *Langmuir* **2001**, *17*, 4471–4474.

[46] Gopinadhan, M.; Ahrens, H.; Gunther, J. U.; Steitz, R.; Helm, C. A. *Macromolecules* **2005**, *38*, 5228–5235.

[47] Schmitt, J.; Grunewald, T.; Decher, G.; Pershan, P. S.; Kjaer, K.; Losche, M. *Macromolecules* **1993**, *26*, 7058–7063.

[48] Hong, H. P.; Steitz, R.; Kirstein, S.; Davidov, D. *Adv. Mater.* **1998**, *10*, 1104.

[49] von Klitzing, R.; Mohwald, H. *Langmuir* **1995**, *11*, 3554–3559.

[50] Neff, P. A.; Naji, A.; Ecker, C.; Nickel, B.; Von Klitzing, R.; Bausch, A. R. *Macromolecules* **2006**, *39*, 463–466.

[51] Hara, M. *Editor, Polyelectrolytes: Science and Technology. ed.* **1993**, p 399 pp.

[52] Debye, P.; Hückel, E. *Physik Z.* **1923**, *24*, 185.

[53] Schönhoff, M. *J. Phys.: Condens. Matter* **2003**, *15*, R1781–R1808.

[54] Philipp, B.; Dautzenberg, H.; Linow, K.-J.; Dawydoff, W. *Prog. Polym. Sci.* **1989**, *14*, 91.

[55] Kabanov, V. A. *Usp. Khim* **2005**, *74*, 5.

[56] Bucur, C. B.; Z., S.; Schlenoff, J. B. *J. Am. Chem. Soc.* **2006**, *128*, 13690.

[57] Dautzenberg, H. *Macromolecules* **1997**, *30, (25)*, 7810–7815.

[58] Dautzenberg, H.; Karibyants, N. *Macromolecular Chemistry and Physics* **1999**, *200 (1)*, 118–125.

[59] Tsuchida Eishun, Y. O. K. S. *J. Polym. Sci., Part A: Polym. Chem.* **1972**, *10*, 3397.

[60] Thunemann, A. F.; Muller, M.; Dautzenberg, H.; Joanny, J. F. O.; Lowne, H. In *Polyelectrolyte Complexes. In Polyelectrolytes With Defined Molecular Architecture II*; Vol. 166, p ., Ed.; Springer: Berlin, 2004.

[61] Kabanov, A. V.; Kabanov, V. A. *Bioconjugate Chem.* **1995**, *6*, 7.

[62] Tsuchida, E. *J. Macromol. Sci. Chem.* **1994**, *A13*, 1.

[63] Cohen Stuart, M.; Hofs, B.; Voets, I. K.; de Keizer, A. *Curr. Opinion Coll. & Interf. Sci.* **2005**, *10*, 30.

[64] Arys, X.; Fischer, P.; Jonas, A. M.; Koetse, M. M.; Laschewsky, A.; Legras, R.; Wischerhoff, E. *J. Am. Chem. Soc.* **2003**, *125*, 1859–1865.

[65] Zhai, L.; Cebeci, F.; Cohen, R.; ; Rubner, M. *Nano Letters* **2004**, *4 (7)*, 1349–1353.

[66] Arys, X.; Jonas, A. M.; Laschewsky, A.; R., L. *Supramolecular Polymers* **2000**, 505–563.

[67] Kotov, N. V. *Nanostructured Materials* **1999**, *12, (5-8)*, 789–796.

[68] Sukhishvili, S. A.; Granick, S. J. *J. Am. Chem. Soc.* **2000**, *122*, 9550–9551.

[69] Sukhishvili, S. A.; Granick, S. *Macromolecules* **2002**, *35*, 301–310.

[70] Hong, J. D.; Lowack, K.; Schmitt, J.; Decher, G. *Prog. Colloid Polym. Sci.* **1993**, *93*, 98–104.

[71] v. d. Schee, H. A.; Lyklema, J. *J. Phys. Chem.* **1984**, *88*, 6661–6667.

[72] Bharadwaj, S.; R., M.; T., H. D. *Langmuir* **2006**, *22*, 6093–6101.

[73] Wong, J.; Zastrow, H.; Jaeger, W.; v. Klitzing, R. *Langmuir* **2009**, *25*, 14061–14070.

[74] Nazaran, P.; Bosio, V.; Jaeger, W.; Anghel, D. F.; v. Klitzing, R. *J. Phys. Chem. B* **2007**, *111*, 8572–8581.

[75] Dodoo, S.; Steitz, R.; Laschewsky, A.; von Klitzing, R. *Phys. Chem. Chem. Phys.* **2011**, *13*, 10318–10325.

[76] Plech, A.; Salditt, T.; Muenster, C.; Peisl, J. *J. Colloid and Interface Science* **2000**, *223*, 74–82.

[77] Dubas, S.; Schlenoff, J. *Macromolecules* **1999**, *32*, 8153–8160.

[78] Lavalle, P.; Gergely, C.; Cuisinier, F. J. G.; Decher, G.; Schaaf, P.; Voegel, J. C.; Picart, C. *Macromolecules* **2002**, *35*, 4458–4465.

[79] Caruso, F.; Rodda, E.; Furlong, D.; Niikura, K.; Okahata, Y. *Anal. Chem.* **1997**, *69*, 2043–2049.

[80] Ladam, G.; Schaad, P.; Voegel, J.; Schaaf, P.; Decher, G.; Cuisinier, F. *Langmuir* **2000**, *16*, 1249–1255.

[81] Picart, C.; Lavalle, P.; Hubert, P.; Cuisinier, F. J. G.; Decher, G.; Schaaf, P.; Voegel, J. C. *Langmuir* **2001**, *17*, 7414–7424.

[82] Ruths, J.; Essler, F.; Decher, G.; Riegler, H. *Langmuir* **2000**, *16*, 8871–8878.

[83] Picart, C.; Mutterer, J.; Richert, L.; Luo, Y.; Prestwich, G. D.; Schaaf, P.; Voegel, J.-C.; Lavalle, P. *PNAS* **2002**, *99*, 12531–12535.

[84] Holm, C.; Kékicheff, P.; Podgornik, R. *Electrostatic effects in soft matter and biophysics*; Kluwer Academic Publishers, Dodrecht, The Netherlands, 2001.

[85] Israelachvilli, J. N. *Intermolecular and Surface Forces*, 2nd ed.; Academic Press; San Diego, 1992.

[86] Butt, H.-J.; Graf, K.; Kappl, M. *Physics and Chemistry of Interfaces*; Wiley-VCH; Weinheim, 2nd edition, 2003.

[87] Nargessi, R. D.; Smith, D. S. *Methods Enzylmol.* **1998**, *122*, 67.

[88] Bosio, V.; Dubreuil, G. F. A., F. Bogdanovic *Colloids and Surfaces A: Physicochem. Eng. Aspects* **2004**, *243*, 147–155.

[89] Roe, R. J. In *Methods of X-ray and Neutron Scattering in Polymer Science*; Binder, K., Ed.; Oxford University Press, Inc., 2000.

[90] Golnik, A.; Bernhard, C.; Humlicek, J.; Kläser, M.; Cardona, M. *Phys. Stat. Sol. B* **1999**, *215*, 553.

[91] Born, M.; Wolf, E. In *Principle of Optics*; 6th ed.„ Ed.; Pergamon Press, New York, 1980.

[92] Satija, S. K.; Majkrzak, C. F.; Russell, T. P.; Sinha, S. K.; Sirota, E. B.; Hughes, G. J. *Macromolecules* **1990**, *23*, 3860–3864.

[93] Howse, J. R.; Manzanares-Papayanopoulos, E.; McLure, I. A.; Bowers, J.; Steitz, R.; Findenegg, G. H. *J. Chem. Phys.* **2002**, *116*, 7177–7188.

[94] Mezei, F.; Golub, R.; Klose, F.; Toews, H. *Phys. B* **1995**, *213*, 898–900.

[95] Steitz, R.; Leiner, V.; Siebrecht, R.; von Klitzing, R. *Colloids Surf., A* **2000**, *163*, 63–70.

[96] Parratt, L. G. *Phys. Rev.* **1954**, *95*, 359–369.

[97] Farinato, R.; Dubin, P. *Colloid - Polymer Interaction: from fundamentals to practice*; John Wiley & Son, Inc., 1999.

[98] Wong, J. E.; Rehfeldt, F.; Hanni, P.; Tanaka, M.; von Klitzing, R. *Macromolecules* **2004**, *37*, 7285–7289.

[99] Schmidt, S.; Motschmann, H.; Hellweg, T.; von Klitzing, R. *Polymer* **2008**, *49*, 749–756.

[100] Sauerbrey, G. *Zeitschrift fuer Physik* **1959**, *155*, 206–222.

[101] Hook, F.; Rodahl, M.; Brzezinski, P.; Kasemo, B. *Langmuir* **1998**, *14*, 729–734.

[102] Smith, K. L. *Electron. Wireless World* **1986**, *July*, 51–53.

[103] Rodahl, M.; Höök, F.; Krozer, A.; Brzezinski, P.; Kasemo, B. *Rev. Sci. Instrum.* **1995**, *66*, 3924.

[104] Miller, M. D.; Bruening, M. L. *Chem. Mater.* **2005**, *17*, 5375–5381.

[105] Gopinadhan, M.; Ivanova, O.; Ahrens, H.; Guenther, J.; Steitz, R.; Helm, C. A. *J. Phys. Chem. B* **2007**, *111*, 8426–8434.

[106] Collins, K. D.; Neilson, G. W.; Enderby, J. E. *Biophys. Chem.* **2007**, *128*, 95–104.

[107] Hofmeister, F. *Arch. Exp. Pathol. Pharmakol.* **1888**, *24*, 247–260.

[108] Ivanova, O.; Soltwedel, O.; Gopinadhan, M.; Koehler, R.; Steitz, R.; Helm, C. A. *Macromolecules* **2008**, *41*, 7179–7185.

[109] Voigt, U.; Jaeger, W.; Findenegg, G. H.; von Klitzing, R. *J. Phys. Chem. B* **2003**, *107*, 5273–5280.

[110] Voigt, U.; Khrenov, V.; Thuer, K.; Hahn, M.; Jaeger, W.; von Klitzing, R. *J. Phys.: Condens. Matter* **2003**, *15*, S213–S218.

[111] Mjahed, H.; Voegel, J.; Senger, B.; Chassepot, A.; Rameau, A.; Ball, V.; Schaaf, P.; Boulmedais, F. *Soft Matter* **2009**, *5*, 2269–2276.

[112] Yaminsky, V.; Vogler, E. *Curr. Opin. Colloid Interface Sci.* **2001**, *6*, 342–349.

[113] Schwarz, B.; Schönhoff, M. *Colloids Surf., A* **2002**, *198*, 293–304.

[114] Schlenoff, J. B.; Rmaile, A. H.; Bucur, C. B. *J. Am. Chem. Soc.* **2008**, *130*, 13589–13597.

[115] Dautzenberg, H.; Gornitz, E.; Jaeger, W. *Macromol. Chem. Phys.* **1998**, *199*, 1561–1571.

[116] Peppas, N. A.; Khare, A. R. *Adv. Drug Delivery Rev.* **1993**, *11*, 1–35.

[117] Dubas, S. T.; Schlenoff, J. B. *Langmuir* **2001**, *17*, 7725–7727.

[118] Sukhorukov, G. B.; Schmitt, J.; Decher, G. *Phys. Chem. Chem. Phys.* **1996**, *100*, 948–953.

[119] Bongaerts, J. H.; Cooper-White, J. J.; Stokes, J. R. *Biomacromolecules* **2009**, *10*, 1287–1294.

[120] Salomäki, M.; Laiho, T.; Kankare, J. *Macromolecules* **2004**, *37*, 9585–9590.

[121] Ninham, B. W.; Yaminsky, V. *Langmuir* **1997**, *13*, 2097–2108.

[122] Antipov, A.; Sukhorukov, G.; Mohwald, H. *Langmuir* **2003**, *19*, 2444–2448.

[123] Steitz, R.; Leiner, V.; Tauer, K.; Khrenov, V.; Von Klitzing, R. *Appl. Phys. A: Mater. Sci. Process.* **2002**, *74*, S519–S521.

[124] Farhat, T.; Yassin, G.; Dubas, S.; Schlenoff, J. *Langmuir* **1999**, *15*, 6621–6623.

[125] Kugler, R.; Schmitt, J.; Knoll, W. *Macromol. Chem. Phys.* **2002**, *203*, 413–419.

[126] Schwarz, B.; Schönhoff, M. *Langmuir* **2002**, *18*, 2964–2966.

[127] McCormick, M.; Smith, R.; Graf, R.; Barrett, C.; Reven, L.; Spiess, H. *Macromolecules* **2003**, *36*, 3616–3625.

[128] Smith, R.; Reven, L.; Barrett, C. *Macromolecules* **2003**, *36*, 1876–1881.

[129] Dodoo, S.; Balzer, T., B. Hugel; Laschewsky, A.; von Klitzing, R. *Soft Material* **2011**, Accepted.

[130] Kellogg, G. J.; Mayes, A. M.; Ferreira, M.; Rubner, M. F.; Satija, S. K. *Langmuir* **1996**, *12*, 5109–5113.

[131] Kim, B.-S.; Choi, J.-W. *Biotechnology and Bioprocess Engineering* **2007**, *12*, 323–332.

[132] Glinel, K.; Dejugnat, C.; Prevot, M.; Schlöler, B.; Schönhoff, M.; von Klitzing, R. *Colloids Surf A* **2007**, *303*, 3–13.

[133] Sukhishvili, S. A. *Current Opinion in Colloid & Interface Science* **2005**, *10*, 37–44.

[134] Caruso, F.; Lichtenfeld, H.; Donath, E.; Möhwald, H. *Macromolecules* **1999**, *32*, 2317–2328.

[135] Garg, A.; Heflin, J. R.; Gibson, H. W.; Davis, R. M. *Langmuir : the ACS journal of surfaces and colloids* **2008**, *24*, 10887–94.

[136] Hook, F.; Rodahl, M.; Kasemo, B.; Brzezinski, P. *Proc. Natl. Acad. Sci. U. S. A.* **1998**, *95*, 12271–12276.

[137] Hook, F.; Rodahl, M.; Brzezinski, P.; Kasemo, B. *J. Colloid Interface Sci.* **1998**, *208*, 63–67.

[138] Kolarik, L.; Furlong, D. N.; Joy, H.; Struijk, C.; Rowe, R. *Langmuir* **1999**, *15*, 8265–8275.

[139] Sui, Z.; Salloum, D.; Schlenoff, J. B. *Langmuir* **2003**, *19*, 2491–2495.

[140] Sun, B.; Flessner, R. M.; Saurer, E. M.; Jewell, C. M.; Fredin, N. J.; Lynn, D. M. *J. Colloid Interface Sci.* **2011**, *355*, 431–441.

[141] Shovsky, A.; Bijelic, G.; Varga, I.; Makuska, R.; Claesson, P. M. *Langmuir* **2011**, *27*, 1044–1050.

[142] Ankerfors, C.; Ondaral, S.; Wagberg, L.; Odberg, L. *J. Colloid Interface Sci.* **2010**, *351*, 88–95.

[143] Mueller, M.; Ouyang, W.; Kessler, B. *Spectrochimica Acta Part A - Molecular and Biomolecular Spectroscopy* **2010**, *77*, 709–716.

[144] Tedeschi, C.; Caruso, F.; Möhwald, H.; Kirstein, S. *Journal of the American Chemical Society* **2000**, *122*, 5841–5848.

[145] Linford, M. R.; Auch, M.; Möhwald, H. *Journal of the American Chemical Society* **1998**, *120*, 178–182.

[146] Fukao, N.; Kyung, K.-H.; Fujimoto, K.; Shiratori, S. *Macromolecules* **2011**, *44*, 2964–2969.

[147] Chang, C.-C.; Lin, S.; Chu-Su, Y.; Lin, C.-W. *Sensor Letters* **2011**, *9*, 404–408.

[148] Schuewer, N.; Klok, H.-A. *Langmuir* **2011**, *27*, 4789–4796.

[149] Mhanna, R. F.; Voeroes, J.; Zenobi-Wong, M. *Biomacromolecules* **2011**, *12*, 609–616.

[150] Köhler, R.; Dönch, I.; Ott, P.; Laschewsky, A.; Fery, A.; Krastev, R. *Langmuir* **2009**, *25*, 11576–11585.

[151] Feldötö, Z.; Varga, I.; Blomberg, E. *Langmuir* **2010**, *26*, 17048–17057.

[152] Krim, J.; Solina, D. H.; Chiarello, R. *Phys. Rev. Lett.* **1991**, *66*, 181–184.

[153] Rodahl, M.; Kasemo, B. *Sensors Actuators, A* **1996**, *54*, 448–456.

[154] Urbakh, M.; Daikhin, L. *Langmuir* **1994**, *10*, 2836–2841.

[155] Martin, S. J.; Frye, G. C.; Ricco, A. J. *Anal. Chem.* **1993**, *65*, 2910.

[156] Urbakh, M.; Daikhin, L. *Phys. Rev., B* **1994**, *49*, 4866–4870.

[157] Cho, K. C.; Leung, W. P.; Mok, H. Y.; Choy, C. L. *Biochim. Biophys. Acta* **1985**, *830*, 36.

[158] Edmonds, P. D. *Bioelectromagnetics* **1982**, *3*, 157.

[159] Decher, G.; Lvov, Y.; Schmitt, J. *Thin Soild Films* **1994**, *244*, 772–777.

[160] Picart, C.; Ladam, G.; Senger, B.; Voegel, J.-C.; Schaaf, P.; Cuisinier, F. J. G.; Gergely, C. *J. Chem. Phys.* **2001**, *115*, 1086–1094.

[161] Garza, J.; Schaaf, P.; Muller, S.; Ball, V.; Stoltz, J.; Voegel, J.; Lavalle, P. *Langmuir* **2004**, *20*, 7298–7302.

[162] Kovacevic, D.; van der Burgh, S.; de Keizer, A.; Stuart, M. A. C. *Langmuir* **2002**, *18*, 5607–5612.

[163] Elbert, D. L.; Herbert, C. B.; Hubbell, J. A. *Langmuir* **1999**, *15*, 5355–5362.

[164] Lavalle, P.; Picart, C.; Mutterer, J.; Gergely, C.; Reiss, H.; Voegel, J.-C.; Senger, B.; Schaaf, P. *J. Phys. Chem. B* **2004**, *108*, 635–648.

[165] Salomäki, M.; Vinokurov, I. A.; Kankare, J. *Langmuir* **2005**, *21*, 11232–11240.